Final Scientific/Technical Report – DE-FG02-06ER64184

Reporting Period: 15 November 2002 – 15 January 2007

Submission Date: November 2, 2007

Title: In Situ Immobilization of Uranium in Structured Porous Media via Biomineralization at the Fracture/Matrix Interface – Subproject to Co-PI Eric E. Roden

Investigators: Eric E. Roden (Subproject PI)*
The University of Alabama
Department of Biological Sciences
A122 Bevill Building 7th Avenue
Tuscaloosa, AL 35487

* As of August 2005: University of Wisconsin, Department of Geology and Geophysics, 1215 West Dayton Street, Madison, WI 53706

Table of Contents

1. Executive Summary

Overview

Although the biogeochemical processes underlying in situ bioremediation technologies are increasingly well understood, field-scale heterogeneity (both physical and biogeochemical) remains a major obstacle to successful field-scale implementation. In particular, slow release of contamination from low-permeability regions (primarily by diffusive/dispersive mass transfer) can hinder the effectiveness of remediation. The research described in this report was conducted in conjunction with a project entitled "In Situ Immobilization of Uranium in Structured Porous Media via Biomineralization at the Fracture/Matrix Interface**"**, which was funded through the Field Research element of the former NABIR Program (now the Environmental Remediation Sciences Program) within the Office of Biological and Environmental Research. Dr. Timothy Scheibe (Pacific Northwest National Laboratory) was the overall PI/PD for the project, which included Scott Brooks (Oak Ridge National Laboratory) and Eric Roden (formerly at The University of Alabama, now at the University of Wisconsin) as separately-funded co-PIs. The overall goal of the project was to evaluate strategies that target bioremediation at interfaces between high- and low-permeability regions of an aquifer in order to minimize the rate of contaminant transfer into high-permeability/high fluid flow zones. The research was conducted at the Area 2 site of the Field Research Center (FRC) at Oak Ridge National Laboratory (ORNL). Area 2 is a shallow pathway for migration of contaminated groundwater to seeps in the upper reach of Bear Creek at ORNL, mainly through a ca. 1 m thick layer of gravel located 4-5 m below the ground surface. Hydrological tracer studies indicate that the gravel layer receives input of uranium from both upstream sources and from diffusive mass transfer out of highly contaminated fill and saprolite materials above and below the gravel layer. We sought to test the hypothesis that injection of electron donor into this layer would induce formation of a redox barrier in the less conductive materials above and below the gravel, resulting in decreased mass transfer of uranium out these materials and attendant declines in groundwater U(VI) concentration. Details regarding the planning, execution, and results of the in situ biostimulation experiment will be provided in separate peer-reviewed publications by the project PIs and colleagues. This report summarizes research activities conducted at The University of Alabama (2002-2005) and the University of Wisconsin (2005-2007) in support of the field experiment.

Sediment core analyses

A comprehensive assessment of the abundance and redox speciation of solid-phase iron and uranium compounds in Area 2 sediments was achieved through analysis of multiple (10 total) sediment cores. The analyses revealed a distinct enrichment in uranium (up to a few μmol per gram of dry sediment, equivalent to several hundred ppm) at the base of the fill zone, with the zone of U enrichment extending 0.5-1 m above and below the gravel located at the fill-saprolite interface. Although only ca. 10% of the total measured uranium pool was recovered as U(VI) by wet chemical extraction of bulk wet sediment, determinations made on anaerobically-dried, size-fractionated materials indicated a more equal distribution of uranium between U(VI) and residual (presumably reduced) nitric acid-soluble phases. We speculate that the wet chemical extraction for bulk U(VI) (100 mM $NaHCO_3$) did not fully solubilize uranium from the clay-rich microporous materials that are characteristic of ORNL saprolite materials. High

concentrations of solid-phase Fe (up to ca. 300 μm per gram of dry sediment) were present throughout Area 2 sediments, with crystalline Fe(III) oxides (soluble in citrate/dithionite) being 5-10 times more abundant than dilute (0.5M) HCl-soluble amorphous Fe(II) and Fe(III) phases. The high concentrations of Fe(III) oxides in the saprolite materials suggests that much of the solid-phase U(VI) is associated with Fe(III) oxide surfaces. These results lead us to speculate that a major source of U(VI) input to Area 2 groundwaters is diffusive mass transfer from U-enriched zones on either side (i.e. above and below) of the high-flow gravel layer. **Based on this assessment, a ca. 3 m thick depth interval bracketing the gravel layer was targeted for the in situ biostimulation experiment.** We anticipated that diffusive/advective input of electron donor to U-enriched sediments on either side of (as well as within) the gravel layer would lead to coupled reduction of solid-phase Fe(III) and U(VI), thus reducing the input of U to the high-flow gravel layer.

The influence of in situ ethanol biostimulation on the redox speciation of Fe and U in Area 2 sediments was assessed by comparing stimulated and unstimulated sediment in terms of (i) the ratio of 0.5M HCl-extractable Fe(II) to total citrate/dithionite (C/D)-extractable Fe, which was expected to increase as a result of ethanol-driven Fe(III) reduction activity; and (ii) the ratio of $NaHCO_3$-extractable U(VI) to the sum of $NaHCO_3$-extractable U(VI) and residual HNO_3-extractable U, which was expected to decrease as a result of ethanol-driven U(VI) reduction activity. The results collectively indicated that in situ biostimulation had a significant impact on the relative abundance of reduced Fe compounds, particularly in sediments from below the gravel layer. However, the relative abundance of U(VI) was not significantly altered, even though groundwater U(VI) concentrations decreased significantly in the vicinity of borehole MLS-F during in situ biostimulation. In these comparisons, the ratio U(VI) to total U was relatively high in all the materials analyzed, which together with the high intrinsic variability in solid-phase U abundance made detection of a significant change in relative U(VI) difficult or impossible. In addition, controlled experimental studies of solid-phase U(VI) reduction in Area 2 sediments indicated that only a fraction of the total U(VI) of Area 2 sediment is subject to microbial (or abiotic) reduction.

The abundance of culturable ethanol-, acetate, and hydrogen-oxidizing iron-reducing and sulfate-reducing organisms was assessed in stimulated vs. unstimulated sediment core materials from within and just below the gravel layer. There was no obvious impact of biostimulation on the abundance of these organisms. However, this exercise yielded several pure iron- and sulfate-reducing isolates. Detailed studies of the physiology of these and other isolates from ethanol-stimulated FRC Area 2 sediments (conducted as part of other ERSP-funded research) are underway.

Sediment slurry experiments

Preliminary experiments. Preliminary sediment slurry incubation experiments were conducted with Area 2 materials in order to evaluate the potential for stimulation microbial U(VI) reduction (and other microbial respiratory pathways) using ethanol (10 mM) as the electron donor. These experiments showed that both native Fe(III)-reducing microbial populations and the well-characterized Fe(III)/U(VI)-reducing bacterium *Geobacter sulfurreducens* had the potential to

reduce sediment-associated U(VI). However, only ca. 50% of total sediment U(VI) was subject to microbial reduction, a result consistent with other recent ERSP-funded research.

Slurry experiment with native microflora. A detailed assessment of terminal electron acceptor metabolism and U(VI) reduction by native microflora was conducted with slurries of highly U-contaminated, Fe(III) oxide-rich Area 2 sediments from just below the gravel/saprolite interface. A classical pattern of electron acceptor consumption over time was observed, with nitrate consumed first (day 0-4), followed by reduction (without a lag) of Fe(III) (day 4-9) and sulfate (day 9-12); methane production ensued after a ca. 1 week lag period. U(VI) reduction took place mainly during the period of Fe(III) reduction; only minor changes in the relative abundance U(VI) were observed during the ensuing sulfate-reducing and methanogenic phases. Reverse transcribed 16S rRNA clone libraries and measurements of phospholipid fatty acids (PLFA) abundance and the incorporation of ^{13}C-ethanol into PLFAs revealed major increases in the abundance of organisms related to *Dechloromonas*, *Geobacter*, and *Oxalobacter*. PLFAs indicative of Fe(III)/U(VI)-reducing *Geobacter* species showed a distinct increase in the amended slurries, and analysis of PLFA $^{13}C/^{12}C$ ratios confirmed the incorporation of ethanol into signature PLFAs of *Geobacter*. Although no significant increase in the abundance of PLFAs indicative of sulfate-reducing bacteria (SRB) was observed, a distinct increase in the abundance of ^{13}C-labeled PLFAs indicative of *Desulfobacter*, *Desulfotomaculum*, and *Desulfovibrio* was observed during the brief period of sulfate reduction which followed the Fe(III) reduction phase.

A follow-up experiment was conducted with subsamples of the reduced slurries to assess possible metabolic (as opposed to geochemical) reasons for incomplete U(VI) reduction observed in the ethanol-amended slurries. Duplicate slurry subsamples were amended with nothing (control), 5 mM ethanol, 5 mM ethanol + 10 mmol L^{-1} of synthetic amorphous Fe(III) oxide, 5 mM ethanol + 2 mM SO_4^{2-}, or 5 mM ethanol + 0.1 mM AQDS. Addition of Fe(III) oxide and sulfate were designed to stimulate DIRB and SRB activities. AQDS is a soluble electron shuttling compound that accelerates rates of microbial Fe(III) oxide reduction in sediments, and that may stimulate solid-associated U(VI) reduction by reacting with U(VI) associated with sediment surfaces that are inaccessible to direct microbial reduction. None of the treatments stimulated significant additional U(VI) reduction, despite the presence of active microbial metabolism as indicated by additional Fe(II) accumulation, sulfate consumption, and CH_4 production. These results indicate that the main limitation posed on residual U(VI) reduction was geochemical rather than microbiological in nature, and highlight the need for studies on the physiochemical nature of the non-reducible U(VI) species.

Gravel layer biogeochemistry. An experiment was conducted to address the unusual biogeochemistry of the gravel layer at Area 2. Visual examination of sediment cores suggested that Fe in the gravel materials was reduced, as indicated by their dark grey color in contrast to the yellow-orange color of the Fe(III) oxide-rich fill and saprolite sediments. Solid-phase Fe measurements confirmed that the gravel sediments are in fact enriched in solid-associated Fe(II) and depleted in total Fe(III) oxide content. These observations were perplexing given that both thermodynamic and kinetics-based models of redox speciation argue against the co-existence of high concentrations of solid-associated Fe(II) in aquifers containing significant concentrations of nitrate (mean Area 2 nitrate concentrations are 0.5-1 mM). Fine-grain material from the gravel

layer was incubated in artificial groundwater to gain insight into what is actually happening within the gravel layer in terms of redox metabolism. Nitrate (2 mM final concentration) was added to the slurries every few days to mimic the input of nitrate from upstream groundwater input. To our surprise, all of the nitrate added during the first 20 days of incubation was rapidly consumed, and at the same time a large increase in Fe(II) and dissolved acetate was observed. These results suggest that the gravel materials are being supplied with some form of organic carbon which is capable of preventing incoming nitrate from reacting with solid-phase Fe(II) compounds. If this is true, then the concentration of nitrate in Area 2 groundwaters is the result of a dynamic balance between nitrate input and enzymatic consumption within the gravel layer. A long-term semicontinuous culture experiment with Area 2 gravel materials will be initiated in the near future through other ERSP-funded research in order to compare in detail the redox metabolism of the gravel material with and without ethanol input.

Groundwater microbial community analyses

A total of over 300 groundwater samples were collected for possible microbial community analysis during the in situ biostimulation experiment. The filters have been archived at -80 °C (at ORNL) since the time of collection. A subset of these filters was analyzed via a standard nonculture-based molecular technique, Denaturing Gradient Gel Electrophoresis (DGGE) of PCR-analyzed 16S rRNA gene fragments, in order to assess the impact of ethanol biostimulation on groundwater microbial community composition in one of the multi-level sampling wells. The DGGE analyses indicated that biostimulation was accompanied by an increase in the abundance (as indicated by the presence and density of bands on the DGGE gels) of known nitrate-, metal- and sulfate-reducing organisms (e.g. *Dechloromonas*, *Geobacter*, *Aquaspirillum*, *Desulfobacter*, *Desulfovibrio*). The results are consistent with the observed geochemical response to ethanol stimulation, which included rapid and complete removal of nitrate, significant accumulation of dissolved Fe (and Mn), and later coupled loss of sulfate and uranium from solution. We plan to conduct two additional types of analyses on an expanded selection of the archived groundwater microbiota samples, including bulk PLFA content in collaboration with Dr. Robert Findlay at The University of Alabama, and gel element microarray analysis of 16S rDNA in collaboration of Dr. Darrell Chandler at Akonni Biosystems (formerly at Argonne National Laboratory). Comparison of these two independent sets of data should provide direct insight into the linkages between ethanol input, microbial community development, and groundwater geochemistry (including uranium removal).

Biogeochemical reaction model development

Development of conceptual and numerical models of biogeochemical processes in biostimulated sediments was an important individual research focus for co-PI Roden. The primary product of this work is a reaction-based model (coded in Fortran 95) called TEAPREVU, which stands for Terminal Electron Accepting Processes in a hypothetical Representative Elementary Volume of Uranium contaminated subsurface sediment. The model was developed to simulate the results of the batch slurry experiment with FRC Area 2 sediment, with the idea that the developed framework would eventually be incorporated into a field-scale reactive transport simulation of in situ biostimulation at Area 2. The model accounts for complete (to HCO_3^-) or incomplete (to acetate) oxidation of ethanol, as well as oxidation of

acetate to HCO_3^- and/or CH_4, via 18 different TEAP pathways. Each of the TEAP reactions are dependent on the biomass of one or more distinct microbial populations chosen based on current knowledge of the kinds of organisms likely to proliferate in response to biostimulation of subsurface sediments. The model reproduced the slurry incubation results quite well, which suggests that the strategy for simulating the interaction between the different TEAPs is generally valid. A modified version of TEAPREVU was incorporated (by Yilin Fang at PNNL) into a general biogeochemical reaction simulation framework (BIOGEOCHEM) which in turn was linked with a three-dimensional field-scale reactive transport model (HYDROGEOCHEM) of the Area 2 experimental site. The model was used to help design the in situ ethanol biostimulation experiment, and it successfully simulated the early-time aquifer response to ethanol amendment.

A collaboration was initiated with Dr. Qusheng Jin at the University of Oregon, as a result of his desire to create a model of our Area 2 slurry experiment en route to development of a field-scale reactive transport simulation of the results of biostimulation push-pull tests with ethanol at Area 2. The structure of Jin's model is similar to that of TEAPREVU; however, a key aspect of the new model is that, unlike TEAPREVU, the production and consumption of molecular hydrogen (H_2) is included within the reaction network. The model accurately reproduced all of the results of the slurry experiment, including the kinetics of ethanol consumption and transient acetate accumulation, as a function of the biomass and metabolism of various functional metabolic groups These results clearly illustrate how physiologically-based reaction models can capture the basic patterns of redox metabolism that are typically observed in sedimentary environments. We plan to transfer the structure of the new model to Yilin Fang at PNNL so that it can incorporated (in place of the microbial physiology components of TEAPREVU) into the field-scale reactive transport for Area 2 and used to simulate the overall results of the in situ biostimulation experiment.

2. Introduction

A. Overview of study site

This research was conducted at the Area 2 site of the Field Research Center (FRC) at Oak Ridge National Laboratory (ORNL) (see Fig. 1). At this site, a ca. 1 m thick layer of limestone gravel is located at 4-5 m depth (see Fig. 2). The gravel layer is sandwiched between an overlying layer of disturbed fill material, and 2-3 m of undisturbed shale saprolite derived from the underlying Nolichucky Shale bedrock. The undisturbed saprolite is highly weathered bedrock that has unconsolidated character but retains much of the bedding and fracture structure of the parent rock (shale with interbedded limestone). The fill was put in place when contaminated soils were excavated and replaced by native saprolite from an uncontaminated area within Bear Creek Valley. The gravel layer was presumably installed prior to addition of the fill in order to provide a stable surface for the operation of heavy machinery. Unfortunately, the gravel layer is a now pathway for migration of uranium-contaminated groundwater to seeps in the upper reach of Bear Creek. Hydrological tracer studies indicate that this layer receives input of uranium from both upstream sources and from diffusive mass transfer out of highly contaminated fill and saprolite materials above and below the gravel layer.

B. In situ biostimulation experiment

The culmination of the overall project was an 11-month in situ ethanol biostimulation experiment carried out between September 2005 and August 2006. In this experiment, a solution containing 10 mM ethanol was injected into three wells (FW212, FW213, and FW214; see Fig. 1) once a day for 1 hr. The injected solution moved southward under natural gradient flow toward Bear Creek. Groundwater samples for geochemical analysis were collected regularly from several monitoring locations, including five multilevel sampling (MLS) wells. At selected times and locations, larger volumes of groundwater (1-2 L) were collected and filtered to obtain samples for microbial biomass and community analysis. This report summarizes research activities conducted at The University of Alabama (2002-2005) and the University of Wisconsin (2005-2007) in support of the field experiment, which included (1) chemical and microbiological characterization of sediment cores from Area 2; (2) sediment slurry experiments with Area 2 materials which evaluated the biogeochemical response to ethanol amendment and the potential for U(VI) reduction; (3) analysis of the response of groundwater microbial communities to in situ biostimulation. In addition, biogeochemical reaction models of microbial metabolism in ethanol-stimulated sediments, developed based on sediment slurry experiments, are described.

3. Analysis of Area 2 sediment cores

A. Methods

Core collection and handling. Undisturbed sediment cores (3.8 cm diameter) were collected by David Watson (the FRC manager) and colleagues at ORNL with a pneumatic hammer-driven coring device (Geoprobe®). Polyurethane core tubes were cut into ca. 50 cm segments and sealed with plastic caps immediately upon retrieval. The cores were shipped on ice and held at 4 °C prior to analysis.

Solid-phase iron. Solid-phase amorphous Fe(II) and Fe(III) oxide phases were quantified by extracting replicate (2 or 3) 1-2 g samples of wet sediment in 5-10 mL of 0.5 M HCl (Lovley and Phillips, 1986) for 1 hr, followed by colorimetric analysis of Fe(II) with ferrozine. Total Fe in the HCl extracts was determined by after the addition of hydroxylamine-HCl, and amorphous Fe(III) concentrations were calculated from the difference between total Fe and Fe(II). The total Fe(III) oxide content of parallel samples was determined by extraction in 10 mL of 0.2 M sodium citrate/ 0.35 M acetic acid (pH 4.8) plus 0.5 g of sodium dithionite (citrate/dithionite extraction) for 1 hr (Poulton and Canfield, 2005), and measuring the Fe(II) content of the extracts with ferrozine.

Solid-phase uranium. Solid-phase U(VI) was determined by extracting 1-2 g of wet sediment in 9 mL of anoxic 100 mM $NaHCO_3$ (Phillips et al., 1995). The samples were placed on a rotary shaker for 1 hr, centrifuged for 10 min at ca. 5000 × g, and a 1 mL aliquot of the supernatant was transferred to 9 mL of 0.01M HNO_3. The remaining supernatant was discarded, and 9 mL of 10% HNO_3 was added to the pellet. The samples were shaken for 16 hr, centrifuged and diluted 1:10 in distilled H_2O. Dissolved uranium, total U(VI), and residual uranium concentrations were analyzed with a Kinetic Phosphorescence Analyzer (Chemcheck Instruments, Richland, WA).

Size-fractionated characterization. Material from two cores (GP-01 and GP-02; see Fig. 1) was dried (either in air or in an anaerobic chamber) and then subjected to particle size fractionation (> 4000 μm, 2000-4000 μm, 1000-2000 μm, 106-1000 μm, < 106 μm) using different sized sieves. The isolated size fractions (1 g subsamples) were analyzed for Fe and U content. Samples dried in the anaerobic chamber were analyzed for both Fe and U abudance and redox speciation as described above. Air dried samples were analyzed for total citrate/dithionite-extractable Fe and total 10% HNO_3-extractable U only. The pH of bulk sediment samples from core GP-02 was determined by suspending 1-2 g of wet material in 10 mL of anaerobic 10 mM $CaCl_2$ overnight, and then measuring the pH of the solution with an Orion Model 700 pH meter.

Microbial enumerations. On one occasion, a roll-tube based (Hungate, 1969) dilution-to-extinction method was used to enumerate and isolate ethanol-, acetate, and hydrogen-oxidizing iron-reducing and sulfate-reducing organisms in stimulated vs. unstimulated sediment core materials from within and just below the gravel layer. Synthetic amorphous Fe(III) oxide was used as the electron acceptor for growth of iron-reducing organisms. The tubes from the last positive dilutions in cultures of biostimulated sediments were used for isolation and phylogenetic identification of representative microorganisms. The isolates were grown in liquid culture to obtain DNA for 16S rRNA gene sequencing, and the closest relative to each isolate was identified by BLAST searching (Altschul et al., 1997) of the National Center for Biotechnology Information (NCBI) database.

B. Results

Pre-biostimulation characterization. The bulk abundance of solid-phase iron and uranium compounds was analyzed in a total of 8 fresh (wet material) cores from the Area 2 field site (Fig. 3) prior to initiation of the in situ biostimulation experiment. Although there was great deal of variability in both Fe and U concentrations, the analyses clearly revealed a distinct enrichment in U at the base of the fill zone, with the zone of U enrichment extending 0.5-1 m above and below the gravel located at the fill-saprolite interface (Fig. 3A-C). Only ca. 10% of the total measured U pool was soluble in 100 mM $NaHCO_3$, suggesting that most of the solid-phase U was present in the U(IV) oxidation state (Phillips et al., 1995). However, determinations made on anaerobically-dried, size-fractionated materials (see below) showed a more equal distribution of U between $NaHCO_3$- and residual HNO_3-extractable phases. We speculate that the 1-hr $NaHCO_3$ extraction did not fully solubilize U(VI) from the clay-rich microporous materials that are characteristic of ORNL saprolite materials (Gwo et al., 1995).

Relatively high concentrations of solid-phase Fe were present throughout Area 2 sediments (Fig. 3D-F). Crystalline Fe(III) oxides soluble in citrate-dithionite (C/D) were 5-10 times more abundant than 0.5M HCl-extractable Fe(II) and Fe(III) phases. The high concentrations of Fe(III) oxides present in the saprolite materials suggests that much of the solid-phase U(VI) is associated with Fe(III) oxide surfaces, which are known to be strong sorbents of U(VI) in soils and sediments (Barnett et al., 2002). These results lead us to speculate that a major source of U(VI) input to Area 2 groundwaters (e.g. as documented by extensive monitoring of groundwater geochemistry at well GW835) is diffusive mass transfer from U-enriched zones on either side (i.e. above and below) of the high-flow gravel layer. **Based on this assessment, a ca. 3 m thick depth interval bracketing the gravel layer was targeted for the**

in situ biostimulation experiment. We anticipated that diffusive/advective input of electron donor to U-enriched sediments on either side of (as well as within) the gravel layer would lead to reduction of U(VI) (both aqueous and sorbed), thus reducing the input of U to the high-flow gravel layer. The relatively high concentrations of Fe(III) oxide in sediments above and below the gravel layer were expected to provide an ample source of electron-accepting capacity for growth and maintenance of dissimilatory metal-reducing bacterial populations.

Detailed physiochemical characterization (Fe/U abundance and speciation, sediment grain size, pH) was conducted on sediments in the vicinity of the gravel layer at Area 2. Measurements of total Fe and U abundance in materials from core GP-01 (Fig. 4B,C) showed that most of the Fe and U was associated with fine-grained (< 106 μm) materials, except within the gravel zone, where U concentrations were highly variable (often at or near detection) and present as coatings on large gravel particles. Mass-normalized Fe and U contents determined on GP-02 core materials (Fig. 5) provided a similar picture. A scatter plot of total U and Fe contents in the GP-01 materials (Fig. 6) emphasizes the linkage between these elements in Area 2 sediments. As mentioned above, the relative abundance of U(VI) and residual U (presumably U(IV)) was significantly higher in the anaerobically-dried, size-fractionated material from GP-02 (Fig. 5A,B) compared to bulk wet sediment (Fig. 3A,B). The pH of bulk sediment from GP-02 was approximately 6.5 (Fig. 5A, inset).

Post-biostimulation analyses. The influence of in situ ethanol biostimulation on the redox speciation of Fe and U in Area 2 sediments was assessed by comparing stimulated and unstimulated sediment in terms of (i) the ratio of 0.5M HCl-extractable Fe(II) to total citrate/dithionite (C/D)-extractable Fe, which was expected to increase as a result of ethanol-driven Fe(III) reduction activity; and (ii) the ratio of $NaHCO_3$-extractable U(VI) to the sum of $NaHCO_3$-extractable U(VI) and residual HNO_3-extractable U, which was expected to decrease as a result of ethanol-driven U(VI) reduction activity. Comparison of ratios rather than absolute concentrations of redox-sensitive compounds was preferable in light of the large variation in total Fe and U abundance in Area 2 sediments. The comparisons were made on materials from just above and below the gravel layer, where an impact of ethanol input on Fe and U redox speciation was expected to take place.

The first of two such comparison involved sediments that were collected prior to in situ biostimulation (MLS cores A-E and GP cores 03-05) and ca. 8 months after (core MLS-F) the start of the in situ biostimulation experiment. The results indicated that in situ biostimulation had a significant impact on the relative abundance of reduced Fe compounds, particularly in sediments from below the gravel layer (Fig. 7A). However, the relative abundance of U(VI) was not significantly altered (Fig. 7B), even though groundwater U(VI) concentrations decreased significantly in the vicinity of borehole MLS-F during in situ biostimulation (see below). Analogous results were obtained in comparison of sediments collected from within (core FW232) and outside of (core FW105) the zone of biostimulation at the end of the in situ biostimulation experiment. In this case, the impact of ethanol input on the sediment was visually quite apparent (Fig. 8), and a significant increase in relative Fe(II) abundance was evident (Fig. 9A). However, the ratio of U(VI) to total U was actually lower in the core from within the zone of biostimulation.

In both of the above comparisons, the ratio U(VI) to total U was relatively high in all the materials analyzed, which together with the high intrinsic variability in solid-phase U abundance made detection of a significant change in relative U(VI) difficult or impossible. In addition, controlled experimental studies of solid-phase U(VI) reduction in Area 2 sediments (discussed next) indicated that only a fraction of the total U(VI) of Area 2 sediment is subject to microbial (or abiotic) reduction. Based on these findings, it is perhaps not surprising that we were unable to document major shifts in the redox speciation of sediment-associated U in response to in situ biostimulation. Samples of anaerobically-dried and stored sediment from cores FW232 and FW105 have been provided to Eugene Ilton (PNNL) for analysis of U redox speciation by XPS.

The abundance of culturable ethanol-, acetate, and hydrogen-oxidizing iron-reducing and sulfate-reducing organisms was assessed in stimulated vs. unstimulated sediment core materials from within and just below the gravel layer. There was no obvious impact of biostimulation on the abundance of these organisms (Table 1). However, this exercise did yield several pure iron- and sulfate-reducing isolates. Strain ir1g6a (from gravel) is 99% identical to *Geobacter lovleyi* strain SZ; this organism is known to utilize ethanol, acetate, and H_2 as electron donors, and (like virtually all other *Geobacter* species) is presumably capable of U(VI) reduction. Strain ir1g6b (from gravel) is 99% identical to *Geospirillum arsenophilus*, which is known to utilize acetate as an electron donor; its ability to reduce U(VI) has not been tested. Strain ir3g3 (from gravel) is 97% identical to *Pelobacter propionicus*, which is known to utilize ethanol as an electron donor; its ability to reduce U(VI) is also unknown. Strains sr2g8, sr2g1, sr2g6 (isolated from gravel) and are 97-98% identical to *Desulfovibrio ferrireducens* strain CY2; this organism utilizes ethanol and H_2 as electron donors, and is likely (based on previous studies; (Lovley et al., 1993)) to be capable of U(VI) reduction. Strain sr3s4 (isolated from saprolite) is 96% identical to *Desulfovibrio carbinolicus* strain DSM 3852 (*Deltaproteobacteria*). Like *D. ferrireducens*, this organism uses ethanol and H_2 as electron donors and is likely to be capable of U(VI) reduction. Detailed studies of the physiology of these and other isolates from ethanol-stimulated FRC Area 2 sediments are underway through other ERSP-funded research.

4. Area 2 sediment incubation experiments

A. Preliminary experiment

During the early phase of the project (Fall 2003), we conducted a preliminary assessment of the potential for stimulation of Fe(III) and U(VI) reduction in sediments from below the fill-saprolite interface (i.e. sediments from ca. 7-8 m depth) using ethanol (10 mM) as the electron donor. These experiments were conducted because we were initially targeting the intact saprolite for the in situ biostimulation experiment. Sediment samples (ca. 100 g wet weight) were suspended in 50 mL of a Pipes-buffered artificial groundwater designed to mimic the major element composition (excluding nitrate and sulfate) of Area 2 groundwater. Subsamples from the slurries were removed periodically for analysis of the abundance and redox speciation of Fe and U as described in the previous section. The results indicated that all the sediments tested (6 depth intervals each from cores FWB 201 and 202 for a total of 12 slurries with and without ethanol) showed positive potential for stimulation of Fe(III) oxide reduction, as indicated by changes in the ratio of Fe(II) to total Fe in 0.5M HCl extracts (Fig. 10A), and the accumulation of aqueous Fe(II) (Fig. 10B). The abundance of U(VI) was too low in these sediments to obtain

reliable estimates of the potential for U(VI) reduction. However, experiments in which ca. 100 μmol L^{-1} (equal to the maximum bulk concentration of U(VI) observed in sediments from the fill zone at Area 2) of exogenous U(VI) was added (as uranyl-acetate) to the sediment slurries after several weeks of preincubation indicated that the biostimulated sediments were capable of carrying out significant U(VI) reduction, as indicated by an average value of 0.4 for the ratio of U(VI) to total U after ca. two months of incubation (Fig. 10C). In contrast, the unstimulated slurries showed much lower U(VI) reduction (average U(VI) to total U ratio of ca. 0.8). These findings provided important preliminary confirmation that it was possible to stimulate coupled reduction of Fe(III) and U(VI) in Area 2 sediments.

B. Endogenous U(VI) reduction by *G. sulfurreducens*

Slurries of sediment from the zone of maximum U(VI) concentration in core FWB 201 were inoculated with ca. 10^8 cells mL^{-1} of acetate/fumarate-grown *Geobacter sulfurreducens* (Caccavo et al., 1992; Methe, 2003) cells (see Jeon et al. (2004) for a description of methodology) in order to assess the potential for microbial reduction of endogenous U(VI) in Area 2 sediments. The reason for using the dissimilatory iron-reducing culture was that the sediments employed in the experiment had been exposed to air and were completely dry, which led us to anticipate that endogenous metal-reducing populations would be temporarily inactive. This speculation was incorrect, as both the *G. sulfurreducens*-amended and unamended slurries showed complete reduction of aqueous U(VI) and ca. 60% reduction of solid-associated U(VI) after ca. 1 month of incubation in the presence of 10 mM ethanol (Fig. 11A,B). Addition of 0.1 mM AQDS as an electron shuttling compound (Lovley et al., 1996) stimulated Fe(III) reduction (Fig. 11C), but had no major impact on the rate or extent of U(VI) reduction. Other recent ERSP-funded research (discussed below) has also demonstrated incomplete reduction of sediment-associated U(VI). Controls on enzymatic and chemical reduction of solid-associated U(VI) in Area 2 sediments have been addressed in detail in the Burgos et al. 2004-2007 NABIR project (Integrative Studies element).

C. Sediment slurry experiment with native microflora

A detailed assessment of terminal electron acceptor metabolism and U(VI) reduction by native microflora was conducted with slurries of highly U-contaminated, Fe(III) oxide-rich sediments from just below the gravel/saprolite interface (see Fig. 2) in core FWB 215. The results of this study are only briefly summarized here, as a paper describing the experiment in detail has been submitted for publication,(Mohanty et al., 2007) and is provided as an Attachment (#1) to this report. Once again the experiment was conducted with dried, pulverized sediment. The slurries were inoculated with a small (5% vol:vol) quantity of a 1:1 (wet mass:liquid volume) suspension of undried sediment from the same depth interval in order to introduce a healthy natural microflora. The aqueous phase of the slurries was designed to match the groundwater geochemistry at Area 2, and thus contained ca. 1 mM of both nitrate and sulfate as competing electron acceptors. The concentrations of numerous aqueous and solid-phase species were followed over time during a ca. 50-day incubation period.

A classical pattern of electron acceptor consumption over time was observed, with nitrate being consumed first (day 0-4), followed by reduction (without a lag) of Fe(III) (day 4-9) and

sulfate (day 9-12) (see Fig. 1 in Attachment #1). Methane production ensued after a ca. 1 week lag period. The results indicated that ethanol was oxidized directly to CO_2 during the period of nitrate reduction, whereas ethanol appeared to be partially oxidized to acetate during the Fe(III) and sulfate reduction phases, as evidenced by the accumulation of significant quantities of acetate. The acetate was converted to CH_4 and CO_2 during the methanogenic phase of the experiment. A very gradual reduction of nitrate was observed in non-ethanol-amended slurries, indicating the presence of only small quantities of endogenous labile organic matter in the saprolite sediment. U(VI) reduction took place mainly during the period of Fe(III) reduction; only minor changes in the relative abundance U(VI) were observed during the ensuing sulfate-reducing and methanogenic phases. No U(VI) reduction was observed in the non-ethanol-amended slurries. Only ca. 60% of the U(VI) content of the sediment was reduced in the ethanol-amended slurries.

Reverse transcribed 16S rRNA clone libraries and measurements of phospholipid fatty acids (PLFA) abundance and the incorporation of ^{13}C-ethanol into PLFAs were used to characterize the microbial community response to ethanol amendment. The 16S rRNA libraries revealed major increases in the abundance of organisms related to *Dechloromonas*, *Geobacter*, and *Oxalobacter* (see Table 1 in Attachment #1). PLFAs indicative of *Geobacter* showed a distinct increase in the amended slurries, and analysis of PLFA $^{13}C/^{12}C$ ratios confirmed the incorporation of ethanol into signature PLFAs of *Geobacter* (see Fig. 3 in Attachment #1). Although no significant increase in the abundance of PLFAs indicative of sulfate-reducing bacteria (SRB) was observed, a distinct increase in the abundance of ^{13}C-labeled PLFAs indicative of *Desulfobacter*, *Desulfotomaculum*, and *Desulfovibrio* was observed during the brief period of sulfate reduction which followed the Fe(III) reduction phase.

A follow-up experiment was conducted with subsamples of the reduced slurries to assess possible metabolic (as opposed to geochemical) reasons for incomplete U(VI) reduction observed in the ethanol-amended slurries. The PLFA and 16S rRNA clone library data (see above) suggested that DIRB and SRB were present in the slurries during the latter stages of the incubation, and we speculated that depletion of their preferred electron acceptors may have limited their ability to reduce U(VI) reduction in the slurries. Duplicate slurry subsamples were amended with nothing (control), 5 mM ethanol, 5 mM ethanol + 10 mmol L^{-1} of synthetic amorphous Fe(III) oxide, 5 mM ethanol + 2 mM SO_4^{2-}, or 5 mM ethanol + 0.1 mM AQDS. Addition of Fe(III) oxide and sulfate were designed to stimulate DIRB and SRB activities. AQDS is a soluble electron shuttling compound that accelerates rates of microbial Fe(III) oxide reduction in sediments, and that may stimulate solid-associated U(VI) reduction by reacting with U(VI) associated with sediment surfaces that are inaccessible to direct microbial reduction (Jeon et al., 2004). None of the treatments stimulated significant additional U(VI) reduction (see Figure 6 in Attachment #1), despite the presence of active microbial metabolism as indicated by additional Fe(II) accumulation, sulfate consumption, and CH_4 production. AQDS stimulated reduction of residual Fe(III) phases in the sediment, but in contrast to previous studies (Jeon et al., 2004) did not promote solid-associated U(VI) reduction. These results, together with the study of Fe(III) and U(VI) reduction in Area 2 sediment by *G. sulfurreducens* (Fig. 11), indicate that the main limitation posed on residual U(VI) reduction was geochemical rather than microbiological in nature. Other ERSP-sponsored studies have documented incomplete reduction of solid-associated U(VI) in reduced subsurface sediments that contain excess electron

donor and abundant Fe(II) (a potential chemical reductant for U(VI)) (Jeon et al., 2004; Ortiz-Bernad et al., 2004; Wan et al., 2005). While the basis for this phenomenon remains unclear, it likely related to the poor availability of U(VI)-occupied surface sites to enzymatic reduction (Jeon et al., 2004; Ortiz-Bernad et al., 2004), and/or the nature of U(VI) coordination at the solid-water interface (Jeon et al., 2005). The persistence of substantial solid-associated U(VI) during active Fe(III) reduction provides an explanation for the increase in dissolved U(VI) that took place later on during the methanogenic phase of the slurry experiment (see Fig. 1F in Attachment #1): complexation of residual U(VI) by DIC (> 10 mM) produced during methanogenic oxidation of acetate could have easily shifted the balance between aqueous and surface-associated U(VI) (Barnett et al., 2002).

There are two key practical implications of the sediment slurry experiment. First, the results suggest that standard thermodynamics-based conceptual models of TEAPs in sediment should be valid for predicting the response of ORNL FRC Area 2 (and other) subsurface sediments to in situ ethanol amendment, i.e. in terms of the segregation of major TEAPs over space and time. A sequence of TEAPs analogous to that observed in the slurry incubation (up to the point of sulfate reduction) was in fact documented the in situ ethanol biostimulation experiment conducted at the Area 2 research site (see Fig. 13 below). The conformation of the data to thermodynamic theory provides a sound basis for development of microbial physiology-based kinetic models which can reproduce the zonation of TEAPs typically observed over space and/or time in sediment systems (cf. Watson et al. (2003), Wirtz (2003), Thullner et al. (2005), Roden (2008)). In addition, the detection by rRNA and PLFA methods of functional groups of microorganisms known to be associated with major TEAPs (see above) provides confirmation that such groups were in fact activated during ethanol biostimulation.

A second key implication of the slurry experiment is that the redox behavior of uranium, unlike other major redox couples, could not be explained on the basis of standard thermodynamic considerations. The seemingly irreversible association of U(VI) with particle surfaces that are inaccessible to enzymatic (and abiotic) reduction observed here and in other subsurface sediments cannot be rationalized in terms of existing models of aqueous/solid-phase U speciation (Langmuir, 1997). This phenomenon is of practical significance in that it may limit the overall effectiveness of in situ remediation of highly-contaminated U(VI) source zones such as those present at ORNL. Our results highlight the need for studies on the physiochemical nature of the non-reducible U(VI) species.

D. Investigation of gravel layer biogeochemistry

A simple sediment slurry experiment, analogous in general design to that described above, was conducted to address the unusual biogeochemistry of the gravel layer at Area 2. Visual examination of sediment cores suggested that Fe in the gravel materials was reduced, as indicated by their dark grey color in contrast to the yellow-orange color of the Fe(III) oxide-rich fill and saprolite sediments (Fig. 2). The gravel sediments were in fact enriched in solid-associated Fe(II) (Figs. 3D and 5D) and depleted in total Fe(III) oxide content (Figs. 3F and 5F). These observations proved to be problematic for development of the field-scale reactive transport model for Area 2 (discussed below), because both thermodynamic and kinetics-based models of redox speciation argued against the co-existence of high concentrations of solid-associated Fe(II)

in aquifers containing 1 mM nitrate. In order to proceed with the field-scale modeling, the initial Fe(II) content of the gravel layer had to be set equal to zero in order to prevent immediate rapid consumption of nitrate at the start of the simulation (before biostimulation began). An experiment was conducted with the fine-grain (< 106 μm) fraction of pooled material from 4-5 m depth in order to gain insight into what is actually happening within the gravel layer in terms of redox metabolism. Triplicate 25 g portions of material were suspended in 100 mL of Pipes-buffered Area 2 artificial groundwater (see Attachment #1) and incubated under anaerobic conditions. Nitrate (2 mM final concentration) was added to the slurries every few days to mimic the input of nitrate from upstream groundwater input. We were particularly interested to determine whether addition of nitrate would trigger oxidation of solid-associated Fe(II). To our great surprise, all of the nitrate added during the first 20 days of incubation was rapidly consumed, and at the same time a large increase in Fe(II) and dissolved acetate was observed (Fig. 12). Addition of 14 mM nitrate (seven 2 mM addition) was required to trigger oxidation of sediment Fe(II) compounds. These results suggest that the gravel materials are being supplied with some form of organic carbon which is capable of preventing incoming nitrate from reacting with solid-phase Fe(II) compounds. If this is true, then the concentration of nitrate in Area 2 groundwaters is the result of a dynamic balance between nitrate input and enzymatic consumption within the gravel layer. A long-term semicontinuous culture experiment with Area 2 gravel materials will be initiated in the near future through other ERSP-funded research (Burgos et al. and Chandler/Roden 2004 NABIR projects) in order to compare in detail the redox metabolism of the gravel material with and without ethanol input.

5. Groundwater microbial community analyses

A. Groundwater chemistry during in situ biostimulation (data courtesy of S. Brooks, ORNL)

In situ delivery of ethanol to wells FW212, FW213, and FW214 (red circles in Fig. 1) commenced in September 2005. To jump-start microbial activity, and for the purposes of evaluating field-scale mass transfer rates, a 24-hr long injection pulse was used to initiate the ethanol (10 mM) delivery. After the first 24 hr, a pulsed injection strategy was used, consisting of a 1-hr delivery every 24 hrs. Figure 13 shows concentrations of redox-sensitive components in groundwater at multi-level sampler B (MLS-B) during the biostimulation experiment. This sampling well consistently received input of ethanol and provides a representative picture of the impact of biostimulation on groundwater chemistry. The plot shows an initial sharp drop in uranium and sulfate concentrations corresponding to flushing during the initial 24-hr pulse injection. This period was followed by recovery to initial concentrations for the first ca. 200 hrs. Nitrate decreased to near zero within the first few days of the injection. Subsequently, dissolved iron concentrations rose sharply indicating the onset of Fe(III) reduction (manganese reduction is also evident, perhaps slightly earlier than iron reduction). Shortly thereafter, sulfate concentrations began to decline indicating that sulfate reduction became active, and uranium concentrations fell to about 1/3 of the initial concentration after 1200 hrs. The onset of sulfate reduction was not coincident with iron and manganese reduction, but took place later, and uranium reduction was coincident with sulfate reduction but not iron and manganese reduction.

B. Molecular microbial community analysis

A total of over 300 groundwater samples were collected for possible microbial community analysis during the in situ biostimulation experiment. The filters have been archived at -80 °C (at ORNL) since the time of collection. A subset of these filters was analyzed via a standard nonculture-based molecular technique, Denaturing Gradient Gel Electrophoresis (DGGE) of PCR-analyzed 16S rRNA gene fragments (Muyzer et al., 1993), in order to assess the impact of ethanol biostimulation on groundwater microbial community composition in well MLS-B. All analyses were performed by Microbial Insights (Rockford, TN). DNA was extracted from groundwater filters using PowerSoil (MoBio Laboratories) extraction kits. Eubacterial 16S rDNA was amplified using primers 341FGC (GC-clamped oligonucleotide) and 519R as described in Muyzer (1993) with minor modifications. This amplicons were subjected to DGGE using a Biorad D-code gel system maintained at a constant temperature of 60ºC in 0.5X TAE buffer (20mM Tris-acetate, 0.5mM EDTA, pH 8.0). Gradients were formed using 8-10% acrylamide and 30-65% denaturant (100% denaturant is defined as 7M urea, formamide) and the gels were run at 55 V for 16 h. Gels were stained in 0.5X TAE containing 0.5 mg/l of ethidium bromide. Images were captured with an Alpha Imager™ system. Dominant bands were excised, eluted in 50 µL of nanopure water and placed at -20ºC for 1 hr to overnight. The DNA from the bands was then and re-amplified using the same primers and conditions listed above. An Ultra Clean PCR Clean-up DNA Purification Kit (MoBio Laboratories) was used following the manufactures directions. Using 341F as the primer, products were then sequenced by the University of Tennessee, Knoxville, Molecular Biology Resource Facility. Chromatogram files that were received from the sequencing facility were then aligned to known DNA sequences using the Ribosomal Database Project (Cole et al., 2003). Any base pair mismatches are verified with the original chromatogram or changed based upon that chromatogram. The corrected sequence was then submitted to the same database and the top ten matches were received.

The DGGE analyses indicated that biostimulation was accompanied by an increase in the abundance (as indicated by the presence and density of bands on the DGGE gels) of known nitrate-, metal- and sulfate-reducing organisms (e.g. *Dechloromonas*, *Geobacter*, *Aquaspirillum*, *Desulfobacter*, *Desulfovibrio*), as well as other anaerobic organisms such as *Hydrogenomonas* (Figs. 14 and 15). After about 1200 hrs there was a rebound in uranium and sulfate concentrations and a drop in dissolved iron and manganese, suggesting that the rate of biological metal reduction diminished despite continued delivery of ethanol to the groundwater system. The groundwater microbial community analyses indicated a general decline in the abundance of anaerobic respiratory during the period of U(VI) and sulfate rebound (Fig. 15).

C. Additional planned groundwater microbial community analyses

We plan to conduct two additional types of analyses on an expanded selection of the archived groundwater microbiota samples. First, approximately 110 filters will be analyzed for bulk PLFA content in the laboratory of Dr. Robert Findlay at The University of Alabama. Findlay, an acknowledged expert in PLFA analysis (Findlay, 2004), is a colleague of Roden and has agreed to analyze our samples at near cost. These measurements will be useful for constraining total microbial biomass in the groundwater, as well as assessing variations in the

abundance of different major classes of microorganisms throughout the duration of the in situ experiment (see Fig. 13 for an indication of the time points that will analyzed). It is important to note here that samples will be analyzed both from wells on the southeast side of the treatment zone (see Fig. 1) that showed evidence of sustained ethanol input and uranium removal (FW212, MLS-B, MLS-D, and FW216), and from wells on the northwest side (MLS-A, MLS-C) that (for reasons apparently related to variations in the hydrological flow regime) did not receive sufficient ethanol input to trigger major removal of uranium from solution.

An additional nucleic acid-based method for interrogation of microbial community structure will applied to the same groundwater samples analyzed for PLFA content in collaboration with Dr. Darrell Chandler at Akonni Biosystems (formerly at Argonne National Laboratory). As part of ongoing ERSP research and development (Chandler, PI/PD, Roden, Co-PI), Chandler and colleagues developed a metal-, sulfate-, and nitrate-reducer 16S rRNA targeted, microbead-based microarray system, and applied it a number of sediment and groundwater samples from the Old Rifle site in Colorado (Chandler et al., 2006). The methodologies developed provide a basic framework for coupled microarray-based microbial community measurements with predictive models of contaminant fate and transport. Since the time this work was completed, Chandler moved from Argonne to Akonni, where he is developing a new, user-friendly microfluid cartridge and instrument to deploy gel element microarrays (Guschin et al., 1997) for analysis of groundwater microbial communities. The original rRNA microbead array has been translated to a gel element format, expanded to include additional DOE-relevant organisms, and modified to include fluidic sub-circuits for semi-automated rRNA analysis. With minor additional modifications, the new gel element array will be suitable for analysis of 16S rDNA, and this system will be employed to analyze PCR-amplified 16S rRNA genes from a selection of the Area 2 groundwater samples to be analyzed for PLFA content. Comparison of these two independent sets of data should provide direct insight into the linkages between ethanol input, microbial community development, and groundwater geochemistry (including uranium removal).

6. Biogeochemical reaction model development

Development of conceptual and numerical models of biogeochemical processes in biostimulated sediments was an important individual research focus for co-PI Roden. The primary product of this work is a reaction-based model (coded in Fortran 95) called TEAPREVU, which stands for Terminal Electron Accepting Processes in a hypothetical Representative Elementary Volume of Uranium contaminated subsurface sediment. The model was developed to simulate the results of the batch slurry experiment with FRC Area 2 sediment, with the idea that the developed framework would eventually be incorporated into a field-scale reactive transport simulation of in situ biostimulation at Area 2. This work was co-funded by the Burgos et al. NABIR Integrative Studies Element project ("Reaction-Based Reactive Transport Modeling of Iron Reduction and Uranium Immobilization at Area 2 of the NABIR Field Research Center"). A detailed description of the design and implementation of the model for simulation of redox processes in sediments is available on the ORNL FRC web-site (http://public.ornl.gov/nabirfrc/frcdoc12.cfm), and a copy of this description is included as Attachment #2 to this report. The model envisions flow of ethanol-containing fluid through a single reactor cell (the fluid flow rate is set equal to zero to model the batch slurry experiment).

The incoming fluid contains soluble electron acceptors (O_2, NO_3^-, U(VI), SO_4^{2-}) whose abundance, together with the abundance of solid-phase electron acceptors (MnO_2, FeOOH, S^0) in the sediment, control the relative rates of various terminal electron accepting processes (TEAP) and other biogeochemical reactions over time in the reactor. The model accounts for complete (to HCO_3^-) or incomplete (to acetate) oxidation of ethanol, as well as oxidation of acetate to HCO_3^- and/or CH_4, via 18 different TEAP pathways (see Fig. 1 in Attachment #2). Each of the TEAP reactions are dependent on the biomass of one or more distinct microbial populations (8 total) chosen based on current knowledge of the kinds of organisms likely to proliferate in response to biostimulation of subsurface sediments. Growth of these populations is described using the bioenergetics-based approach developed by Rittman and McCarty (2001) for simulation of wastewater (i.e. sewage) treatment, in which the partitioning of organic carbon flow between energy generation and cell biomass production (see Fig. 2 in Attachment #2) is dependent on the free energy of the corresponding TEAP, which is computed dynamically during the simulation as a function of the abundance (concentration and/or activity) of the reactants and products involved in the process. This approach alleviates the need for making a priori assumptions about the biomass yield for the different physiological functional populations. Kinetic constants for uptake of electron donors, electron acceptors, and inorganic nitrogen compounds, as well for the inhibition of specific RTEAPs (37 total) by the presence of more favorable electron acceptors, were either chosen arbitrarily or constrained by the physiological properties of pure culture representatives and/or by values required to reproduce the results of the batch slurry experiment. Each of the RTEAPs results in production of various inorganic compounds, which either accumulate in solution or undergo reactions (sorption and/or mineral precipitation) with the solid-phase. The model also accounts for a wide variety of secondary redox reactions (sensu Van Cappellen and Wang (1996)) that may potentially occur in sedimentary environments (e.g. oxidation of reduced species such as Mn(II), Fe(II), U(IV), S(-II), S^0, and CH_4 by aqueous or solid-phase electron acceptors such as O_2, NO_3^-, MnO_2, and FeOOH; see Table 4 in Attachment #2 for a complete list of reactions), as well as for precipitation/dissolution of mineral phases that may be associated with microbial activity in sediments. In this way the model is capable of simulating time-dependent changes in the abundance of various oxidized and reduced species and mineral phases as a function of the input of external electron acceptors/donors and other aqueous species. This capacity is critical for field-scale simulation of biogeochemical processes in subsurface sediments (Hunter et al., 1998).

The central goal in simulating the Area 2 sediment slurry experiment was to reproduce the basic patterns of organic substrate metabolism, consumption of electron acceptors, and accumulation of reduced end-products of anaerobic respiration. In general the optimized model reproduced these patterns rather well (solid lines in Fig. 3 of Attachment #2). Although the timing and magnitude of the predicted accumulation of acetate resulting from partial oxidation of ethanol (and the subsequent utilization of acetate) did not exactly match the experiment results, the general agreement between the simulation and the data suggests that the developed reaction network provides a reasonable explanation for this pattern of substrate metabolism. The strategy for simulating the interaction between the different TEAPs also seems generally valid, given the close resemblance of the predicted and observed patterns of electron acceptor (NO_3^-, Fe(III), SO_4^{2-}) consumption and reduced end-product accumulation (Fe(II) and CH_4; note that the abundance of reduced sulfur compounds (e.g. HS^-, FeS) was not determined). However, the predicted aqueous/solid speciation of uranium did not match the experimental data. A significant

fraction (ca. 50%) of solid-associated U(VI) failed to desorb during biostimulation and therefore (as discussed above) remained unreduced at the end of the incubation. Understanding the controls on reduction of solid-associated U(VI) (both biotic and abiotic) and development of strategies for accurately simulating the fate of uranium in biostimulated FRC Area 2 sediments is a key goal of the current Burgos et al. NABIR project.

A slightly modified version of TEAPREVU was incorporated (by Yilin Fang at PNNL) into a general biogeochemical reaction simulation framework (Fang et al., 2003; Fang et al., 2005), which in turn was linked with a three-dimensional field-scale reactive transport model (HYDROGEOCHEM) (Yeh et al., 2004) of the Area 2 experimental site. The model was used to help design the in situ ethanol biostimulation experiment described above. The model incorporates variable hydraulic conductivity, porosity, dispersivity, and sediment geochemistry parameters for each of the three major strata (intact saprolite, gravel, and saprolite fill). The Fe and U analyses shown in Figs. 3-5 were used to establish the initial solid-phase geochemical conditions. Model parameters (including enhanced vertical dispersivity representing diffusive/dispersive mass transfer between the gravel layer and saprolite materials above and below) were estimated based on field hydraulic and tracer tests. The model successfully to simulated the early-time aquifer response to ethanol amendment (data not shown). Although the match between model predictions and observations varied across sampling points, in general the relationship was remarkably good given that no parameter fitting was performed based on field observations.

Recently, a collaboration was initiated with Dr. Qusheng Jin at the University of Oregon, as a result of Jin's desire to create a model of our Area 2 slurry experiment en route to development of a field-scale reactive transport simulation of the results of biostimulation push-pull tests with ethanol at Area 2 (Jin et al., 2007b). The latter experiments were conducted by Dr. Chen Zu at Indiana University with input from Jack Istok at Oregon State University, who has conducted extensive in situ push-pull experimentation at the ORNL FRC (Istok et al., 2004). Jin's model was implemented in the geochemical modeling software package Geochemist's Work Bench (GWB) (Bethke, 2002), which has been used previously to simulate microbial redox metabolism in both experimental systems and natural sedimentary environments (Jin and Bethke, 2003, 2005; Jin, 2007). The general structure of the model is similar to that of TEAPREVU in that (i) a predetermined set of microbial functional groups is assumed to catalyze the various catabolic reactions; (ii) thermodynamic calculations are used to compute growth yields and to constrain the favorability of various reaction pathways. A key aspect of the new model is that, unlike TEAPREVU, the production and consumption of molecular hydrogen (H_2) is included within the reaction network. Although H_2 concentrations were not measured in the slurry incubation or the in situ biostimulation experiment, such measurements are frequently made during laboratory and field-scale biostimulation experiments, and have been conducted in ongoing ERSP-funded semicontinuous culture experiments with Area 2 sediments. A diagram of the reaction paths and microbial functional groups in Jin's model is provided in Fig. 16, and lists of the primary dependent variables and reaction path equations are provided in Tables 3 and 4. We have a manuscript in preparation on this model (Jin et al., 2007a), and detailed discussion of its structure and function is beyond the scope of this report. The important point is that the model accurately reproduced all of the results of the slurry experiment, including the kinetics of ethanol consumption and transient acetate accumulation (Fig. 17), as a function of the biomass

(Fig. 18A-C) and metabolism (Fig. 18D-F) of various functional metabolic groups These results clearly illustrate how physiologically-based reaction models can capture the basic patterns of redox metabolism that are typically observed in sedimentary environments. We plan to transfer the structure of the new model to Yilin Fang at PNNL so that it can incorporated (in place of the microbial physiology components of TEAPREVU) into the field-scale reactive transport for Area 2 and used to simulate the overall results of the in situ biostimulation experiment.

7. Research Products

A. Referred publications

Roden, E. E., and T. D. Scheibe. 2005. Conceptual and numerical model of uranium(VI) reductive immobilization in fractured subsurface sediments. *Chemosphere* 59:617-628.

Scheibe, T. D., Y. Fang, C. J. Murray, E. E. Roden, J. Chen, Y.-J. Chien, S. C. Brooks, and S. S. Hubbard. 2006. Transport and biogeochemical reaction of metals in a physically and chemically heterogeneous aquifer. *Geosphere* 2:220-235, 2006.

B. Submitted manuscripts

Mohanty, S., B. Kollah, D. Hedrick, A. Peacock, R. K. Kukkadapu, and E. E. Roden. 2007. Biogeochemical processes and microbial community structure in ethanol-stimulated subsurface sediments. *Environ. Sci. Technol.* Submitted for publication.

C. Manuscripts in preparation

Brooks, S. C., E. E. Roden, S. R. Mohanty, W. Kamolpornwijit, D. Watson, and T. D. Scheibe. 2007. Field-scale biostimulation of uranium(VI) reduction in heterogeneous subsurface sediments. Manuscript in prep.

Jin, Q., S. R. Mohanty, and E. E. Roden. 2007. A physiologically-based microbial reaction model for ethanol-amended uranium-contaminated subsurface sediments. Manuscript in prep.

Mohanty, S. R., E. L. Brodie, B. Kollah, T. C. Hazen, and E. Roden. 2007. Comparative analysis of microbial communities in ethanol-amended subsurface sediment by 16S rRNA clone libraries and a high density phylogenetic DNA microarray. Manuscript in prep.

D. Unpublished reports

Roden, E. E., Y. Fang, T. D. Scheibe, S. C. Brooks, and W. D. Burgos. 2005. TEAPREVU: A numerical simulation model of Terminal Electron-Accepting Processes in a Representative Elementary Volume of Uranium-contaminated subsurface sediment. Available at: http://public.ornl.gov/nabirfrc/frcdoc12.cfm.

E. Presentations at national/international scientific conferences

Roden, E.E. and T.D. Scheibe, Multiple pore region model of uranium(VI) reductive immobilization in structured subsurface media" *Eos Trans. AGU, 83*(47), Fall Meet. Suppl., Abstract B12C-12, 2002.

Scheibe, T. D., Y. Fang, E. E. Roden, S. C. Brooks, Y. Chien, and C. J. Murray, "Microbial Reduction of Fe(III) and U(VI) in Aquifers: Simulations Exploring Coupled Effects of Heterogeneity and Fe(II) Sorption", *EOS Trans. AGU*, 85(17), Jt. Assem. Suppl., Abstract H24A-05, 2004.

Kim, Y., W. Kamolpornwijit, S. C. Brooks, T. D. Scheibe, and E. E. Roden, "Rate and extent of uranium(VI) sorption onto weathered saprolite", *EOS Trans. AGU*, 85(17), Jt. Assem. Suppl., Abstract H41E-03, 2004.

Scheibe, T. D., Y. Fang, E. Roden, S. C. Brooks, S. S. Hubbard, J. Chen, Y.-J. Chien, C. J. Murray, and Y. Xie, "Transport and biogeochemical reaction of metals in a physically and chemically heterogeneous aquifer," Geological Society of America Abstracts with Programs, 36(5):325, Nov. 2004.

Scheibe, T. D., S. C. Brooks and E. E. Roden, "Numerical Simulation of Field-Scale Transport and Biogeochemical Reactions Using a Particle-Based Method," *EOS Trans. AGU*, 85(47), Fall Meet. Suppl., Abstract H21E-1068, 2004.

Mohanty, S., B. Kollah, and E. Roden, "Biogeochemical processes in ethanol-stimulated subsurface sediments", Abstract Q-396, American Society for Microbiology General Meeting, 2005.

Roden, E., Mohanty, S., B. Kollah, T. Scheibe, Y. Fang, and S. Brooks, "Numerical simulation of terminal electron-accepting processes in ethanol-stimulated subsurface sediments", Abstract Q-394, American Society for Microbiology General Meeting, 2005.

Scheibe, T. D.,S. C. Brooks, W. Kamopornwijit, Y. Fang, and E. E. Roden, "Identification of Physical and Chemical Mass Transfer Processes by a Tracer Flush Experiment", *EOS Trans. AGU*, 86(18), Jt. Assem. Suppl., Abstract H51A-02, 2005.

Kim, Y., S. C. Brooks, W. Kamopornwijit, T. D. Scheibe, and E. E. Roden, "Immobilization of uranium (VI) in structured saprolite with microbial U(VI) reduction", *EOS Trans. AGU*, 86(18), Jt. Assem. Suppl., Abstract H51A-06, 2005.

Scheibe, T. D., S. C. Brooks, E. E. Roden, Y. Fang, and W. Kamopornwijit, "In Situ Bioremediation of Uranium in a Heterogeneous Aquifer: Field-Scale Monitoring and Numerical Simulation", EOS Trans. AGU, 87(36), Jt. Assem. Suppl., Abstract H42B-03, 2005.

Scheibe T. D., Y. Fang, E. E. Roden, S. C. Brooks, and A. M. Tartakovsky. 2005. "Simulation of metal biogeochemistry in multiple-porosity groundwater flow systems", Presented by Timothy D. Scheibe (Invited Speaker) at Joint International Symposia for Subsurface Microbiology (ISSM 2005) and Environmental Biogeochemistry (ISEB XVII), 2005.

Roden, E. E., "TEAPREV: A numerical tool for assessing rates of terminal electron-accepting processes in a representative elementary volume of subsurface sediment," Geological Society of America *Abstracts with Programs*, 37(7): 535, 2005.

Fang, Y., T. D. Scheibe, E. E. Roden, and S. C. Brooks, "Field-scale reactive transport simulations of multiple terminal electron accepting processes," Geological Society of America *Abstracts with Programs*, 37(7): 535, 2005.

Mohanty, S., B. Kollah, and E. Roden, "Microbial Community Dynamics in Ethanol-Stimulated Subsurface Sediments", Abstract Q-160, American Society for Microbiology General Meeting, 2006.

Fang, Y., T. Scheibe, E. Roden, W. Kamolpornwijit, and S. Brooks,"3D field-scale reactive transport modeling of in situ immobilization of uranium in structured porous media via biostimulation," in *Proceedings of the XVI International Conference on Computational Methods in Water Resources*, P.J. Binning, P.K. Engesgaard, H.K. Dahle, G.F. Pinder and W.G. Gray (Eds), Copenhagen, Denmark, 2006.

Mohanty, S. R., E. L. Brodie, B. Kollah, T. C. Hazen, and E. Roden. 2007. "Comparative analysis of microbial communities in ethanol-amended subsurface sediment by 16S rRNA clone libraries and a high density phylogenetic DNA microarray", Abstract Q-182, American Society for Microbiology General Meeting, 2006.

F. Workshop Presentations (Roden group only)

Roden, E.E., S.R. Mohanty, and B. Kollah, "Biogeochemical Processes in Ethanol-Amended FRC Area 2 Sediments", U.S. Department of Energy, Natural and Enhanced Bioremediation Program ORNL Field Research Center Meeting, 2004. (Poster presentation)

Roden, E.E., "Knowledge gaps in field-scale bioremediation", U.S. Department of Energy, Natural and Enhanced Bioremediation Program Annual PI Meeting, 2005. (Oral presentation)

Roden, E.E., "TEAPREV: A numerical simulation model of Terminal Electron-Accepting Processes in a Representative Elementary Volume of subsurface sediment", U.S. Department of Energy, Natural and Enhanced Bioremediation Program ORNL Field Research Center Meeting, 2005. (Poster presentation)

Mohanty, S.R., B. Kollah, E.E. Roden, "Biogeochemical Processes and Microbial Community Structure in Ethanol-Amended FRC Area 2 Sediments", U.S. Department of Energy,

Natural and Enhanced Bioremediation Program ORNL Field Research Center Meeting, 2005. (Oral presentation)

Mohanty, S.R., B. Kollah, E.E. Roden, "Biogeochemical Processes and Microbial Community Structure in Ethanol-Amended FRC Area 2 Sediments", U.S. Department of Energy, Natural and Enhanced Bioremediation Program ORNL Field Research Center Meeting, 2005. (Poster presentation)

Mohanty, S.R., B. Kollah, E.E. Roden, "Biogeochemical Processes and Microbial Community Structure in Ethanol-Amended FRC Area 2 Sediments", U.S. Department of Energy, Natural and Enhanced Bioremediation Program ORNL Field Research Center Meeting, 2005. (Poster presentation)

8. References cited

Altschul, S. F., T. L. Madden, A. A. Schaffer, J. H. Zhang, Z. Zhang, W. Miller, and D. J. Lipman. 1997. Gapped BLAST and PSI-BLAST: a new generation of protein database search programs. Nucleic Acids Res. 25:3389-3402.

Barnett, M. O., P. M. Jardine, and S. C. Brooks. 2002. U(VI) adsorption to heterogeneous subsurface media: application of a surface complexation model. Environ. Sci. Technol. 36:937-942.

Bethke, C. M. 2002. Geochemist's Work Bench, Release 4.0. University of Ilinois,

Caccavo, F., R. P. Blakemore, and D. R. Lovley. 1992. A hydrogen-oxidizing, Fe(III)-reducing microorganism from the Great Bay estuary, New Hampshire. Appl. Environ. Microbiol. 58:3211-3216.

Chandler, D. P., A. E. Jarrell, E. E. Roden, A. D. Peacock, and P. E. Long. 2006. Suspension array analysis of 16S rRNA from Fe- and SO_4^{2-}-reducing bacteria in uranium contaminated sediments undergoing bioremediation. Appl. Environ. Microbiol. 72.

Cole, J. R., B. Chai, T. L. Marsh, R. J. Farris, Q. Wang, S. A. Kulam et al. 2003. The Ribosomal Database Project (RDP-II): previewing a new autoaligner that allows regular updates and the new prokaryotic taxonomy. Nucleic Acids Res. 31:442-443.

Fang, Y., G. T. Yeh, and W. D. Burgos. 2003. A general paradigm to model reaction-based biogeochemical processes in batch systems. Wat. Resour. Res. 39:1083-1108.

Fang, Y., T. D. Scheibe, E. E. Roden, and S. C. Brooks. 2005. Field-scale reactive transport simulations of multiple terminal electron accepting processes. Abstract submitted to the Annual Meeting and Exposition of the Geological Society of America, Salt Lake City, UT, October 2005.

Findlay, R. H. 2004. Determination of microbial community structure using phosopholipid fatty acid profiles. In G. A. Kowalchuk, F. J. de Bruijn, I. M. Head, A. D. Akkermans, and J. D. van Elsas (eds.). Molecular Microbial Ecology Manual, 2nd Edition, pp. 983-1004. Springer, New York.

Guschin, D. Y., B. K. Mobarry, D. Proudnikov, D. A. Stahl, B. E. Rittmann, and A. D. Mirzabekov. 1997. Oligonucleotide microchips as genosensors for determinative and environmental studies in microbiology. Appl. Environ. Microbiol. 63:2397-2402.

Gwo, J. P., P. M. Jardine, G. V. Wilson, and G. T. Yeh. 1995. A multiple-pore-region concept to modeling mass transfer in subsurface media. J. Hydrol. 164:217-237.

Hungate, R. E. 1969. A roll tube method for cultivation of strict anaerobes. Methods Microbiol. 3B:117-132.

Hunter, K. S., Y. Wang, and P. VanCappellen. 1998. Kinetic modeling of microbially-driven redox chemistry of subsurface environments: coupling transport, microbial metabolism and geochemistry. J. Hydrol. 209:53-80.

Istok, J. D., J. M. Senko, L. R. Krumholz, D. Watson, M. A. Bogle, A. Peacock et al. 2004. In situ bioreduction of technicium and uranium in a nitrate-contaminated aquifer. Environ. Sci. Technol. 28:468-475.

Jeon, B. H., M. O. Barnett, W. D. Burgos, B. A. Dempsey, and E. E. Roden. 2005. Chemical reduction of U(VI) by Fe(II) at the solid-water interface using synthetic and natural iron(III) oxides. Environ. Sci. Technol. 39:5642-5649.

Jeon, B. H., S. D. Kelly, K. M. Kemner, M. O. Barnett, W. D. Burgos, B. A. Dempsey, and E. E. Roden. 2004. Microbial reduction of U(VI) at the solid-water interface. Environ. Sci. Technol. 38:5649-5655.

Jin, Q. 2007. Control of hydrogen partial pressures on the rates of syntrophic microbial metabolisms: a kinetic model for butyrate fermentation. Geobiology 5:35-48.

Jin, Q., and C. M. Bethke. 2003. A new rate law describing microbial respiration. Appl. Environ. Microbiol. 69:2340-2348.

Jin, Q., and C. M. Bethke. 2005. Predicting the rate of microbial respiration in geochemical environments. Geochim. Cosmochim. Acta 69:1133-1143.

Jin, Q., S. R. Mohanty, and E. E. Roden. 2007a. A physiologically-based microbial reaction model for ethanol-amended uranium-contaminated subsurface sediments. Manuscript in prep.

Jin, Q., C. Zu, and Z. Zhen. 2007b. Geomicrobial reaction modeling approach to in situ microbial kinetics in a contaminated aquifer at Oak Ridge, Tennessee, USA. Groundwater Submitted for publication.

Langmuir, D. 1997. Aqueous Environmental Geochemistry. Prentice Hall, Upper Saddle River, NJ.

Lovley, D. R., and E. J. P. Phillips. 1986. Availability of ferric iron for microbial reduction in bottom sediments of the freshwater tidal Potomac River. Appl. Environ. Microbiol. 52:751-757.

Lovley, D. R., E. E. Roden, E. J. P. Phillips, and J. C. Woodward. 1993. Enzymatic iron and uranium reduction by sulfate-reducing bacteria. Mar. Geol. 113:41-53.

Lovley, D. R., J. D. Coates, E. L. Blunt-Harris, E. J. P. Phillips, and J. C. Woodward. 1996. Humic substances as electron acceptors for microbial respiration. Nature 382:445-448.

Methe, B. A. 2003. Genome of *Geobacter sulfurreducens*: metal reduction in subsurface environments. Science 302:1967-1969.

Mohanty, S., B. Kollah, D. Hedrick, A. Peacock, R. K. Kukkadapu, and E. E. Roden. 2007. Biogeochemical processes and microbial community structure in ethanol-stimulated subsurface sediments. Environ. Sci. Technol. Submitted for publication.

Muyzer, G., E. C. Dewaal, and A. G. Uitterlinden. 1993. Profiling of complex microbial populations by denaturing gradient gel electrophoresis analysis of polymerase chain reaction-amplified genes coding for 16S rRNA. Appl. Environ. Microbiol. 59:695-700.

Ortiz-Bernad, I., R. T. Anderson, H. A. Vrionis, and D. R. Lovley. 2004. Resistance of solid-phase U(VI) to microbial reduction during in situ bioremediation of uranium-contaminated groundwater. Appl. Environ. Microbiol. 70:7558-7560.

Phillips, E. J. P., E. R. Landa, and D. R. Lovley. 1995. Remediation of uranium contaminated soils with bicarbonate extraction and microbial U(VI) reduction. J Ind Microbiol 14:203-207.

Poulton, S. W., and D. E. Canfield. 2005. Development of a sequential extraction procedure for iron: implications for iron partitioning in continentally derived particulates. Chem. Geol. 214:209-221.

Rittmann, B. E., and P. L. McCarty. 2001. Environmental Biotechnology. McGraw-Hill, Boston.

Roden, E. E. 2008. Microbiological controls on geochemical processes 1: Fundamentals and case study on microbial Fe(III) reduction. Kinetics of Water-Rock Interactions. Springer, New York.

Thullner, M., P. Van Cappellen, and P. Regnier. 2005. Modeling the impact of microbial activity on redox dynamics in porous media. Geochim. Cosmochim. Acta 69:5005-5019.

VanCappellen, P., and Y. Wang. 1996. Cycling of iron and manganese in surface sediments: a general theory for the coupled transport and reaction of carbon, oxygen, nitrogen, sulfur, iron, and manganese. Am. J. Sci. 296:197-243.

Wan, J., T. K. Tokunaga, E. Brodie, Z. Wang, Z. Zheng, D. Herman et al. 2005. Reoxidation of bioreduced uranium under reducing conditions. Environ. Sci. Technol. 39:6162-6169.

Watson, I. A., S. E. Oswald, R. U. Mayer, Y. Wu, and S. A. Banwart. 2003. Modeling kinetic processes controlling hydrogen and acetate concentrations in an aquifer-derived microcosm. Environ. Sci. Technol. 37:3910-3919.

Wirtz, K. A. 2003. Control of biogeochemical cycling by mobility and metabolic strategies of microbes in sediments: an integrated model study. FEMS Microbial Ecology 46:295-306.

Yeh, G. T., Y. Li, P. M. Jardine, W. D. Burgos, Y. L. Fang, M. H. Li, and M. D. Siegel. 2004. HYDROGEOCHEM 5.0: A Three-Dimensional Model of Coupled Fluid Flow, Thermal Transport, and HYDROGEOCHEMical Transport through Variable SaturatedConditions - Version 5.0. Oak Ridge National Laboratory.

Table 1. Abundance of ethanol-, acetate-, and hydrogen-oxidizing dissimilatory iron-reducing microorganisms (DIRMs) and sulfate-reducing microorganisms (SRMs) from biostimulated vs. unstimulated FRC Area 2 sediments. All abundances are in cells per gram of wet sediment.

		DIRMs	DIRMs	DIRMs	SRMs	SRMs	SRMs
Material	Condition	Ethanol	Acetate	Hydrogen	Ethanol	Acetate	Hydrogen
Saprolite	Unstimulated	4.1×10^3	3.0×10^2	2.9×10^2	3.7×10^3	4.0×10^3	2.1×10^4
Saprolite	Stimulated	2.1×10^2	4.4×10^2	2.2×10^2	6.9×10^3	4.4×10^4	5.0×10^4
Gravel	Stimulated	1.1×10^4	1.3×10^5	3.5×10^3	8.7×10^1	2.1×10^3	2.7×10^1

Table 2. Summary of phylogenetic analyses of 16S rDNA fragments from DGGE gels prepared with DNA extracted from Area 2 groundwater samples (ports 3, 4, and 5 of well MLSB) during the first 4.5 months of the in situ biostimulation experiment. The band ID numbers correspond to the labeled bands in Fig. 13.

MLSB 3		MLSB 4		MLS B 5	
Band ID	Closest Genus	Band ID	Closest Genus	Band ID	Closest Genus
2.1	Oxalobacteraceae	3.1	Aquaspirillum	4.1	Aquaspirillum
2.2	Aquaspirillum	3.2	Chromobacterium	4.2	Chromobacterium sp
2.3	Dechloromonas	3.3	Aquaspirillum	4.3	Aquaspirillum sp
2.4	Chromobacterium	3.4	Chromobacterium	4.4	Chromobacterium sp
2.5	Hylemonella	3.5	Chromobacterium	4.5	Chromobacterium sp
2.6	Dechloromonas	3.6	Chromobacterium	4.6	Chromobacterium sp.
2.7	Dechloromonas	3.7	Hylemonella	4.7	Dechloromonas sp
2.8	Dechloromonas	3.8	Dechloromonas	4.8	Dechloromonas sp.
5.1	Desulfosporosinus	6.1	Geobacter sp	11.1	Clostridiales bacteriu
5.2	Oxalobacteraceae	6.2	Geobacter sp	11.2	Aquaspirillum
5.3	Aquaspirillum	6.3	Geobacter sp.	11.3	
5.4	Acidovorax	6.4	Geobacter sp.	11.4	Burkholderiales
5.5	Dechloromonas	6.5	Geobacter sp.	11.5	Hydrogenothermus
5.6	Chromobacterium	6.6	Chromobacterium	11.6	Hydrogenothermus
5.7	Dechloromonas	8.1	Geobacter sp.	11.7	Geobacter
7.1	Aquaspirillum	8.2	Clostridiales	11.8	Desulfosarcina
7.2	Geobacter sp.	8.3	Hydrogenothermus	11.9	Termite group 1
7.3	Hydrogenothermus	8.4	Hydrogenimonas	11.10	Desulfobacter
7.4	Hydrogenimonas	8.5	Hydrogenothermus	14.1	Nitrospira
7.5	Hydrogenothermus	8.6	Hydrogenothermus	14.2	Acidovorax
7.6	Geobacter bremensis	8.7	Geobacter bremensis	14.3	Clostridium
7.7	Chromobacterium sp.	8.8	Geobacter	14.4	Aquaspirillum
7.8	Dactylosporangium	8.9	Dactylosporangium	14.5	Geobacter
9.1	Aquaspirillum	10.1	Clostridiales bacteriu	14.6	Hydrogenothermus
9.2	Geobacter	10.2	Aquaspirillum	14.7	
9.3	Clostridiales	10.3	Geobacter	14.8	Brevundimonas
9.4	Hydrogenothermus	10.4		14.9	Marinobacter
9.5	Desulfobacter	10.5	Burkholderiales bacteri	14.10	Agrobacterium vitis
9.6	Desulfosarcina	10.6	Hydrogenothermus	14.11	Desulfovibrio
9.7	Geobacter	10.7	Desulfosarcina	14.12	Desulfovibrio
9.8	Chloroflexus	10.8	Geobacter	14.13	Desulfovibrio
9.9		10.9	Termite group 1	14.14	
12.1	Aquaspirillum	13.1	Nitrospira	14.15	Desulfovibrio
12.2	Geobacter sp	13.2	Clostridium sp	17.1	Photobacterium sp.
12.3	Hydrogenothermus	13.3	Aquaspirillum	17.2	Aquaspirillum
12.4	Geobacter	13.4	Geobacter	17.3	Geobacter
12.5	Geobacter bremensis	13.5	Hydrogenothermus	17.4	Aquaspirillum
12.6	Desulfobacter	13.6	Brevundimonas	17.5	Geobacter
12.7		13.7	Geobacter	17.6	Acinetobacter
15.1	Aquaspirillum	13.8	Agrobacterium	17.7	Uncultured bacterium
15.2	Geobacter sp	13.9	Desulfovibrio	17.8	Azoarcus
15.3	Hydrogenothermus	13.10	Desulfovibrio	17.9	Propionibacter
15.4	Desulforhopalus	13.11	Desulfovibrio	17.10	
15.5	Desulfovibrio	16.1	Photobacterium	17.11	Desulfovibrio
15.6	Propionibacter	16.2	Aquaspirillum	20.1	Moorella
15.7	Desulfovibrio	16.3	Geobacter	20.2	Aquaspirillum
15.8		16.4	Aquaspirillum	20.3	Geobacter
18.1	Desulfobulbus	16.5	Geobacter	20.4	Azospirillum
18.2	Aquaspirillum	16.6		20.5	Geobacter
18.3	Geobacter	16.7	Hydrogenothermus	20.6	Geobacter
18.4	Aquaspirillum	16.8	Geobacter	20.7	Agrobacterium
18.5	Clostridium	16.9	Dechloromonas	20.8	Desulfovibrio
18.6	Geobacter	16.10	Magnetic bacterium	20.9	Methylocystis
18.7	Thauera	16.11		20.10	Propionibacter
		19.1	Photobacterium	20.11	Desulfonema
		19.2	Moorella		
		19.3	Desulfobulbus		
		19.4	Aquaspirillum		
		19.5	Azospirillum		
		19.6	Hydrogenothermus		
		19.7	Geobacter		
		19.8	Agrobacterium		
		19.9	Desulfovibrio		
		19.10	Methylocystis		
		19.11			
		19.12	Desulfovibrio		

Table 3. Primary dependent variables in the GWB simulation of the Area 2 sediment slurry experiment.

Number	Type*	Name	Abbreviation	Initial Value
(1)	ED	CH_3CH_2OH (Ethanol)	CH3CH2OH	0.009 (mol L^{-1})
(2)	ED, FP	CH_3COO^- (Acetate)	CH3COO	0.0 (mol L^{-1})
(3)	ED, FP	H_2	H2	1.0×10^{-9} (mol L^{-1})
(4)	EA	NO_3^-	NO3	0.0012 (mol L^{-1})
(5)	EA	FeOOH (s)	FeOOH	0.032 (mol L^{-1})
(6)	EA	SO_4^{2-}	SO4	0.0011 (mol L^{-1})
(7)	RM, EA	HCO_3^-	HCO3	0.0005 (mol L^{-1})
(8)	RM	N_2	N2	0.0005 (mol L^{-1})
(9)	RM	Fe(II)	Fe2	0.0 (mol L^{-1})
(10)	RM	HS^-	HS	0.0 (mol L^{-1})
(11)	RM	CH_4	CH4	0.0 (mol L^{-1})
(12)	FP, RM	H^+	H	3.2×10^{-7} (mol L^{-1})
(13)	MP	$FeCO_3$(s)	FeCO3	0.0 (mol L^{-1})
(14)	MP	FeS(s)	FeS	0.0 (mol L^{-1})
(15)	MB	Organic Carbon-Oxidizing Denitrifying Microorganisms	DM1	XXXX (g L^{-1})
(16)	MB	Organic Carbon-Oxidizing Dissimilatory Iron-Reducing Microorganisms	DIRM1	XXXX (g L^{-1})
(17)	MB	Organic Carbon-Oxidizing Sulfate-Reducing Microorganisms	SRM1	XXXX (g L^{-1})
(18)	MB	Ethanol-Metabolizing Methanogenic Microorganisms	MGM1	XXXX (g L^{-1})
(19)	MB	Ethanol-Fermenting Microorganisms	FM	XXXX (g L^{-1})
(20)	MB	Acetate-Oxidizing Methanogenic Microorganisms	MGM2	XXXX (g L^{-1})
(21)	MB	H_2-Oxidizing Denitrifying Microorganisms	DM2	XXXX (g L^{-1})
(22)	MB	H_2-Oxidizing Dissimilatory Iron-Reducing Microorganisms	DIRM2	XXXX (g L^{-1})
(23)	MB	H_2-Oxidizing Sulfate-Reducing Microorganisms	SRM2	XXXX (g L^{-1})
(24)	MB	H_2-Oxidizing Methanogenic Microorganisms	MGM3	XXXX (g L^{-1})

* ED = Electron donor; EA = Electron acceptor; FP = Fermentation product; RM = Respiration metabolite; MP = Mineral precipitate; MB = Microbial biomass

Table 4. Metabolic energy-generating terminal electron-accepting processes (TEAPs) in the GWB simulation of the Area 2 sediment slurry experiment.

No.	Reaction	Catalyzed By
(1)	$CH_3CH_2OH + 2.4NO_3^- + 0.4H^+ \rightarrow 2HCO_3^- + 1.2N_2 + 2.2H_2O$	DM1
(2)	$CH_3CH_2OH + 4FeOOH + 7H^+ \rightarrow CH_3COO^- + 4Fe^{2+} + 7H_2O$	DRM1
(3)	$CH_3CH_2OH + 0.5SO_4^{2-} \rightarrow CH_3COO^- + 0.5HS^- + 0.5H^+ + H_2O$	SRM1
(4)	$CH_3CH_2OH + HCO_3^- \rightarrow CH_3COO^- + 0.5CH_4 + 2H_2O$	MGM1
(5)	$CH_3CH_2OH + H_2O \rightarrow CH_3COO^- + 2H_2 + H^+$	FM
(6)	$CH_3COO^- + 1.6NO_3^- + 0.6H^+ \rightarrow 2HCO_3^- + 0.8N_2 + 0.8H_2O$	DM1*
(7)	$CH_3COO^- + 8FeOOH + 15H^+ \rightarrow 2HCO_3^- + 8Fe^{2+} + 12H_2O$	DRM1*
(8)	$CH_3COO^- + SO_4^{2-} \rightarrow 2HCO_3^- + HS^-$	SRM1*
(9)	$CH_3COO^- + H_2O \rightarrow HCO_3^- + CH_4$	MGM2
(10)	$H_2 + 0.4NO_3^- + 0.4H^+ \rightarrow 0.2N_2 + 1.2H_2O$	DM2
(11)	$H_2 + 2FeOOH + 4H^+ \rightarrow 2Fe^{2+} + 4H_2O$	DRM2
(12)	$H_2 + 0.25SO_4^{2-} + 0.25H^+ \rightarrow 0.25HS^- + H_2O$	SRM2
(13)	$H_2 + 0.25HCO_3^- + 0.25H^+ \rightarrow 0.25CH_4 + 0.75\ H_2O$	MGM3

* reactions subject to noncompetitive inhibition by CH_3CH_2OH.

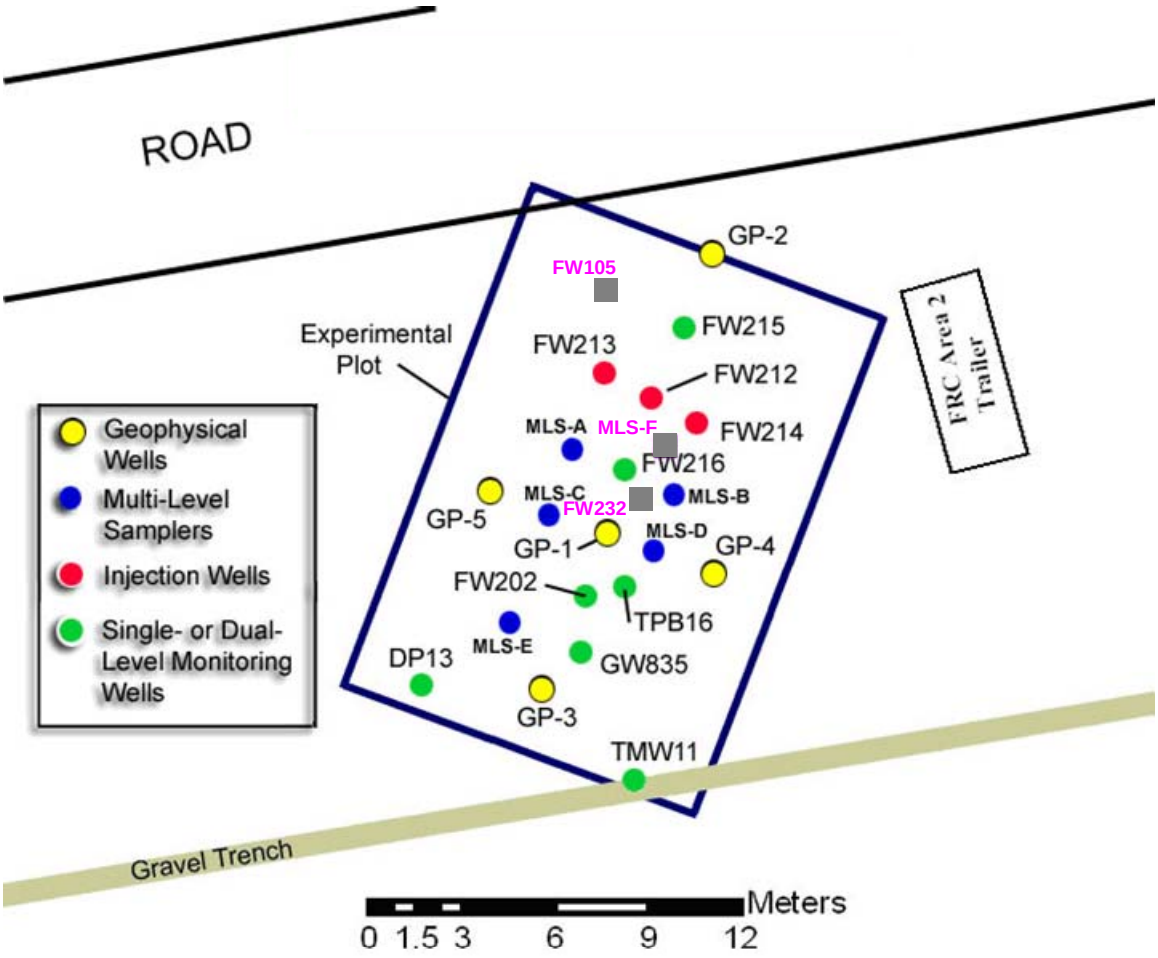

Fig. 1. Plan view map of the Area 2 study site at the ORNL FRC, showing the location of various boreholes. The gray squares with pink lettering indicate the location of cores collected during (MLS-F) or after (FW232 and FW105) the in situ biostimulation experiment.

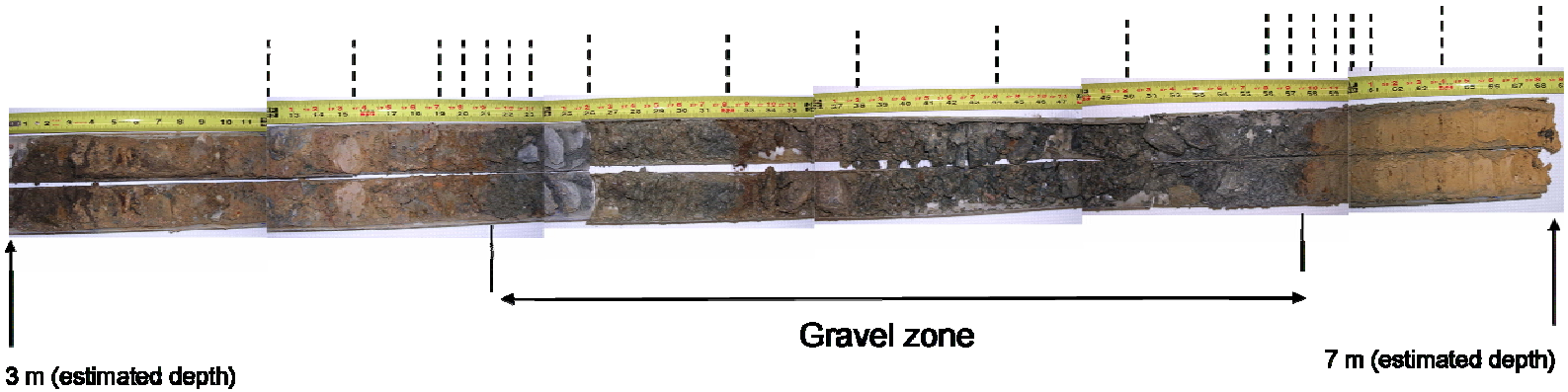

Fig. 2. Composite photos of a sediment core (GP-01) from Area 2 at the ORNL FRC, showing the gravel layer between 4 and 5 m depth. Dashed lines indicate the depth intervals subjected to particle size fractionation prior to solid-phase Fe and U analysis.

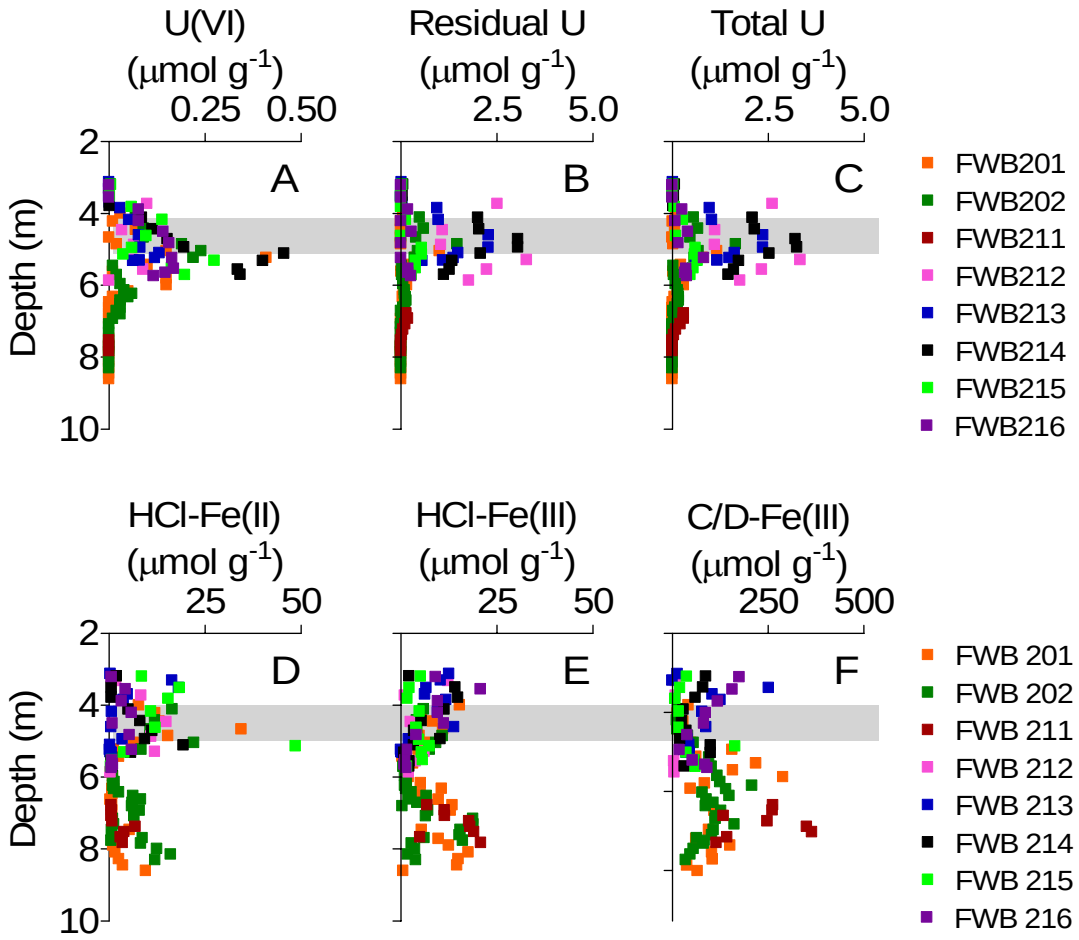

Fig. 3. Solid-phase U (A-C) and Fe (D-F) content of sediments from 8 different cores from Area 2 at the ORNL FRC. Each symbol represents the average of duplicate or triplicate subsamples. Grey bars indicate the approximate location of the gravel layer.

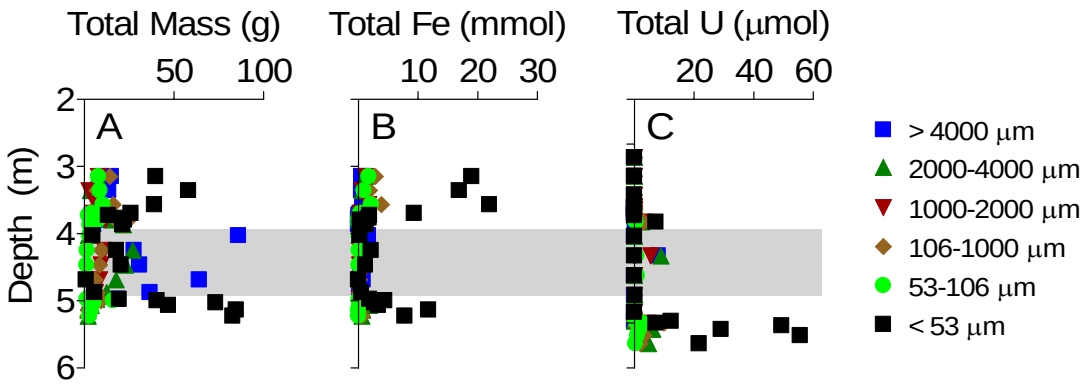

Fig. 4. Total mass, Fe, and U content of different size fraction of sediment materials from core GP-01. Total Fe and U contents represent the mass-normalized concentration (μmol g^{-1}) multiplied by the total mass of sediment in a given size interval. Grey bar indicates the approximate location of the gravel layer.

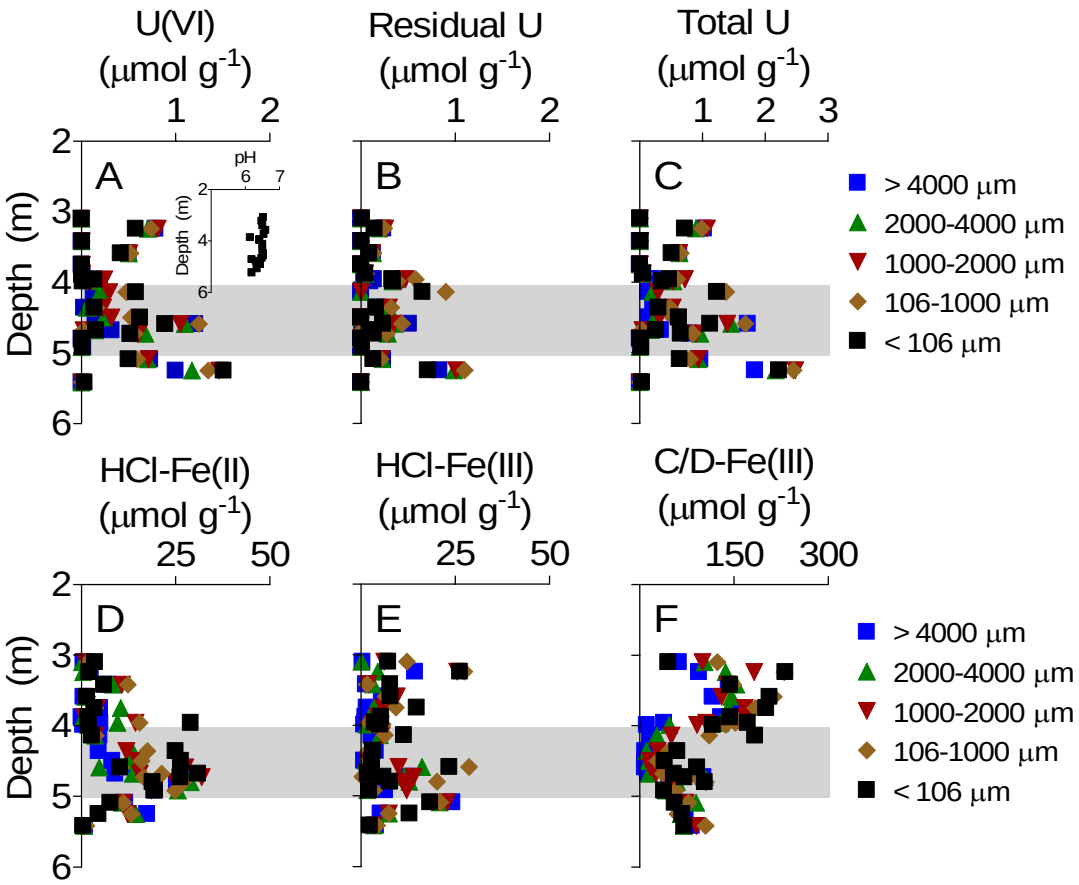

Fig. 5. Solid-phase U and Fe content of different size fractions of anaerobically-dried sediment materials from core GP-02. Grey bars indicate the approximate location of the gravel layer.

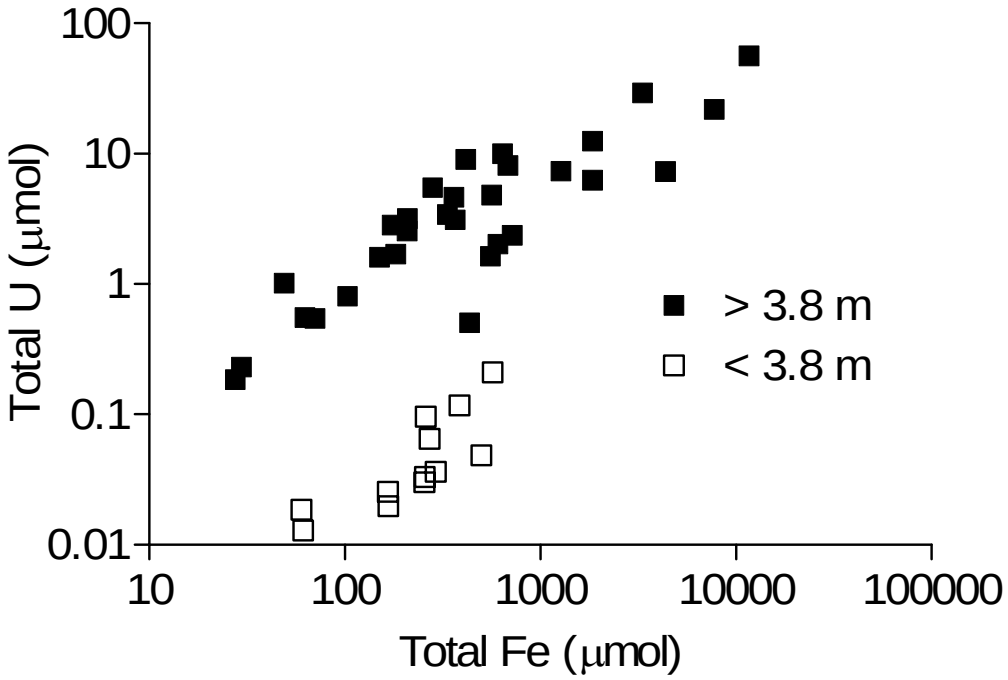

Fig. 6. Relationship between total solid-phase U and Fe content of size-fractionated sediment materials from core GP-01 (data from Fig. 4). Samples from depths greater than 3.8 m represent the most highly-contaminated materials within, just above, and just below the gravel layer at Area 2 (see Fig. 3).

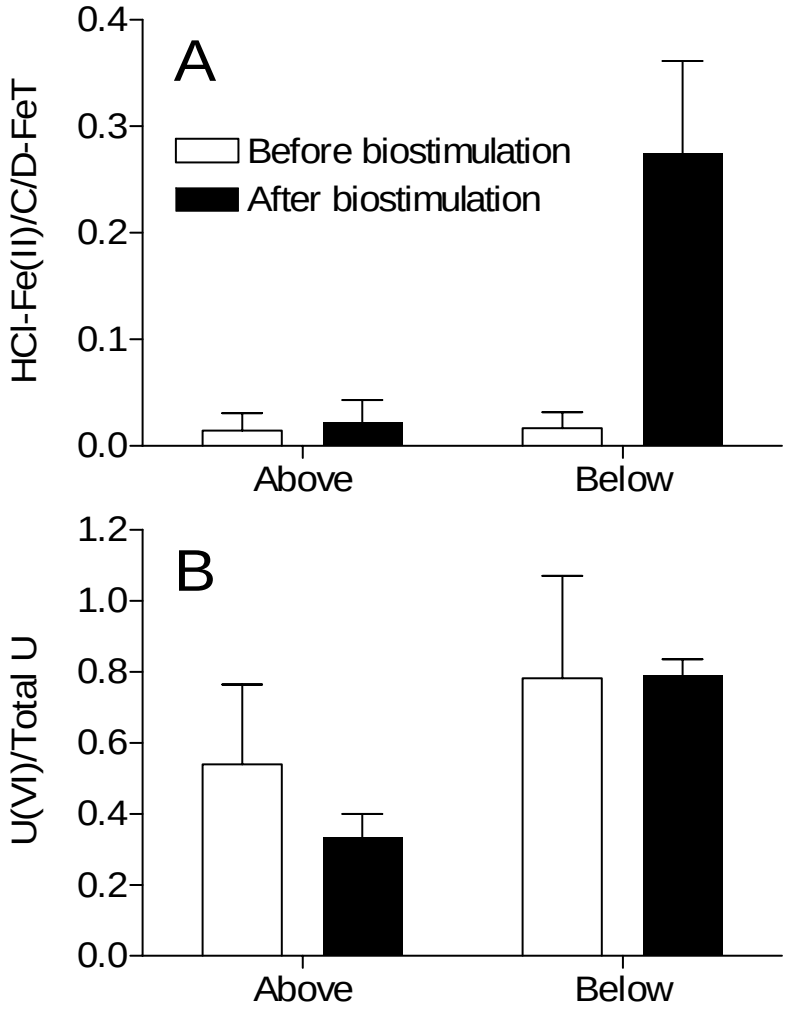

Fig. 7. Influence of in situ ethanol biostimulation on the redox speciation of Fe (A) and U (B) in Area 2 sediments. The "before biostimulation" data correspond to average values for 2-cm segments of sediment directly above or below the gravel layer, obtained from cores MLS-A, MLS-B, MLS-C, MLS-D, MLS-E, GP-03, GP-04, and GP-05 (8 cores total) that were collected in the spring of 2005, 4-6 months prior to the start of the in situ biostimulation experiment. The "after biostimulation" data correspond to average values for three successive 1-cm segments of sediment directly above or below the gravel layer, obtained from core MLS-F that was collected in May 2006, 8 months after the start of the in situ biostimulation experiment. Error bars represent ± 1 standard deviation.

Fig. 8. Photos of sediment in the vicinity of the gravel layer at Area 2 from cores collected within (FWB232; upper set) and outside of (FB105; lower set) the zone of biostimulation at the end of the in situ biostimulation experiment. Note the distinct darkening of materials in the biostimulated sediments, which is indicative of Fe(III) oxide reduction activity.

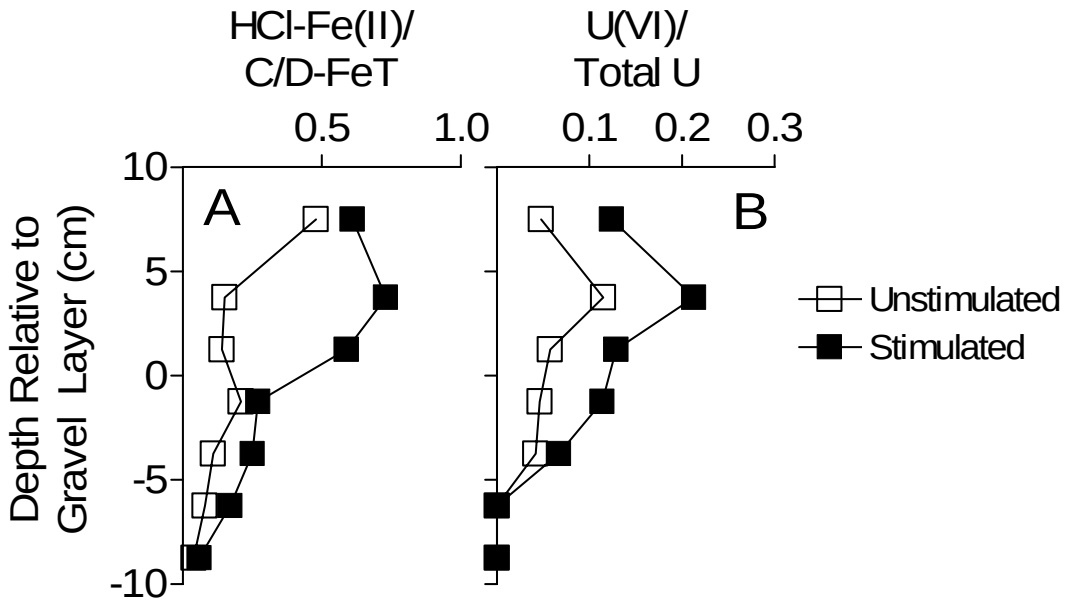

Fig. 9. Influence of in situ ethanol biostimulation on the redox speciation of Fe (A) and U (B) in Area 2 sediments. The "stimulated" and "unstimulated" data refer to measurements made on single 0.5 g subsamples of anaerobically-dried sediment from cores FW232 and FW105, which were collected within and outside of the zone of in situ biostimulation (see Fig. 1), respectively, just after the termination of the in situ experiment.

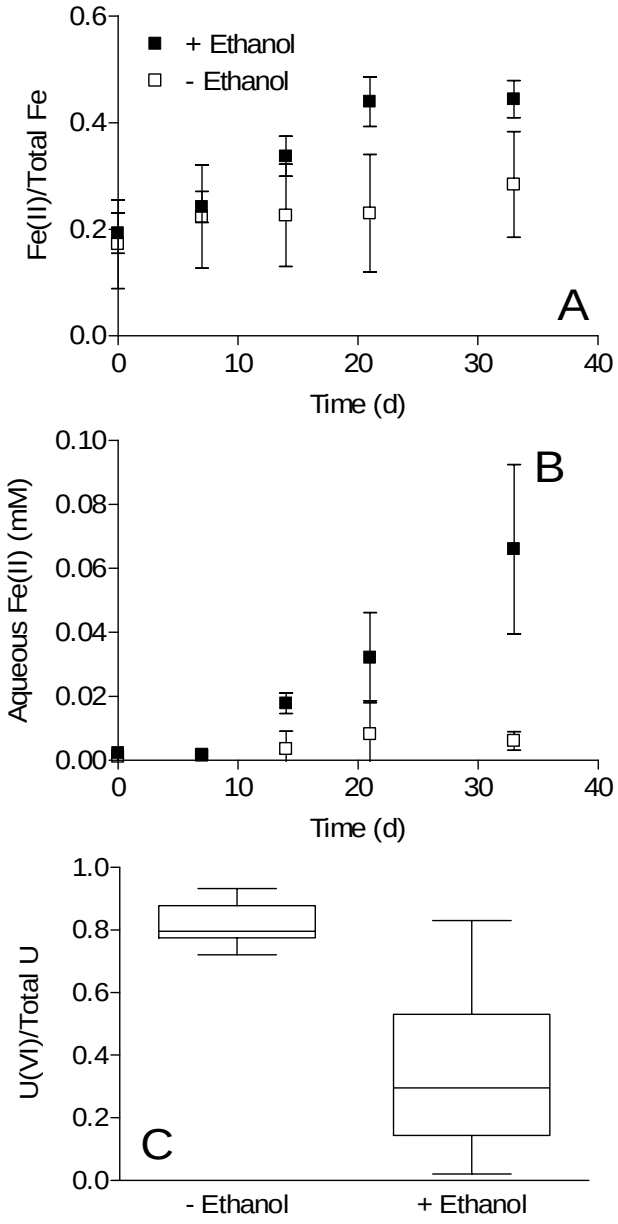

Fig. 10. Influence of ethanol amendment on the redox speciation of Fe (A,B) and U (C) in slurries of Area 2 saprolite material from below the zone of major U contamination (12 slurries each, ± ethanol, from ca. 7-8 meters depth; see Fig. 3). In order to assess the potential for U(VI) reduction, ca. 100 μmol L^{-1} (bulk) of uranyl-acetate was added to the slurries after several weeks of incubation, and the relative abundance of $NaHCO_3$-extractable U(VI) was then determined after an additional 60 days of incubation. Error bars in panels A and B show ± 1 standard deviation. The lines, boxes, and bars in the box and whisker shown in panel B indicate the median value, the 25^{th} to 75^{th} percentile, and the total range of values, respectively.

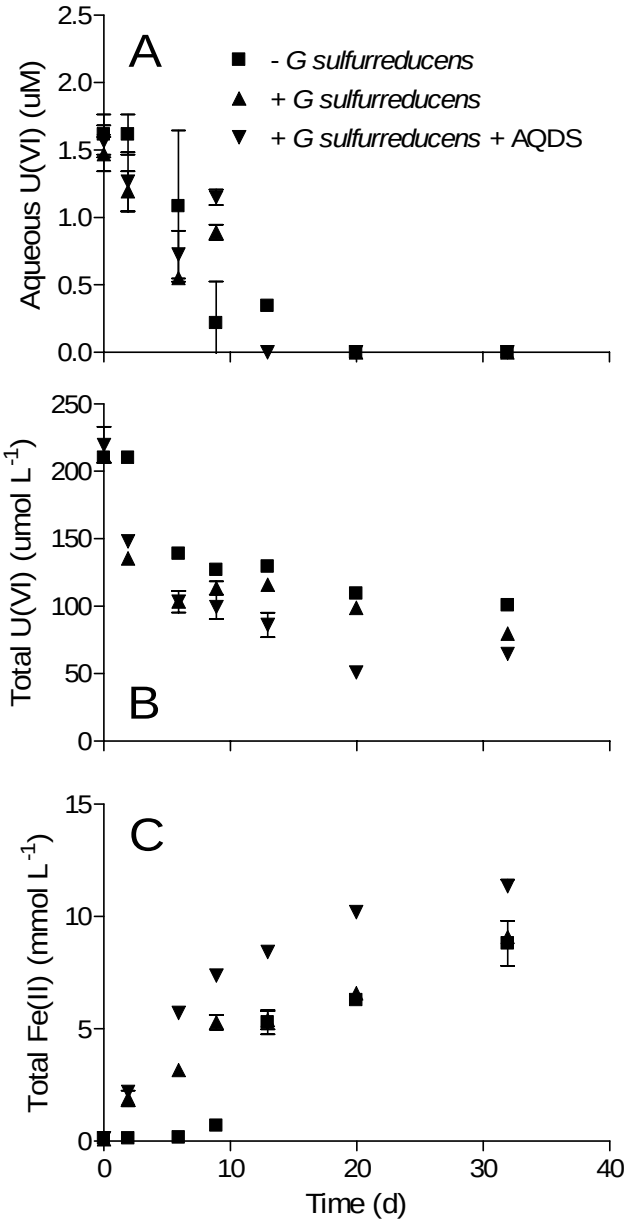

Fig. 11. Reduction of endogenous U(VI) (A,B) and Fe(III) (C) in ethanol (10 mM) amended slurries of sediment from the zone of maximum U contamination just below the gravel layer at Area 2 (see Fig. 3). Acetate/fumarate-grown cells of *G. sulfurreducens* (ca. 10^8 mL^{-1}) were added to some of the slurries to stimulate U(VI) and Fe(III) reduction. Data represent the mean ± range of duplicate slurries.

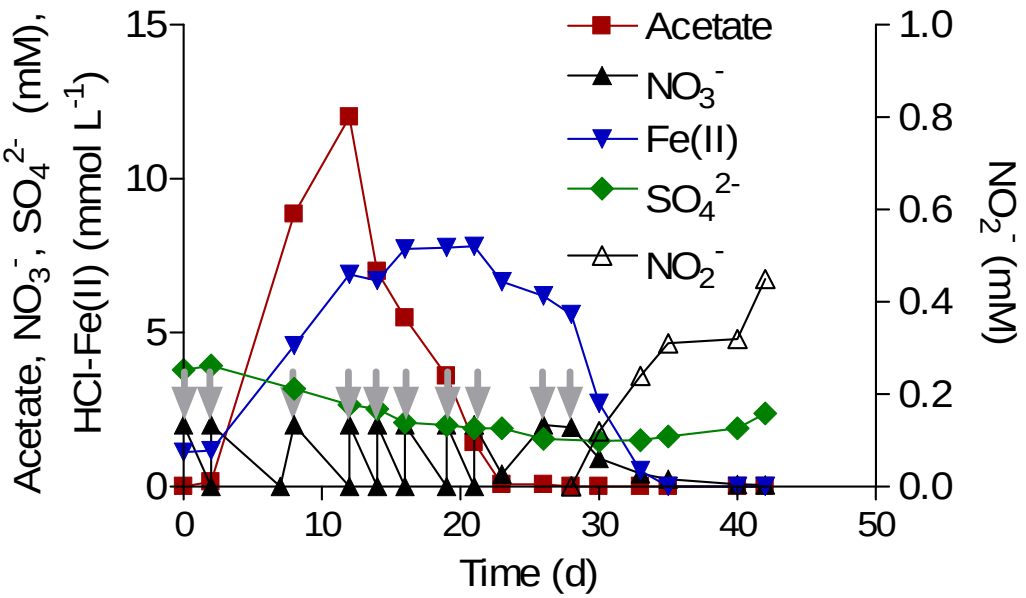

Fig. 12. Redox metabolism in anaerobic slurries of Area 2 gravel material (< 106 μm fraction). The slurries were amended periodically with 2 mM NO_3^- (grey arrows) until oxidation of sediment Fe(II) compounds took place. Symbols show the mean of triplicate slurries.

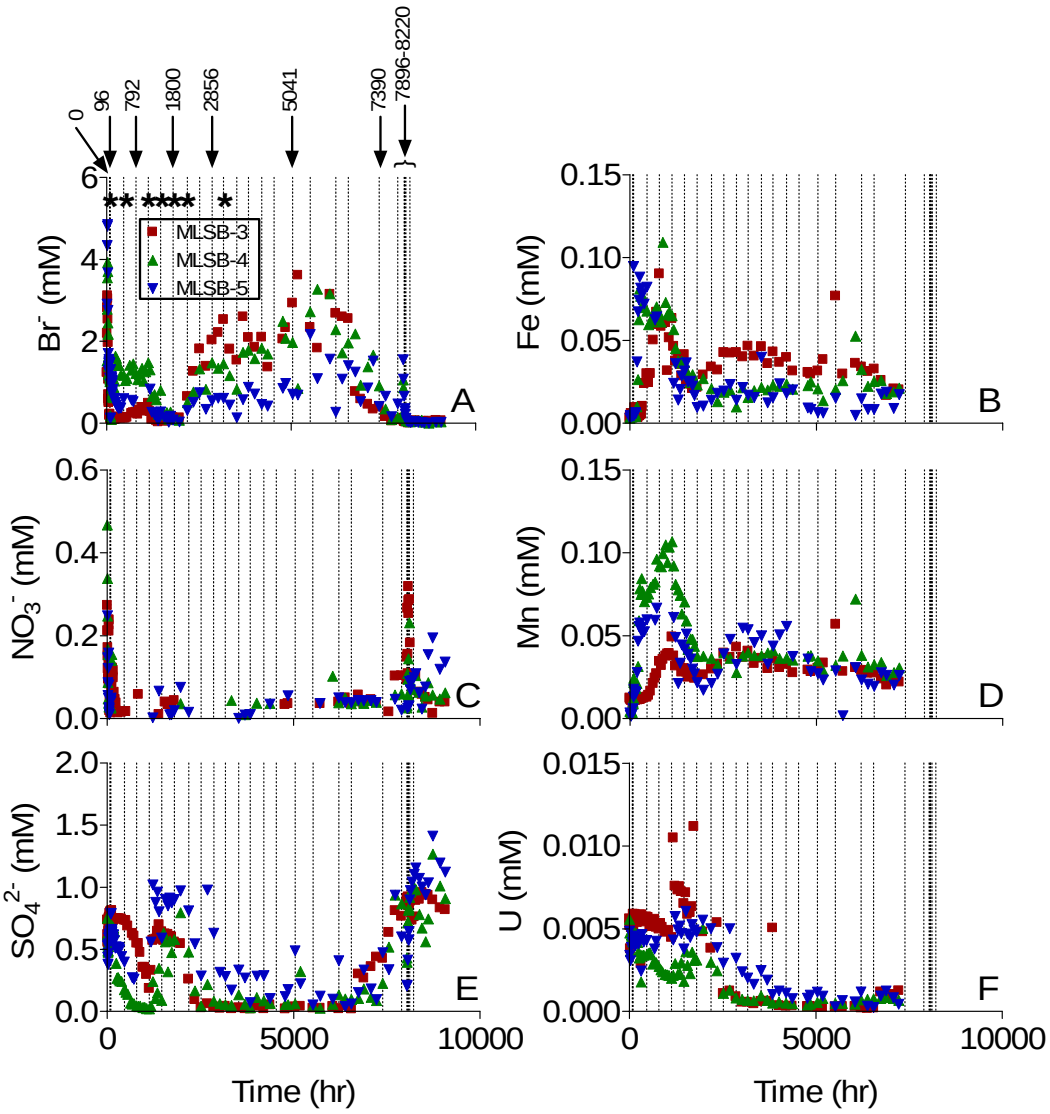

Fig. 13. Concentration of selected redox-sensitive elements in multi-level sampling (MLS) well MLSB during the first 4.5 months of the in situ biostimulation experiment. Different symbols correspond to sampling ports 3, 4, and 5 within the MLS. Time zero corresponds to initiation of ethanol injection in late September 2005. Dashed vertical lines indicate times when groundwater samples were filtered for microbial community analysis. Asterisks indicate groundwater samples that were analyzed by DGGE (see Figs. 14-15); arrows indicate groundwater samples that are slated for analysis of PLFA content.

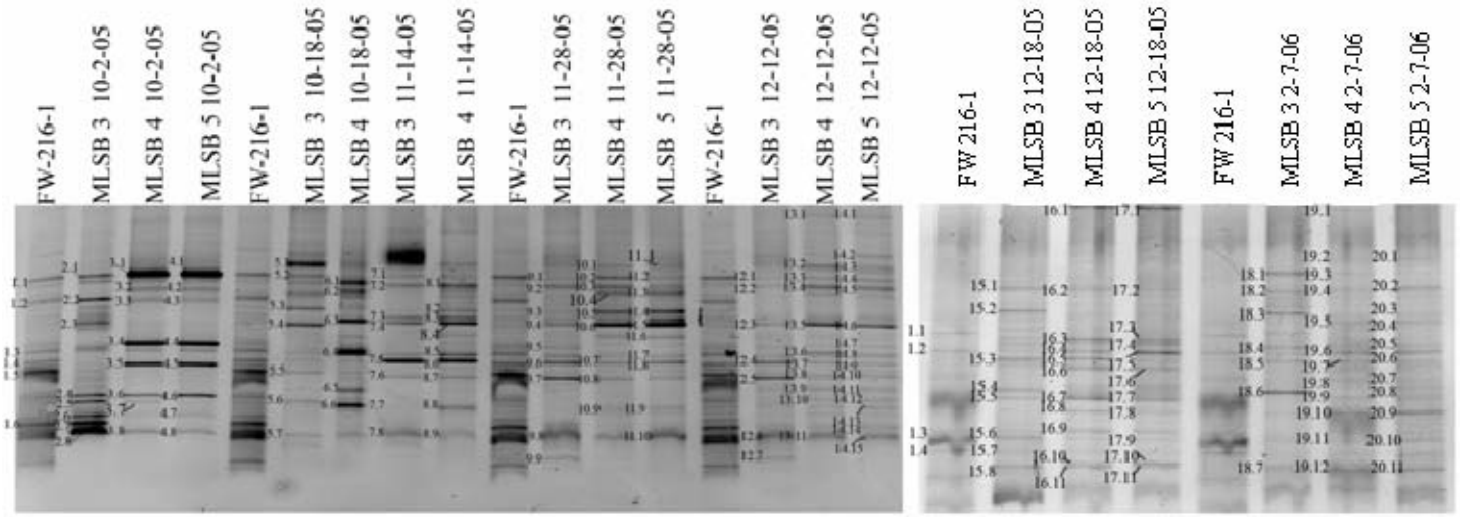

Fig. 14. DGGE gels prepared with DNA extracted from Area 2 groundwater samples (ports 3, 4, and 5 of well MLSB) during the first 4.5 months of the in situ biostimulation experiment. The ID numbers correspond to bands that were excised and reamplified for sequencing (see Table 2).

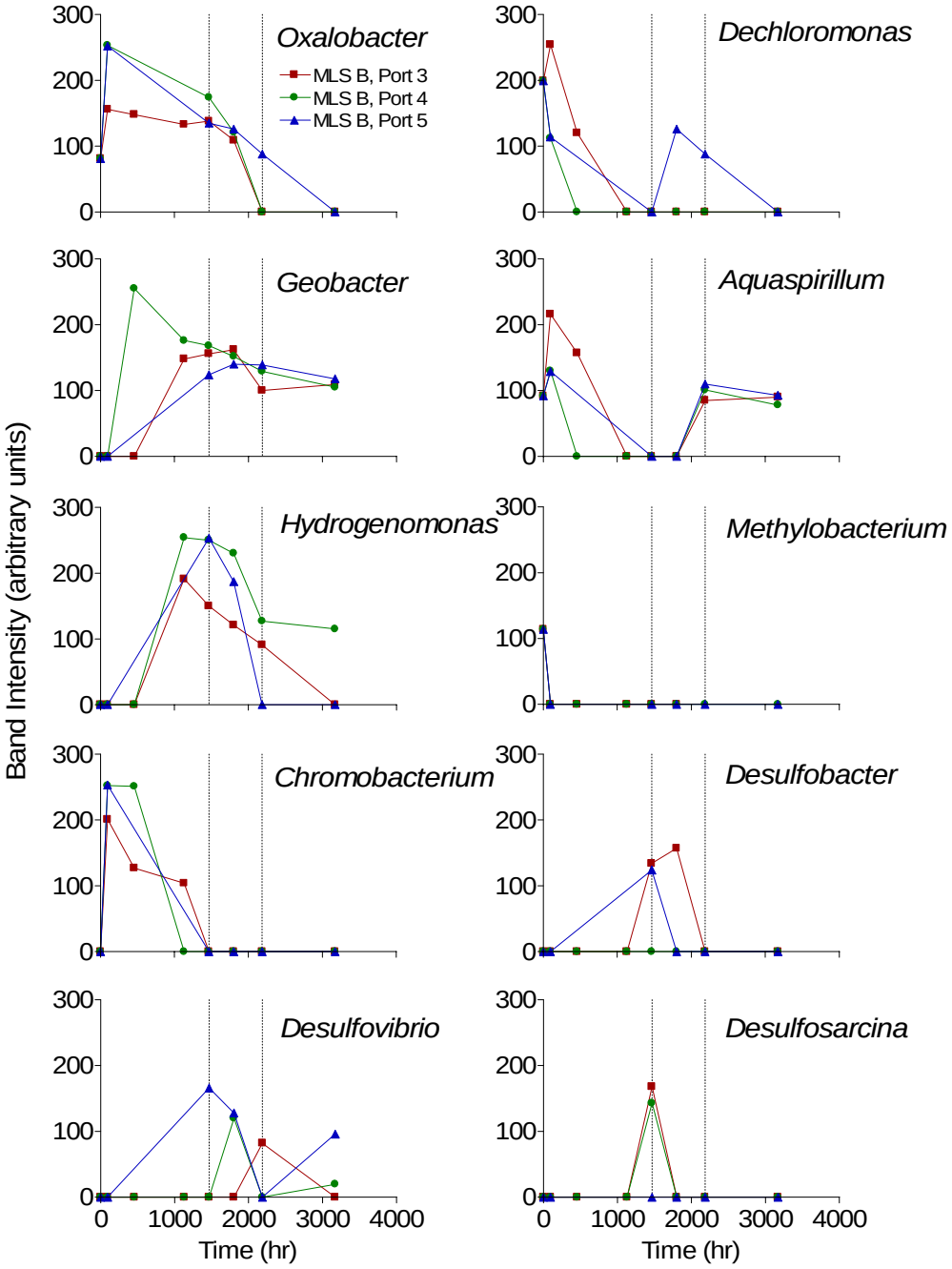

Figure 15. Changes in microbial community structure within Area 2 groundwater (ports 3, 4, and 5 from well MLSB) during the first 4.5 months of the in situ biostimulation experiment, assessed through DGGE analysis of PCR-amplified 16S rRNA genes. The dashed vertical lines in each panel indicate the period of U(VI) and sulfate rebound between ca. 1500 and 2200 hours). Images of the DGGE gels are provided Fig. 13, and a detailed summary of the band sequence analyses is provided in Table 2.

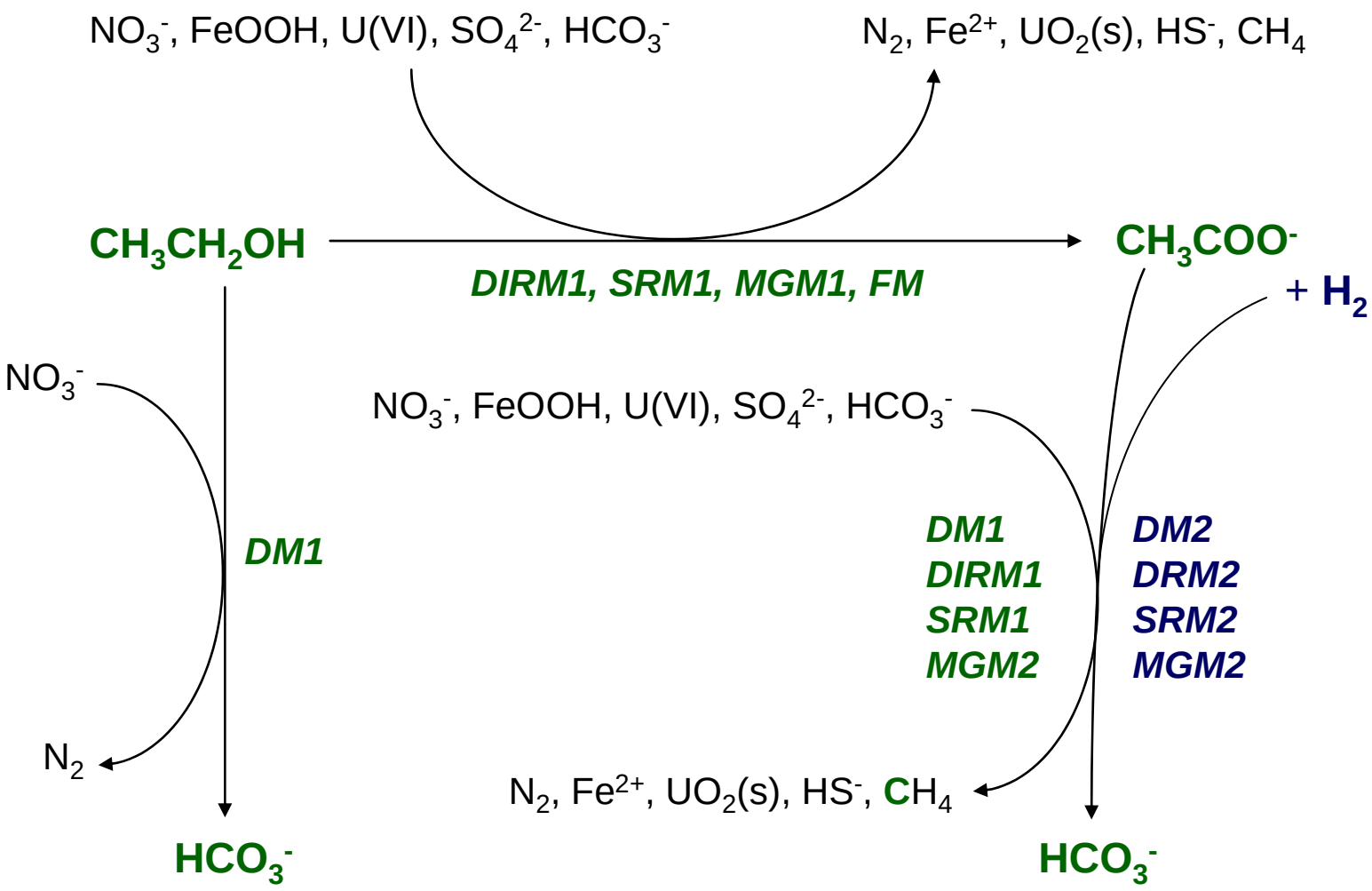

Fig. 16. Substrate reaction paths in the Geochemist's Work Bench simulation (courtesy of Q. Jin, University of Oregon) of the Area 2 sediment slurry experiment. This simulation, unlike TEAPREVU, includes molecular hydrogen (H_2) as an end-product of ethanol metabolism and an electron donor for anaerobic respiration and methanogenesis.

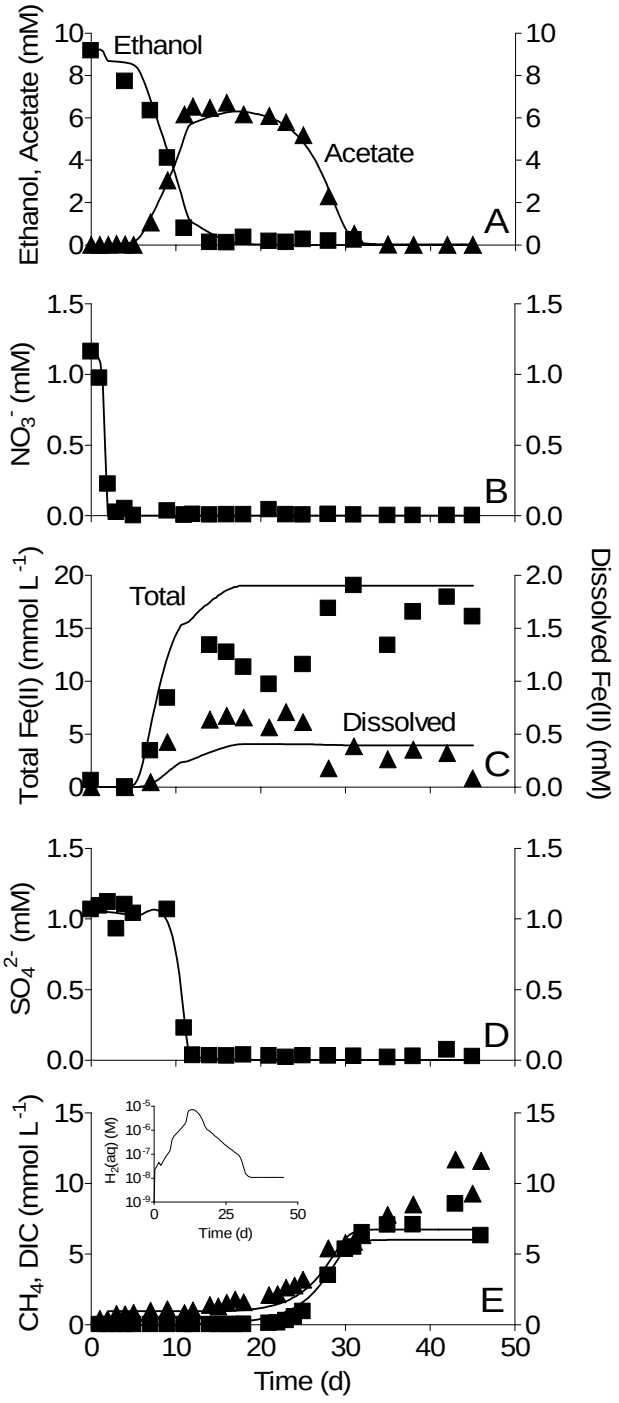

Fig. 17. Results of the Geochemist's Work Bench simulation (courtesy of Q. Jin, University of Oregon) of the Area 2 sediment slurry experiment. Solid lines shows simulated values.

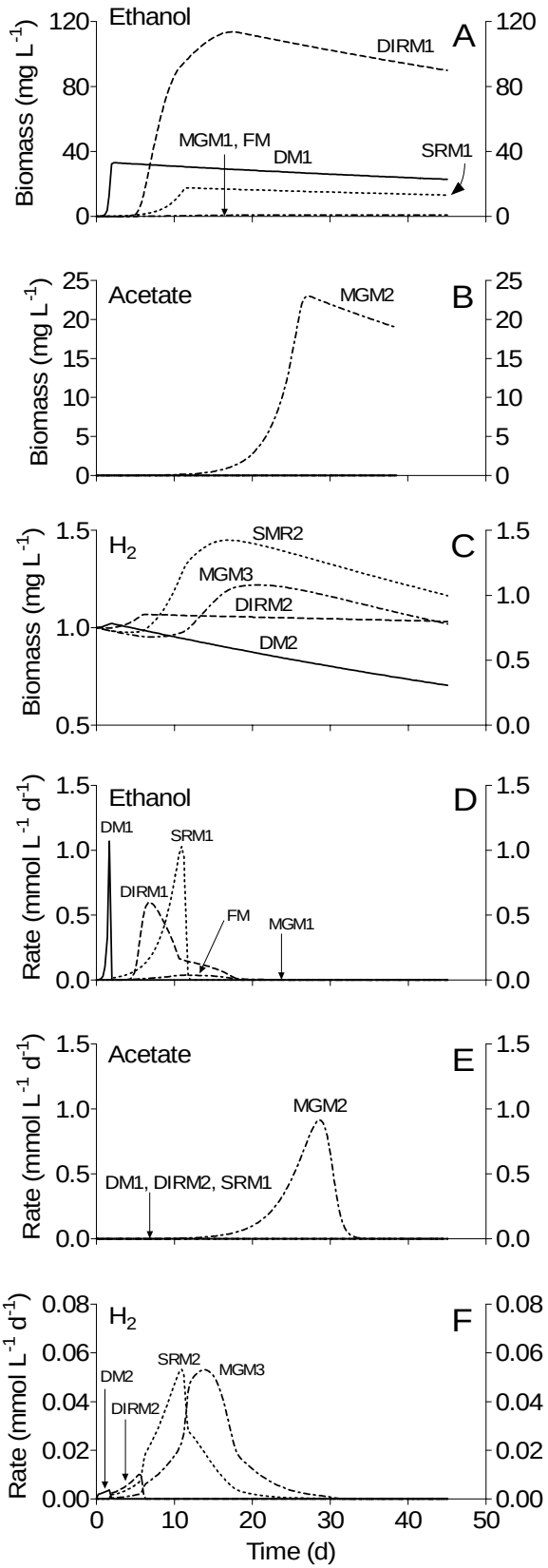

Fig. 18. Microbial biomass (A-C) and metabolic rates (D-F) from the Geochemist's Work Bench simulation (courtesy of Q. Jin, University of Oregon) of the Area 2 sediment slurry experiment. The population designations correspond to those in Fig. 16.

Biogeochemical Processes In Ethanol Stimulated Uranium Contaminated Subsurface Sediments

SANTOSH R. MOHANTY[1]
BHARATI KOLLAH[1],
DAVID B. HEDRICK[2],
AARON D PEACOCK[2],
RAVI K. KUKKADAPU[3], AND
ERIC E. RODEN[*,1]

[1]Department of Geology and Geophysics
1215 W. Dayton St.
University of Wisconsin
Madison, WI 53706

[2]Center for Biomarker Analysis
The University of Tennessee
Knoxville, TN 37932

[3]Pacific Northwest National Laboratory
P.O. Box 999, MSIN K8-96
Richland, WA 37932

*Corresponding Author:
Phone: 608-890-0724; fax: 608-262-0693; email: eroden@geology.wisc.edu

A laboratory incubation experiment was conducted with uranium-contaminated subsurface sediment from Area 2 at the U.S. Department of Energy Field Research Center at Oak Ridge National Laboratory to assess the biogeochemical and microbial community response to ethanol amendment, specifically with respect to the temporal sequence of terminal electron-accepting processes (TEAPs) and the potential for U(VI) reduction. A classical sequence of TEAPs was observed in ethanol-amended slurries, with NO_3^- reduction, Fe(III) oxide reduction, SO_4^{2-} reduction, and CH_4 production proceeding in sequence until all of the added ethanol (9 mM) was consumed. Approximately 60% of the 100 mM $NaHCO_3$-extractable U(VI) content of the sediment was reduced during the period of Fe(III) reduction. No additional U(VI) reduction took place during the sulfate-reducing and methanogenic phases of the experiment. Only gradual reduction of nitrate, and no reduction of U(VI), took place in ethanol-free slurries. Stimulation of additional Fe(III) or sulfate reduction in the ethanol-amended slurries failed to promote further U(VI) reduction. Reverse transcribed 16S rRNA clone libraries and measurements of phospholipid fatty acids (PLFA) abundance and the incorporation of ^{13}C-ethanol into PLFAs were used to characterize the microbial community response to ethanol amendment. The 16S rRNA libraries revealed major increases in the abundance of organisms related to *Dechloromonas*, *Geobacter*, and *Oxalobacter*. PLFAs indicative of *Geobacter* showed a distinct increase in the amended slurries, and analysis of PLFA $^{13}C/^{12}C$ ratios confirmed the incorporation of ethanol into signature PLFAs of *Geobacter*. Although no significant increase in the abundance of PLFAs indicative of sulfate-reducing bacteria (SRB) was observed, a distinct increase in the abundance of ^{13}C-labeled PLFAs indicative of *Desulfobacter*, *Desulfotomaculum*, and *Desulfovibrio* was observed during the brief period of sulfate reduction which followed the Fe(III) reduction phase. Our results show that bulk biogeochemical processes in ethanol-amended sediments can be reliably interpreted in terms of standard conceptual models of TEAPs in sediments. However, the redox and aqueous/solid-phase speciation of uranium is complex and cannot be explained on the basis of simplified thermodynamic considerations.

Introduction

The oxidized form of uranium [U(VI)] is relatively soluble (largely as U(VI)-carbonate complexes) and mobile in most oxic circumneutral pH sedimentary environments (*1*). U(VI) can be reduced enzymatically by dissimilatory iron- and sulfate-reducing bacteria, leading to removal of uranium from solution through precipitation of the insoluble U(IV) mineral phase uraninite [UO_2(s)] (*2,3*). Recent studies have demonstrated that in situ stimulation of microbial U(VI) reduction activity, through addition of acetate or ethanol as electron donor, can be used to precipitate UO_2(s) in U(VI)-containing aquifers (*4-7*). Analysis of groundwater and sediment microbial communities in situ and in laboratory sediment incubations have consistently demonstrated that dissimilatory iron-reducing bacteria (DIRB) in the family *Geobacteraceae* are responsible for U(VI) reduction in acetate-amended sediments in which Fe(III) oxide reduction is the predominant respiratory pathway (*5,8-12*). However, the microbial agents responsible for U(VI) reduction in more complex systems, where multiple terminal electron-accepting processes (TEAPs) co-exist and compete with one another, have yet to be rigorously defined. For example, although growth of *Geobacteraceae* clearly took place during acetate biostimulation at the Rifle site in CO (*5,13*), proliferation of other types of respiratory organisms such as sulfate-reducing bacteria (SRB) clearly occurred (*12*) with important consequences for long-term U(VI) reduction activity (*5*). Recent studies of ethanol-driven biostimulation in subsurface sediments at the U.S. Department of Energy Field Research Center (FRC) at Oak Ridge National Lab (ORNL) have suggested that nitrate-, iron-, and sulfate-respiring organisms, as well as a variety of other phylogenetic groups, may play a role in U(VI) reduction (*7,11,14-16*). In contrast, the shift from metal-reducing to methanogenic conditions in biostimulated FRC Area 2 sediments apparently retarded U(VI) reduction and altered the long-term stability of UO_2(s) (*17*).

Assessing the linkage between aqueous/solid-phase geochemical conditions, microbial community development, and patterns of U(VI) reduction activity represents continuing a challenge for in situ uranium bioremediation research. The objective of this work was to examine these linkages in suspensions (slurries) of ethanol-amended, uranium-contaminated subsurface sediment from Area 2 at the ORNL FRC. Microbial communities associated with shifts in TEAPs were assessed by 16S rRNA gene (clone library analysis of 16S rDNA and reverse-transcribed 16S rRNA) and phospholipid fatty acid (PLFA) techniques, including stable isotope probing (^{13}C incorporation) of PLFAs. The results verify existing conceptual models of the temporal segregation of TEAPs in sediments, and provide a data set for development of microbial physiology-based reaction models suitable for incorporation into field-scale reactive transport simulations of ethanol-driven redox metabolism.

Experimental Section

Site Description. Sediment for the slurry incubation experiment was obtained from Area 2 at the ORNL FRC (see http://www.esd.ornl.gov/nabirfrc). The Area 2 site is a shallow pathway for migration of contaminated groundwater to seeps in the upper reach of Bear Creek at ORNL. Hydraulic monitoring at the site indicates that the depth to ground water is ca. 4.5 meters below the land surface. Detail descriptions of the stratigraphy and sediment/groundwater characteristics of Area 2 are available elsewhere (*18*). Dissolved oxygen concentrations in are generally less than 50 μM, and nitrate concentrations vary between 0.5 and 1 mM. The average dissolved uranium concentration is 5 μM. PHREEQC (*19*) simulations with the best available aqueous phase uranium speciation constants (*20,21*) indicate that under the pH (ca. 6.5) and dissolved pCO_2 (ca. 1.7) conditions of groundwater at Area 2, dissolved U(VI) is present almost exclusively as $Ca_2UO_2(CO_3)_3$, UO_2CO_3, and $UO_2(CO_3)_2^{2-}$ complexes.

A typical geologic profile at Area 2 consists of ca. 6 m of reworked fill and saprolite at the surface underlain by 2-3 m of intact saprolite, with weathered Nolichucky Shale bedrock below the saprolite. The bulk mineralogy of the intact saprolite consists of approximately equal amounts of (i) quartz, anorthite, calcite, and dolomite; and (ii) microcline, illite, kaolinite, and vermiculite; the reworked fill contains larger amounts (ca. 80% by weight) of the former materials (*18*). Sediments within the reworked fill and just below the fill-saprolite boundary contain high concentrations of uranium (up to 3 μmol g^{-1}) (Figure S1). Approximately 10% of total HNO_3-extractable uranium is recoverable as U(VI) by anaerobic extraction with 100 mM $NaHCO_3$ (*22*), with maximum U(VI) concentrations of ca. 0.5 μmol g^{-1} at the bottom of the reworked fill (Figure S1). The solid-phase U(VI) is likely associated with amorphous and/or crystalline Fe(III) oxides, which are present at concentrations up to 25 and 250 μmol g^{-1} within the reworked fill and underlying saprolite (Figure S2).

Slurry Preparation. Core material from the zone of maximum total U(VI) concentration was dried, ground with a mortar and pestle, and passed through a 0.5 mm sieve. The 0.5M HCl- and citrate/dithionite (C/D)-extractable Fe contents of the dried sediment (ca. 130 μmol g^{-1}) were determined as previously described (*23*). One hundred twenty-five g of dry sediment was suspended in 500 mL of a Pipes-buffered artificial groundwater (PBAGW835) designed to mimic the groundwater in well 835 at Area 2. The composition of PBAGW835 was as follows: $CaCl_2.2H_2O$, 1.85 mM; $CaSO_4.2H_2O$, 1.0 mM; $Ca(NO_3)_2.4H_2O$, 0.5 mM, $MgCl_2.6H_2O$ 1.1 mM, KCl 0.16 mM, $Na_{1.5}$-Pipes 10 mM. The slurry was prepared in a 1-L glass bottle fitted with a cap that incorporated a glass pressure tube with a thick rubber stopper through which samples could be collected by needle and syringe. The pH of the slurry was adjusted to 6.5 prior to bubbling with 100% N_2 to render the slurry anoxic. The slurries were inoculated with a small

quantity (2% vol/vol) of a suspension of undried sediment (10 g in 20 mL of PBAGW835) from the same depth interval. Two slurries were amended with 9 mM of ^{13}C-ethanol, and two slurries were left unamended. The slurries were incubated in the dark at 20 °C, and sampled periodically by syringe and needle for various aqueous and solid-phase geochemical parameters.

General analytical techniques. Dissolved Fe(II) concentrations in the slurries were determined by filtering (inside an anaerobic chamber) a 0.2-1.0 mL aliquot of slurry through a 0.22 μm nylon syringe filter directly into ferrozine (1 g L^{-1} in 50 mM Hepes) and reading the A_{562} with a Shimadzu UV-1201V spectrophotometer. Total (aqueous + solid-phase) Fe(II) was determined by extracting 0.5 mL slurry samples in 5 mL of 0.5 M HCl for 1h, followed by colorimetric analysis of Fe(II) with ferrozine. Total Fe in the HCl extracts was determined by after the addition of hydroxylamine-HCl, and Fe(III) concentrations were calculated from the difference between total Fe and Fe(II). The C/D-extractable Fe content of the slurries was determined by extracting 0.5 mL samples in 5 mL of 0.2 M sodium citrate/ 0.35 M acetic acid (pH 4.8) plus 0.5 g of sodium dithionite for 1h, and measuring the Fe(II) content of the extracts with ferrozine.

Samples for dissolved uranium were filtered (inside an anaerobic chamber) through a 0.22 μm nylon syringe filter into 0.01M HNO_3. Total (aqueous + solid-phase) U(VI) was determined by extracting 1 mL of slurry in 9 mL of anoxic 100 mM $NaHCO_3$ (*22*). The samples were placed on a rotary shaker for 1 h, centrifuged for 10 min at ca. 5000 × g, and a 1 mL aliquot of the supernatant was transferred to 9 mL of 0.01M HNO_3. The remaining supernatant was discarded, and 9 mL of 10% HNO_3 was added to the pellet. The samples were shaken for 1 hr, centrifuged and diluted 1:10 in distilled H_2O. Dissolved uranium, total U(VI), and residual uranium concentrations were analyzed with a Kinetic Phosphorescence Analyzer (KPA-11; Chemcheck Instruments, Richland, WA).

Samples for determination of acetate, nitrate, sulfate, and ethanol were obtained by filtration, and then exposed to atmospheric O_2 for ca. 30 min in order to oxidize Fe(II) (*24*). The samples were then centrifuged to remove Fe(III) oxide precipitates and stored frozen until analysis. Acetate, nitrate, and sulfate were analyzed on a Dionex model DX 100 ion chromatograph equipped with an IonPac®AS14 analytical column. Ammonium concentrations were determined colorimetrically (*25*)with a detection limit of 1 μM. Ethanol concentrations were determined on filtered samples by an enzymatic method (STAG; R-Biopharm GmbH, Darmstadt, Germany) with a detection limit of XX μM.

The partial pressure of CH_4 and CO_2 in the headspace of the slurry bottles was determined with a gas chromatograph (Shimadzu GC- 14A) equipped with a flame ionization detector and methanizer. Measured pCO_2 values were used to estimate DIC concentrations based Henry's law and the pH of the slurries (*26*). pH values were determined on 1 mL slurry samples with an Orion model 710A equipped with a Corning minielectrode.

^{57}Fe Mössbauer spectroscopy. Mössbauer analysis of the pristine sediment was performed on air-dried samples, while those of bioreduced sediments were performed on suspension subsamples that were filtered, washed, and dried in an anoxic chamber. Details of the Mössbauer instrumentation and sample preparation procedure were reported by Kukkadapu et al. (*27*). The prepared Mössbauer disks of the bioreduced sediments were stored at −80 °C in an anoxic chamber until analysis. A closed-cycle cryostat (ARS, Allentown, PA) was employed for low temperature (12K) measurements.

The Mössbauer data were modeled with the *Recoil* software using a Voigt-based spectral fitting routine (*28*). In the Voigt-based method, each distribution [quadrupole splitting distribution (QSD) and hyperfine field distribution (HFD)] is represented by a sum of Gaussians

having different positions, widths, and relative areas. The number of Gaussians used for a given fit was the minimum required for good statistics. The coefficients of variation of the spectral areas of the individual sites generally ranged between 1% and 2% of the fitted value. The following guidelines were used in the modeling of the Mössbauer data: (i) all doublets were assumed to be symmetric, (ii) for sextets, the ratios of the spectral areas of peak 1 to peak 3, and peak 2 to peak 3 were fixed at 3 and 2, respectively, (iii) coupling was not allowed between δ (isomer shift) or the CS (center shift) with the distributed hyperfine parameter [quadrupole splitting (Δ or QS)], and (iv) coupling was not allowed between the quadrupole shift parameter (ε) and the distributed hyperfine parameter (z).

PLFA and stable carbon isotope ratio analysis. Bacterial PLFA analyses were performed on 10-mL subsamples collected from duplicate slurries at different time points during the incubation. The samples were freeze-dried prior to extraction with the single-phase chloroform–methanol–buffer system of Bligh and Dyer (*29*), as modified by White et al. (*30*). The total lipid extract was fractionated into neutral lipids, glycolipids, and polar lipids by silicic acid column chromatography (*31*). The polar lipids were transesterified to the fatty acid methyl esters (FAMEs) by a mild alkaline methanolysis (*31*), with the Mayberry and Lane (*32*) method to protect cyclopropane PLFA and release plasmalogen ethers as dimethylacetals. The FAMEs were analyzed by gas chromatography/mass spectroscopy (GC/MS) using an Agilent 6890 series gas chromatograph interfaced to an Agilent 5973 mass-selective detector with a 50-m nonpolar column (0.2-mm I.D., 0.11-lm film thickness) with a temperature program of 100^{o}C initial temperature, 10^{o} C min^{-1} to 150^{o}C for a minute, 3^{o} C min^{-1} to 282^{o}C for 5 min with injector temperature at 270^{o}C and detector at 290^{o}C. Total analysis time was 55 min.

Measurements of stable carbon isotope ratios ($^{13}C/^{12}C$) in the detected PLFAs were performed on a Finnigan Delta Plus isotope ratio mass spectrometer (Thermo, Austin, TX) coupled to a GC-III Combustion interface and an Agilant 6890 gas chromatograph (Palo Alto, CA). The fatty acid methyl esters were separated on an HP-1 column (dimensions 50 m x 200 μm) with constant pressure at 43.7 psi. The oven (column) temperature was programmed to increase fro 60 to 150 ^{o}C at 10 ^{o}C min^{-1}, then to 312 ^{o}C at 3 ^{o}C min^{-1}.

Respiratory quinone analysis. The neutral lipid fraction of the Bligh and Dyer extract after fractionation on silicic acid columns was examined for respiratory ubiquinone and menaquinone isoprenologues by high-performance liquid chromatography/atmospheric pressure photoionization tandem mass spectrometry (HPLC/APPI/MS/MS) (*33,34*).

Nucleic acid extraction. All materials and solutions used for nucleic acid extraction were treated with the RNase inhibitor DEPC prior to use. Nucleic acids were extracted from subsamples of the ethanol-amended slurries (pooled 10-mL subsamples of duplicates) using method as described in Hurt et al. (*35*). This method involves grinding in liquid N_2, freeze-thawing and extended heating (65^{o}C) in high-salt denaturating buffer (pH 7.0) containing 4M guanidine isothiocyanate, and in extraction buffer (pH 7.0) containing 1% hexadecylmethylammonium bromide (CTAB) and 2% SDS. Following centrifugation, the supernatant was removed from the pellet and nucleic acids were extracted in chloroform and then precipitated in 0.6 vol isopropanol by centrifugation at 9000 *g* for 20 min. The nucleic acid pellet was resuspended in RNase-free H_2O, and RNA was separated from DNA using a Qiagen (Santa Clarita, CA) DNA/RNA purification system. The isolated RNA was incubated with RNase free DNAase (Promega, USA) at 37 ^{o}C for 35 min to remove traces of coextracted DNA. Complete removal of DNA from nucleic acid extracts was verified by PCR.

Reverses transcription and PCR amplification of 16S rRNA. Reverse transcription of 16S rRNA was performed using RETROscript kit (Ambion, USA) as specified by the manufacturer, with 907R primer (5-CCG TCA ATT CMT TTR AGT TT) serving as the reverse primer. The resulting cDNA was PCR amplified with 27f (5-AGA GTT TGA TCM TGG CTC AG) in combination with 907R. The PCR reaction (50 μL total volume) contained 1μL template cDNA, 5 μL 10X buffer (Applied biosystems, USA), 4 mM $MgCl_2$, 50 μM of each deoxynucleoside triphosphate (Epicenter Technologies, USA), 0.3 mM of each primer (MWG-Biotech, USA) and 2.5 U of *Taq* DNA polymerase (New England Biolabs, USA). PCR amplification was performed in a DNA thermal cycler (iCycler, Biorad) with an initial denaturation step (2 min, 94^{o}C) followed by 28 cycles of denaturation (30 s, 94^{o}C), annealing (45 s, 50^{o}C) and elongation (30 s, 72^{o}C). The final elongation step was extended to 8 min.

Cloning and sequencing. Amplicons obtained by RT-PCR were purified using QIAquick (QIAGEN #28106) according to manufacturer's instructions. The pGem®-T vector System II (Promega #A3600) was used according to manufacturer's instructions to generate clone libraries. Randomly selected clones were checked for correct insert size via standard vector-targeted PCR and gel electrophoresis. Both M13F and M13R primers were used separately for Big Dye terminator sequencing reaction as specified by the manufacturer (Applied Biosystems). Dye terminators were removed by CleanSEQ kits (Agencourt, USA) as per manufacturer instruction. Sequences were commercially obtained from the University of Wisconsin-Madison Biotechnology Center. Each sequence was analyzed by means of GenBank using BLAST (*36*) as well as the Ribosomal Database Project – II (*37*) in order to identify the closest relative. Sequences which were identified as chimeric were discarded. A value of 95% similarity in 16S rRNA sequence was established as a conservative cut-off for assignment of genus-level

phylogenetic affiliation (*38*). The final sets of sequences have been submitted to GenBank (Accession numbers XXXX –XXXX).

Results

Microbial redox metabolism. Ethanol (initial concentration 9 mM) was completely consumed within 2 weeks in the ethanol-amended slurries (Figure 1A). Substantial accumulation of acetate (up to ca. 7 mM) took place in conjunction with ethanol metabolism. A clearly defined temporal pattern of TEAPs was observed in the ethanol-amended slurries, with NO_3^- reduction, Fe(III) reduction, SO_4^{2-} reduction, and CH_4 production proceeding in sequence (Figure 1B-E, solid symbols) until all of the electron donor was consumed. Production of CH_4 (and DIC) was coupled to consumption of acetate after ca. 20 d incubation. Only a slow consumption of NO_3^- took place in the non-amended slurries; no reduction of Fe(III) or SO_4^{2-}, or production of CH_4 was observed (Figs. 1B-E, open symbols).

Approximately 60% of $NaHCO_3$-extractable U(VI) was reduced during the Fe(III) reduction phase between 4 and 12 d in the ethanol-amended slurries (Figure 1F). No further U(VI) reduction took place during the ensuing periods of sulfate reduction and methanogenesis. No significant reduction of $NaHCO_3$-extractable U(VI) took place in the unamended slurries. Dissolved U(VI) concentrations remained less than 1 μM in the non-amended slurries (Figure 1F, open triangles). In contrast, dissolved U(VI) concentrations increased to 2-3 μM during the period of CH_4 production in the ethanol-amended slurries (Figure 1F, closed triangles).

Phospholipid fatty acid (PLFA) and quinone analysis. The bulk abundance of PLFAs was significantly higher in ethanol-amended slurries compared to the unamended controls (Fig 2A). The ratio of ubiquinones to menaquinones was lower in the ethanol-amended slurries (Figure 2B). The latter result makes sense since both ubiquinones and menaquinones are utilized in

aerobic and denitrifying respiratory metabolism, whereas menaquinones are predominant in anaerobic respiratory pathways (*39*), which were obviously stimulated by ethanol addition.

All of the 19 individual PLFAs detected by GC/MS were more abundant in the ethanol-amended slurries (compare Figs. 3A and 3B). Three specific PLFAs (16:1w7C, 16:0, and 18:1w7C) showed a pronounced response to biostimulation. These same PLFAs, and well as several others (10Me16:0, i17:0, a17:0, cy17:0, 18:1w9c) showed significant incorporation of ^{13}C from the added ^{13}C-ethanol (Figure 3C).

16S rRNA clone libraries. Samples obtained from the prestimulation (0 d) time point did not provide sufficient rRNA for reverse transcription; hence a library was constructed with extracted 16S rDNA which was sufficient to provide template for PCR. Most of these clones belonged to the family *Clostrideaceae* (Table 1). Upon incubation with ethanol, reverse-transcribed 16S rRNA sequences related to the genera *Dechloromonas*, *Geobacter*, *Oxalobacter* became predominant in the 16S rRNA libraries, accounting for 66-88% of total clones. These three sequence types accounted for 13%, 31% and 22% of clones recovered at the end of the NO_3^- reduction phase (4 d sample); 10%, 41%, 22% at the end of the Fe(III) reduction phase (9 day sample); and 14%, 49%, and 20% at the end of the SO_4^{2-} reduction phase (day 14 sample). The frequency of *Dechloromonas* and *Geobacter* clones remained similar during methanogenic phase (day 23 and 35 samples), whereas the abundance of *Oxalobacter* declined.

Discussion

Fe(III) reduction. There were no systematic change in the amount of Fe(III) solubilized by 0.5M HCl extraction in either the ethanol-amended (1.7 ± 0.8 mmol L^{-1}) or unamended sediments (1.8 ± 1.0 mmol L^{-1}) slurries, which suggests that reduction of crystalline Fe(III) mineral phases (a small amount of which dissolved in the 0.5M HCl) was responsible for the

observed Fe(II) production. Low-temperature (12K) Mössbauer measurements revealed that the pristine (unreduced) sediment contained significant quantities of goethite (ca. 70% of total Fe) and phyllosilicate Fe (ca. 25% of total Fe), together with a small amount of hematite (< 5% of total Fe) (Figure 4A). Approximately 20% of the phyllosilicate Fe was in the Fe(II) redox state in the unreduced material; this ratio increased to greater than 60% in ethanol-amended samples collected at the end of the incubation experiment (Figure 4B). Decreases in the goethite and phyllosilicate Fe(III) contents of the reduced sediment, estimated by simulation of Mössbauer spectra, suggested that approximately equal amounts of 0.5M HCl-extractable Fe(II) were produced by goethite and phyllosilicate Fe(III) reduction. Mössbauer analysis of 0.5M HCl-extracted reduced sediment (Figure 4C) verified that 0.5M HCl extraction liberated most (> 75%) of the reduced phyllosilicate domains, as indicated by the similar phyllosilicate Fe(II)/Fe(III) ratios in the pristine (0.2) and 0.5 HCl-extracted reduced (0.25) material (see ref. (*40*) for more detailed discussion). In general our results are in agreement with other recent work on ORNL saprolite materials which indicate that both Fe(III) oxide (goethite) and phyllosilicate Fe(III) (e.g. illite) are quantitatively important electron acceptors for bacterial Fe(III) respiration (*40,41*).

Microbial community response to ethanol amendment. The three PLFAs (16:1w7C, 16:0, and 18:1w7C) which showed the most pronounced response to biostimulation in terms of total lipid biomass (Figure 2A,B) and ^{13}C incorporation (Figure 2C) are known to be abundant in the cell membranes of DIRB such as *Geobacter* and *Shewanella* (*42,43*). The high frequency of *Geobacteraceae*-related clones in 16S rRNA libraries from the ethanol-amended slurries (Table 1), together with the extensive Fe(III) activity observed in ethanol-amended slurries (Figure 1C), suggest that organisms from the *Geobacteraceae* (but not *Shewanella*) were stimulated by

ethanol addition. This conclusion is consistent with other recent studies of the response of Fe(III) oxide-bearing subsurface sediments to acetate or ethanol addition (*5,9,11,12*). These PLFAs are, however, widely distributed in other types of gram-negative bacteria (*44*), and it is likely that some portion of the response to biostimulation could be attributed to proliferation of other bacterial groups, including those discussed below.

Organisms related to *Dechloromonas* and *Oxalobacter* were present in relatively high frequency in the 16S rRNA libraries (Table 1). It is not possible to definitively infer a physiological function for these organisms in terms of response to ethanol addition. *Dechloromonas* is a denitrifying (and perchlorate-reducing) taxa that is widely-distributed in soil and sedimentary environments (*45*), and has been detected in 16S rDNA libraries from uncontaminated ORNL sediments (*11*). Such organisms may have been active during the initial nitrate reduction phase of the experiment, as observed in recent studies of acetate metabolism in freshwater sediments (*46*). The lack of significant ammonium production during nitrate reduction (data not shown) is consistent with denitrification as the main pathway for nitrate consumption. It is not clear, however, what role these organisms may or may not have played in the latter stages of the incubation when methanogenesis was the predominant TEAP.

Oxalobater is an anaerobic, oxalate-metabolizing organism which ubiquitous in natural sediments (*47,48*), and which has (like *Dechloromonas*) been detected in 16S rDNA libraries from uncontaminated subsurface sediments at ORNL (*49*). Oxalate degradation by *Oxalobacter* proceeds via a novel proton motive force-generating mechanism (*50*) which leads to production of equimolar amounts of CO_2 and formate (*51*). Serial (10-fold) dilution of ethanol-amended slurry samples (obtained at the end of the incubation experiment) in oxalate-containing growth medium (ATCC medium 1514) indicated growth (observed microscopically) up to 10^{-4} dilution,

which verified that oxalate-degrading organisms were present in the slurry. We speculated that organisms related to *Oxalobacter* could have played a role in ethanol degradation and/or Fe(III) reduction in the slurries via as yet unknown biochemical mechanisms. However, tests conducted with the type strain (*Oxalobacter formigenes*, ATCC 35274) showed that the organism was unable to grow by ethanol degradation, whereas active growth was observed in identical medium with oxalate (data not shown). *O. formigenes* was also unable to catalyze amorphous Fe(III) oxide reduction with either oxalate, ethanol, or acetate as an electron donor. Detailed enrichment, isolation, and characterization studies are required to determine the physiology of *Oxalobacter* spp. that proliferate in response to ethanol amendment. In addition, determination of the PLFA content of both *Dechloromonas* and *Oxalobacter* would be useful for constraining their potential contribution to PLFA profiles shown in Figure 3.

Neither the bulk PLFA measurements nor the 16S rRNA libraries provided strong evidence for proliferation of sulfate-reducing bacteria (SRB) tied to the brief period of sulfate reduction activity in the ethanol-amended slurries. However, there was a distinct upturn in ^{13}C incorporation into PLFAs indicative of SRBs from the genera *Desulfobacter* (10Me16:0, cy17:0), *Desulfotomaculum* (18:1w9c), and *Desulfovibrio* (i17:0) (*52-54*) between day 9 and 14 (Figure 3C), just at the time when sulfate reduction took place (see Figure 1D). This pattern contrasts with that for putative *Geobacteraceae*-specific PLFA ^{13}C:^{12}C ratios, which were elevated prior both prior to and after day 9. These results illustrate how metabolic stable isotope probing can reveal relatively subtle shifts in microbial community structure that are not discernible through bulk lipid biomarker analysis. The modest but significant apparent stimulation of *Desulfovibrio* is significant in terms of U(VI) reduction potential since

Desulfovibrio, but not *Desulfobacter* or *Desulfotomaculum*, is capable of enzymatic U(VI) reduction (*55*).

Terminal electron-accepting processes in ethanol-amended sediments. The sequence of TEAPs observed in the ethanol-amended slurries (NO_3^- reduction $\rightarrow$ Fe(III) reduction $\rightarrow$ SO_4^{2-} reduction $\rightarrow$ CH_4 production) conformed to classical thermodynamic expectations, with more energetically favorable reactions proceeding less favorable ones (*26,56,57*). Although the segregation of different TEAPs in space and time in sediments is actually determined by the physiological properties of the organisms that catalyze those TEAPs (see refs (*58*) and (*59*) for review), in most (but not all; cf. refs. (*60*) and (*61*)) situations, the sequence of redox reactions first outlined in thermodynamic terms by Ponnamperuma (*56*) (for hydromophic soils) and Froelich and colleagues (*62*) (for marine sediments) are obeyed in natural soil, sediment, and groundwater systems (*26,63*). The results of the subsurface sediment slurry experiments described here (Figure 1) provide an explicit verification of this basic principle.

A redox titration simulation was conducted with the geochemical modeling software PHREEQC (*19*) in order to illustrate how thermodynamic principles can be applied to the interpretation of TEAPs in reaction systems that arise during biostimulation with ethanol. This approach is analogous to that used by Scott and Morgan (*64*) to simulate the response of a model groundwater to input of organic carbon (CH_2O), and by Buffle and Stumm (*65*) to simulate the consumption of oxidants in the hypolimnion of a seasonally statified lake. The input file for the simulation is provided in Table S1. The stability constants (log K values) for various standard aqueous phase species are contained in the default PHREEQC database and were not altered. Optimized stability constants for aqueous U(VI) and U(IV) species (*20*), including provisional constants for Ca-U-CO_3^{2-} complexes ($CaUO_2(CO_3)_3^{2-}$ and $Ca_2UO_2(CO_3)_3$) (*21*), were included in

the input file. Amorphous uraninite (log K = 1.48 for the reaction $U^{+4} + 2H_2O = UO_2(s) + 4H^+$) was assumed to be the U(IV) solid-phase. The pH of the slurry was assumed to remain fixed at the mean value of 6.63 ± 0.09 during the experiment (see Figure 1B inset).

A quantity of reducing equivalents equal to 9 mM of ethanol (108 mmol e^- equiv L^{-1}) was titrated into an aqueous/solid-phase reaction system that mimicked the initial composition of the sediment slurry. The added ethanol was assumed to react instantaneously to thermodynamic equilibrium with the oxidants remaining in the system at any point in the titration according to the following half-reaction:

$$CH_3CH_2OH + 5H_2O = 2CO_3^{2-} + 16H^+ + 12e^- \qquad \log K = 54.65 \qquad (1)$$

The log K for this reaction was calculated from the ΔG_f for ethanol (-181.75 kJ mol^{-1}) given in ref. (*66*), together with standard ΔG_f values for H_2O and CO_3^{2-} (*26*). Although reduction of Fe(III)-bearing phyllosilicates was responsible for a substantial portion of the Fe(II) produced during the incubation (see above), goethite was assumed to be the Fe(III) mineral phase undergoing reduction in the ethanol-amended slurry since the redox properties of natural Fe(III)-bearing phyllosilicates are not well known. The assumed presence and microbial reduction of goethite phases is consistent with mineralogical analyses (electron microscopic imaging and Mössbauer spectroscopy) and microbial reduction experiments conducted with analogous saprolite materials from ORNL (*40,41*). The surface area of the goethite was set equal to 120 m^2 g^{-1} based on simulations of natural goethite reduction in sediments (*59*). Its thermodynamic stability was defined by an operational ΔG_f value of -487 kJ mol^{-1} based on H_2-catalyzed reduction of synthetic goethite phases by *G. sulfurreducens* (*59*). This ΔG_f corresponds to a log K value of 11.61 for the following half-reaction:

$$FeOOH(s) + 3H^+ + e^- = Fe^{2+}(aq) + 2H_2O \qquad (2)$$

Fe(II) produced during goethite reduction was assumed to adsorb to remaining goethite surfaces according to a Langmuir isotherm (*26*) fit (Γ_{max} = 3.67 × 10^{-6} mol sites m^{-2}; log K_{ads} = 3.8) to the aqueous/solid-phase speciation of Fe(II) observed in synthetic Fe(III) oxide reduction experiments with *G. sulfurreducens* (*59*). However, the maximum amount of Fe(II) that could have sorbed to goethite surfaces (ca. 1.25 mmol L^{-1}) was small relative to total solid-phase (HCl-extractable) Fe(II) production (ca. 15 mmol L^{-1}; see Figure 1C). A small amount (ca. 1 mmol L^{-1}) of iron sulfide formation is likely to have taken place during the sulfate reduction phase, and amorphous FeS (log K = -2.96 for the reaction Fe^{2+} + HS^- = FeS + H^+, derived from the ΔG_f value for amorphous FeS (-83.7 kJ mol^{-1}) listed in ref. (*1*)) was therefore allowed to precipitate to equilibrium in the simulation. Sorption of Fe(II) to additional, unspecified mineral surface and/or ion exchange sites (e.g. on Al oxides or phyllosilicates) was assumed to account for the bulk of solid-phase Fe(II) accumulation, since careful mineralogical analysis of microbially-reduced (*Shewanella putrefaciens* Strain CN32) ORNL saprolite failed to provide evidence for formation of distinct Fe(II)-bearing mineral products such as siderite or magnetite (*40*). The molar abundance of such surface sites was defined *a priori* by the bulk measured surface area of the solids (ca. 25 m^2 g^{-1}), the bulk mass loading of the slurry (227 g L^{-1}), and a standard mineral site density of 3.84 × 10^{-6} mol sites m^{-2} recommended by Davis and Kent (*67*). The coefficient for Fe(II) sorption to these sites (Langmuir isotherm) was the only adjustable parameter in the simulation. Higher values of K_{ads} produced a greater degree of Fe(II) sorption, which in turn led to a greater total amount of Fe(III) reduction because of the impact of aqueous Fe(II) on the thermodynamic favorability of goethite reduction (equation 2). Trial-and-error testing showed that a log K_{ads} value of 4.75 produced both a total amount of Fe(III) reduction and an

aqueous/solid phase Fe(II) partitioning (< 2 % in solution; see Figure 1C) comparable to that observed in the experiment.

The simulation accurately reproduced the pattern of TEAPs in the ethanol-amended slurries (Figure 5), with a few important exceptions. First, the measured amount of electron donating equivalents remaining in the system, when plotted against the total number of electron equivalents accounted for by the sum of NO_3^- consumption (5 e^- equiv mol^{-1}), SO_4^{2-} consumption (8 e^- equil mol^{-1}), Fe(II) production (1 e^- equiv mol^{-1}), and CH_4 production (8 e^- equiv mol^{-1}), did not match the linear relationship that was implicit in the simulation (Figure 5A). Incorporation of carbon into microbial biomass and (more importantly) transient accumulation of acetate (see Figure 1A) can account for this result, as well as the lower observed accumulation of DIC compared to the simulation (Figure 5E). A thermodynamics-based approach that takes into account the formation of microbial biomass as part of the redox reaction network has been applied to this dataset to depict the growth of various groups of fermentative and respiratory organisms (*68*). However, only kinetic models (discussed below) can reproduce the accumulation of acetate during partial oxidation of ethanol.

A key disconnect between the experimental data and the simulation results is that the simulation predicted rapid and complete reduction of U(VI) at the beginning of the Fe(III) reduction phase, whereas the actual rate of U(VI) reduction was much slower and did not proceed to completion (Figure 5F). Although sorption of U(VI) to Fe(III) oxide or other sorption/ion exchange sites was not included in the simulation, testing showed that inclusion of such reactions would not have altered the predicted uranium redox speciation. Other studies have documented incomplete reduction of solid-associated U(VI) in reduced subsurface sediments that contain excess electron donor and abundant Fe(II) (a potential chemical reductant

for U(VI)) (*17,23,69*). While the basis for this phenomenon remains unclear, it likely related to the availability of U(VI)-occupied surface sites to enzymatic reduction and/or the nature of U(VI) coordination at the solid-water interface (*23,70*). The persistence of substantial solid-associated U(VI) during active Fe(III) reduction provides an explanation for the increase in dissolved U(VI) that took place later on during the methanogenic phase of the experiment: complexation of residual U(VI) by DIC (> 10 mM) produced during methanogenic oxidation of acetate could have easily shifted the balance between aqueous and surface-associated U(VI) (*71*).

A recent evaluation of the thermodynamic stability of uraninite in the presence of Fe(III) oxides raised the possibility that extraction of sediment-associated U(VI) with high concentrations of DIC at elevated pH could lead to artifactual oxidation of uraninite by residual Fe(III) oxides in the sediment (*72*). The reason for this is that the presence of high DIC and pH conditions moves the uranium redox speciation system into a region where uraninite oxidation by Fe(III) oxides becomes thermodynamically favorable. This same concept was put forward as an explanation for the oxidation of uraninite in high DIC-containing methanogenic column reactors constructed with sediment similar to the material used in our slurry experiments (*17*). If true, this effect would have important practical implications for assessing U(VI) reduction potential in Fe(III) oxide-bearing sediments. PHREEQC was used to evaluate the potential significance of this phenomenon in our experiments: the program was used to simulate the addition of 1 mL of reduced slurry at the end of the redox titration (in which all U(VI) had been converted to uraninite, and in which 18 mmol L^{-1} of residual goethite remained) to 9 mL of anoxic 100 mM $NaHCO_3$ in a 20-mL serum bottle (10 mL headspace). The results indicated that oxidation of uraninite by residual goethite was not thermodynamically favorable under these

conditions, and suggest that the observed persistence of U(VI) in the ethanol-amended slurries was real.

Limitations on U(VI) reduction. A follow-up experiment was conducted with subsamples of the reduced slurries to assess possible metabolic (as opposed to geochemical) reasons for incomplete U(VI) reduction observed in the ethanol-amended slurries. The PLFA and 16S rRNA clone library data (see above) suggested that DIRB and SRB were present in the slurries during the latter stages of the incubation, and we speculated that depletion of their preferred electron acceptors may have limited their ability to reduce U(VI) reduction in the slurries. Duplicate slurry subsamples were amended with nothing (control), 5 mM ethanol, 5 mM ethanol + 10 mmol L^{-1} of synthetic amorphous Fe(III) oxide, 5 mM ethanol + 2 mM SO_4^{2-}, or 5 mM ethanol + 0.1 mM AQDS. Addition of Fe(III) oxide and sulfate were designed to stimulate DIRB and SRB activities. AQDS is a soluble electron shuttling compound that accelerates rates of microbial Fe(III) oxide reduction in sediments (*73*), and that may stimulate solid-associated U(VI) reduction by reacting with U(VI) associated with sediment surfaces that are inaccessible to direct microbial reduction (*23*).

None of the treatments stimulated significant additional U(VI) reduction (Figure 6A), despite the presence of active microbial metabolism as indicated by additional Fe(II) accumulation (Figure 6B), sulfate consumption (Figure 6C), and CH_4 production (Figure 6C). AQDS stimulated reduction of residual Fe(III) phases in the sediment (Figure 6B), but in contrast to previous studies (*23*) did not promote solid-associated U(VI) reduction. Separate studies of Fe(III) and U(VI) reduction in uranium-contaminated Area 2 sediment by *G. sulfurreducens* (10^8 cells mL^{-1} of acetate/fumarate-grown cells; see ref. (*23*) for a description of methods) confirmed that only partial (ca. 50%) U(VI) reduction took place and that AQDS

stimulated Fe(III) reduction but not solid-associated U(VI) reduction (data not shown). Together these results indicate that the main limitation posed on residual U(VI) reduction was geochemical rather than microbiological in nature.

Practical Implications. There are two key practical implications of this study. First, the results suggest that standard conceptual models of TEAPs in sediment should be valid for predicting the response of ORNL FRC Area 2 (and other) subsurface sediments to in situ ethanol amendment, i.e. in terms of the segregation of major TEAPs over space and time. A sequence of TEAPs analogous to that observed in the slurry incubation (up to the point of sulfate reduction) was in fact recently documented in a push-pull test (*74*) and an in situ ethanol biostimulation experiment conducted at the Area 2 research site (S.C. Brooks, T.D. Scheibe, W. Kamolpornwijit, S.R. Mohanty, and E.E. Roden, unpublished data). The thermodynamic (redox titration) simulation approach used to interpret the slurry data is not appropriate for use in field-scale reactive transport simulations of in situ experiments, because ethanol does not react instantaneously to thermodynamic equilibrium in natural low-temperature systems. Nevertheless, the conformation of the data to thermodynamic theory provides a sound basis for development of microbial physiology-based kinetic models which can reproduce the zonation of TEAPs typically observed over space and/or time in sediment systems (cf refs. (*59,75-77*)). In addition, the detection by rRNA and PLFA methods of functional groups of microorganisms known to be associated with major TEAPs (see above) provides confirmation that such groups were in fact activated during ethanol biostimulation. The slurry data have been used as a basis for development of a kinetic microbial reaction model that accurately reproduces the consumption of ethanol, transient accumulation of acetate, and major TEAPs observed in the slurry experiment (*78*) and in a push-pull tests at Area 2 (*74*). An analogous kinetic reaction model (*79*) was incorporated into the

general biogeochemical simulator BIOGEOCHEM (*80,81*), which was in turn linked to the reactive transport code HYDROGEOCHEM (*82*) and used to design and interpret the in situ biostimulation experiment at Area 2.

A second key implication of our findings is that the redox behavior of uranium, unlike other major redox couples, could not be explained on the basis of standard thermodynamic considerations. The seemingly irreversible association of U(VI) with particle surfaces that are inaccessible to enzymatic (and abiotic) reduction observed here and in other subsurface sediments (*23,69,70*) is puzzling and cannot be rationalized in terms of existing models of aqueous/solid-phase U speciation (*1*). This phenomenon is of practical significance in that it may limit the overall effectiveness of in situ remediation of highly-contaminated U(VI) source zones such as those present at ORNL. Our results highlight the need for studies on the physiochemical nature of the such non-reducible U(VI) species.

Acknowledgments

The work was supported by grants DE-FG02-06ER64184 and ER64172-1027487-001191 from the Environmental Remediation Science Program, Office of Biological and Environmental Research, U.S. Department of Energy.

Supporting Information Available

Depth distributions of solid-phase U (Figure S1) and Fe (Figure S2) in FRC Area 2 sediments, and input file for PHREEQC redox titration simulation (Table S1). This material is available free of charge via the Internet at http://pubs.acs.org.

Table 1. Relative proportions of 16S rRNA frequencies in cDNA clone libraries from the ethanol-amended slurries. The libraries were constructed with reverse-transcribed rRNA extracted from pooled 10-mL samples from duplicate slurries. A sequence similarity of 95% was used as cutoff value for genus (or family) level identification. Number in the parenthesis represents total number of clones analyzed.

	Day of Sampling					
Taxa	0 d (90)	4 d (114)	9 d (87)	14 d (77)	23 d (104)	35 d (136)
Azonexus	1	2	0	2	2	1
Anaeromyxobacter	2	1	1	2	0	3
Bacteria from Anoxic soils	0	1	2	3	3	2
Burkholderaceae	2	10	1	0	2	0
Clostrideaceae	40	0	8	2	2	0
Dechloromonas	3	15	9	11	28	40
Desulfotomaculum	4	0	1	0	0	0
Desulfosporomusa	2	0	0	1	0	0
Desulfosporosinus	1	1	0	1	0	1
Flavobacterium	3	0	0	0	0	0
Geobacteraceae	5	35	36	38	43	67
Methylocystis	2	0	0	0	1	0
Methylosinus	0	0	0	0	0	1
Oxalobacter	0	25	19	15	8	12
Ralstonia	1	2	1	0	1	1
Rhodocyclaceae	3	4	2	0	8	1
Solibacter	0	0	1	0	2	5
Uncultured	4	1	4	0	2	0
Others	17	17	2	2	2	2

Figure 1. Redox metabolism in the ethanol-amended (closed symbols) and unamended (open symbols) slurries. Each data point represents the mean of duplicate slurries. The high temporal variability in HCl-extractable Fe(II) content is due to difficulty in obtaining subsamples (via needle and syringe) with uniform particle density.

Figure 2. Total PLFA abundance (A) and ratio of ubiquinone (UB) to menaquinone (MK) abundance in ethanol-amended and unamended slurries. Each data point represents the mean of duplicate slurries.

Figure 3. Specific PLFA abundances in the unamended (A) and ethanol-amended slurries (B), and ^{13}C incorporation into PLFAs in the ethanol-amended slurries, expressed as the ratio of ^{13}C to ^{12}C in the PLFA (C). Each bar represents the mean of duplicate slurries. The designations shown in panel C are provisional, based on the known PLFA contents of relevant groups of microorganisms, including various gram negative (G-) and sulfate-reducing bacteria (SRB), and organisms associated with the genera *Geobacter* (Gb), *Shewanella* (Sh), *Desulfobacter* (Db), *Desulfovibrio* (Dv), and *Desulfotomaculum* (Dm).

Figure 4. Mossbauer (12K) spectra of (a) undreduced, (b) reduced (ethanol-amended), and (c) reduced 0.5M HCl-extracted sediment. Spectra were fitted (lines) as described in the Experimental Section.

Figure 5. Equilibrium thermodynamic simulation of ethanol-amended slurry results using PHREEQC. Reactant or product concentrations (symbols) are plotted against the cumulative

number of electron equivalents accounted for by electron acceptor consumption (NO_3^-, SO_4^{2-}) and end-product accumulation (Fe(II), CH_4). The amount of electron donating equivalents remaining in the slurries (panel A) was computed from the amount of ethanol (12 e^- equiv mol^{-1}) and acetate (8 e^- equiv mol^{-1}) measured in solution at a given time point. Solid lines show results of a redox titration simulation as described in text.

Figure 6. Results of follow-up experiment to assess possible metabolic limitations on residual U(VI) reduction. All slurries except the control were amended with 5 mM ethanol and either 10 mmol L^{-1} of synthetic amorphous Fe(III) oxide, 2 mM sulfate, or 0.1 mM AQDS. Data points represent the means of duplicate slurries.

Figure 1

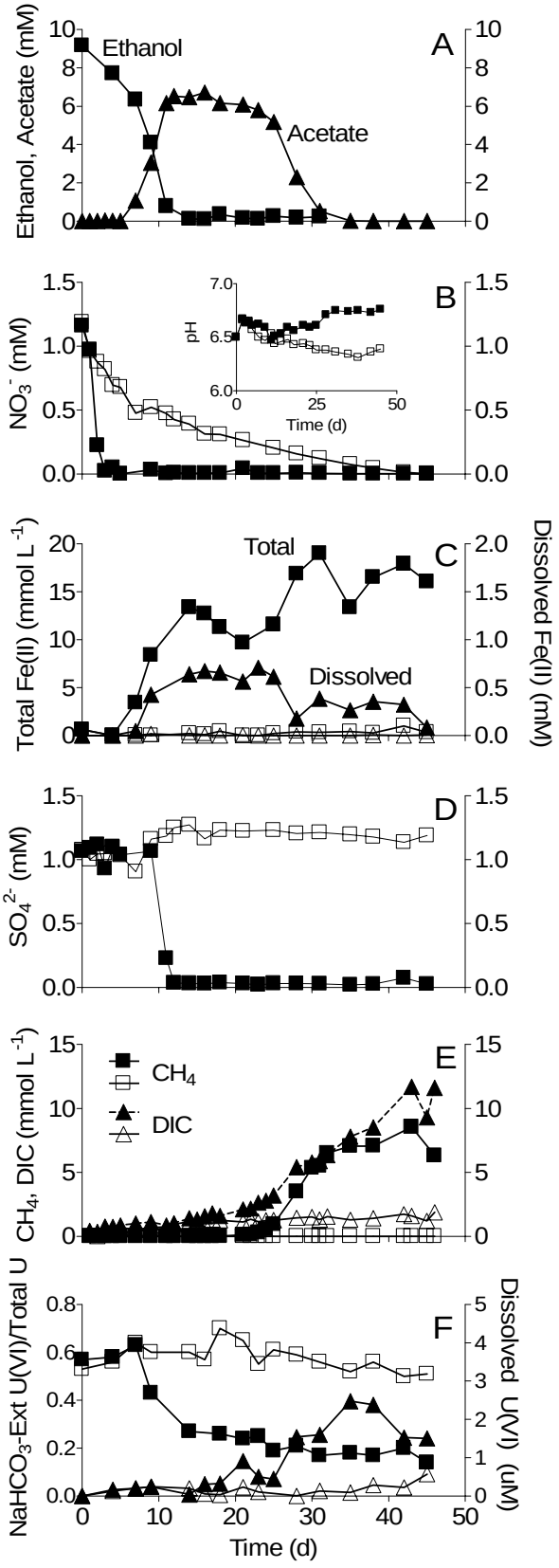
Ethanol
Acetate
A
Ethanol, Acetate (mM)
B
NO_3^- (mM)
pH
Time (d)
Total
Dissolved
C
Total Fe(II) (mmol L^{-1})
Dissolved Fe(II) (mM)
D
SO_4^{2-} (mM)
CH_4
DIC
E
CH_4, DIC (mmol L^{-1})
F
$NaHCO_3$-Ext U(VI)/Total U
Dissolved U(VI) (uM)
Time (d)

Figure 2

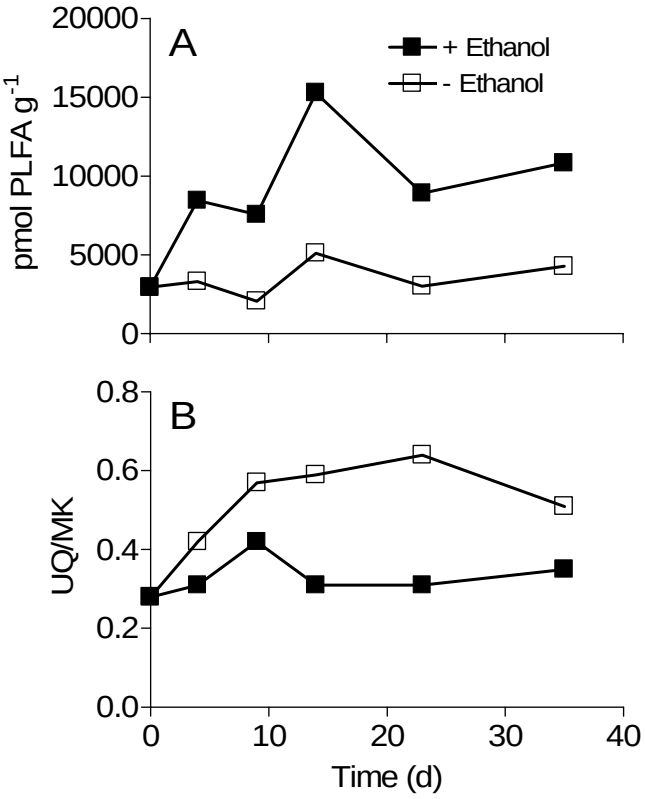
A
+ Ethanol
- Ethanol
pmol PLFA g-1
20000
15000
10000
5000
0
B
UQ/MK
0.8
0.6
0.4
0.2
0.0
0
10
20
30
40
Time (d)

Figure 3

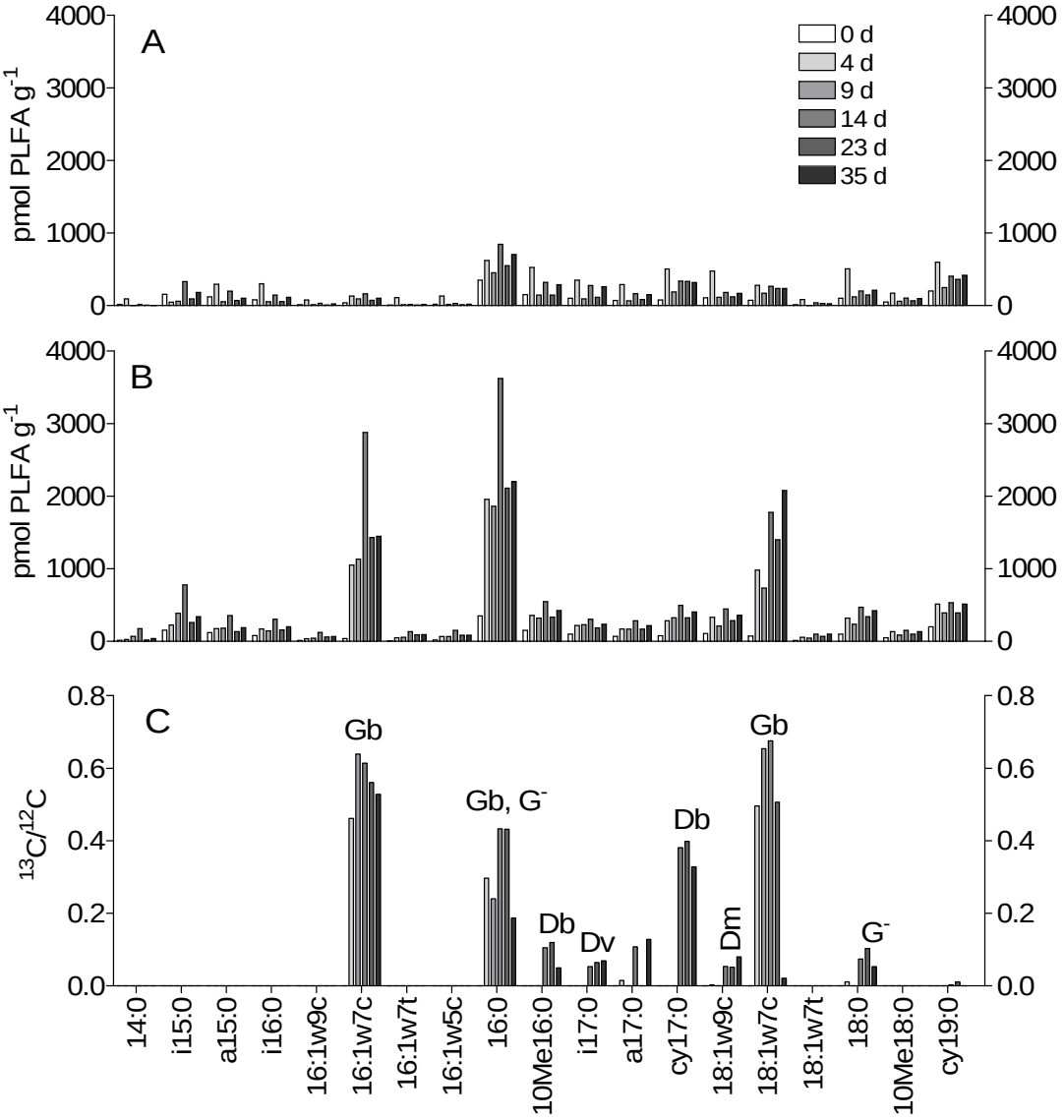
A
B
C
0 d
4 d
9 d
14 d
23 d
35 d
pmol PLFA g-1
13C/12C
Gb
Gb, G-
Db
Dv
Db
Dm
Gb
G-
14:0
i15:0
a15:0
i16:0
16:1w9c
16:1w7c
16:1w7t
16:1w5c
16:0
10Me16:0
i17:0
a17:0
cy17:0
18:1w9c
18:1w7c
18:1w7t
18:0
10Me18:0
cy19:0

Figure 4

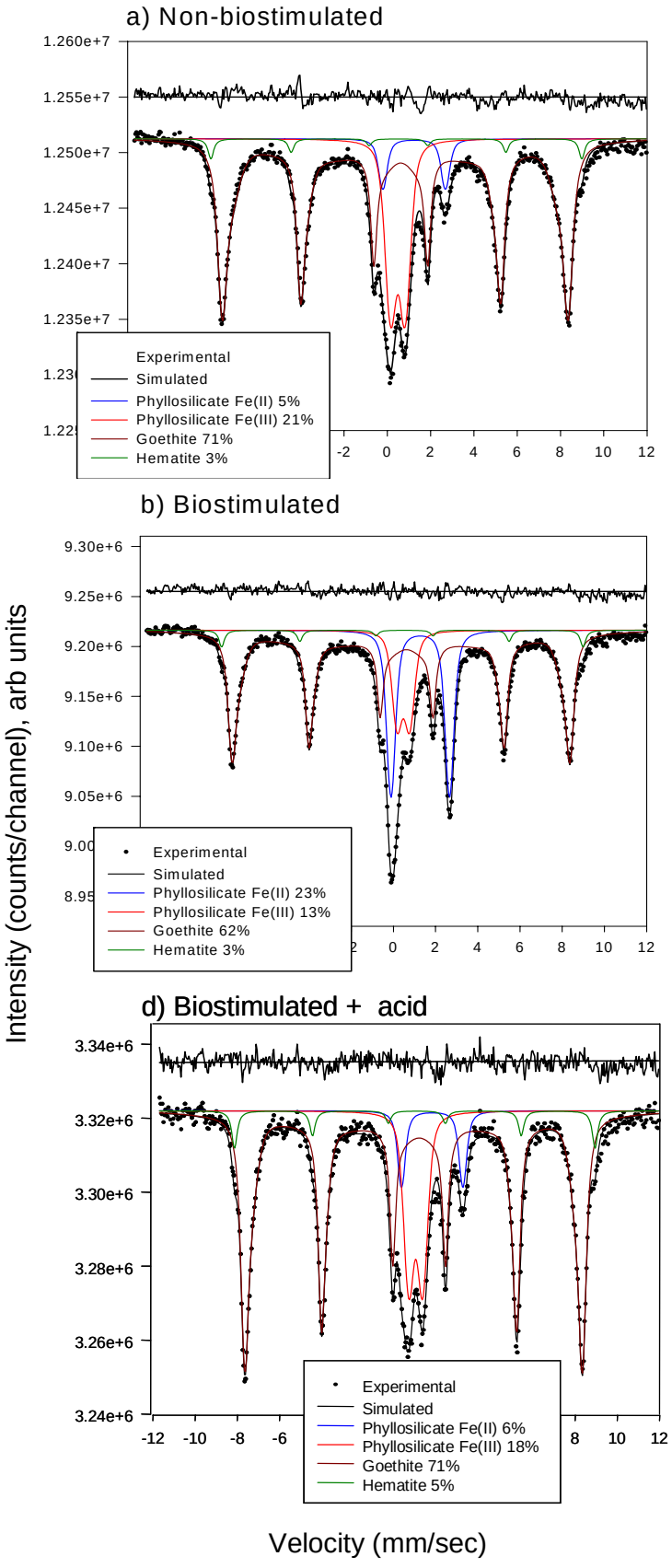
a) Non-biostimulated
1.260e+7
1.255e+7
1.250e+7
1.245e+7
1.240e+7
1.235e+7
Experimental
Simulated
Phyllosilicate Fe(II) 5%
Phyllosilicate Fe(III) 21%
Goethite 71%
Hematite 3%
-2
0
2
4
6
8
10
12
b) Biostimulated
9.30e+6
9.25e+6
9.20e+6
9.15e+6
9.10e+6
9.05e+6
Experimental
Simulated
Phyllosilicate Fe(II) 23%
Phyllosilicate Fe(III) 13%
Goethite 62%
Hematite 3%
d) Biostimulated + acid
3.34e+6
3.32e+6
3.30e+6
3.28e+6
3.26e+6
3.24e+6
Experimental
Simulated
Phyllosilicate Fe(II) 6%
Phyllosilicate Fe(III) 18%
Goethite 71%
Hematite 5%
-12
-10
-8
-6
8
10
12
Intensity (counts/channel), arb units
Velocity (mm/sec)

Figure 5

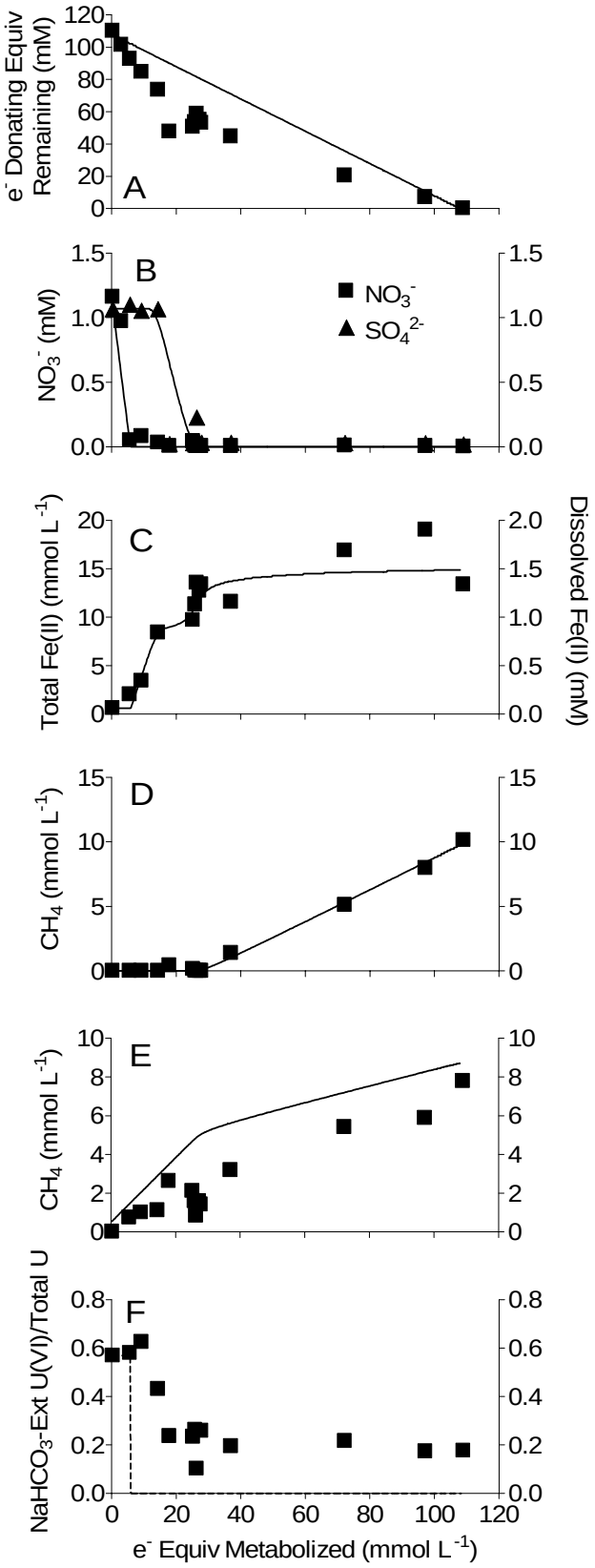
e- Donating Equiv Remaining (mM)
A
B
NO3-
SO4 2-
NO3- (mM)
C
Total Fe(II) (mmol L-1)
Dissolved Fe(II) (mM)
D
CH4 (mmol L-1)
E
CH4 (mmol L-1)
F
NaHCO3-Ext U(VI)/Total U
e- Equiv Metabolized (mmol L-1)

Figure 6

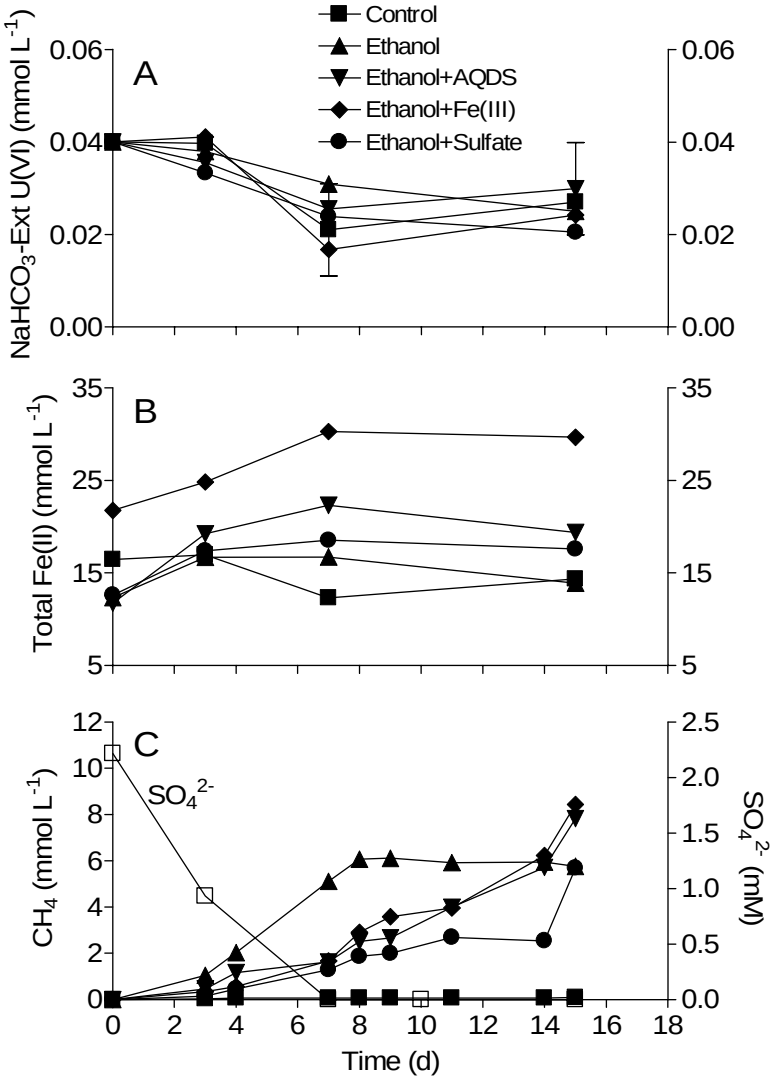
Control
Ethanol
Ethanol+AQDS
Ethanol+Fe(III)
Ethanol+Sulfate
A
B
C
NaHCO3-Ext U(VI) (mmol L-1)
Total Fe(II) (mmol L-1)
CH4 (mmol L-1)
SO4 2-
SO4 2- (mM)
Time (d)

Literature Cited

(1) Langmuir, D. *Aqueous Environmental Geochemistry*; Prentice Hall: Upper Saddle River, NJ, 1997.

(2) Lovley, D. R.; Phillips, E. J. P.; Gorby, Y. A.; Landa, E. R. *Nature* 1991, *350*, 413-416.

(3) Gorby, Y. A.; Lovley, D. R. *Environ. Sci. Technol.* 1992, *26*, 205-207.

(4) Senko, J. M.; Istok, J. D.; Suflita, J. M.; Krumholz, L. R. *Environ. Sci. Technol.* 2002, *36*, 1491-1496.

(5) Anderson, R. T.; Vrionis, H. A.; Ortiz-Bernad, I.; Resch, C. T.; Long, P. E.; Dayvault, R.; Karp, K.; Marutzky, S.; Metzler, D. R.; Peacock, A.; White, D. C.; Lowe, M.; Lovley, D. R. *Appl. Environ. Microbiol.* 2003, *69*, 5884-5891.

(6) Istok, J. D.; Senko, J. M.; Krumholz, L. R.; Watson, D.; Bogle, M. A.; Peacock, A.; Chang, Y. J.; White, D. C. *Environ. Sci. Technol.* 2004, *28*, 468-475.

(7) Wu, W.-M.; Carley, J.; Gentry, T.; Ginder-Vogel, M. A.; Fienen, M.; Mehlhorn, T.; Yan, H.; Caroll, S.; Pace, M. N.; Nyman, J.; Luo, J.; Gentile, M. E.; Fields, M. W.; Hickey, R. F.; Gu, B.; Watson, D.; Cirpka, O. A.; Zhou, J.; Fendorf, S.; Kitanidis, P. K.; Jardine, P. M.; Criddle, C. S. *Environ. Sci. Technol.* 2006, *40*, 3986-3995.

(8) Finneran, K. T.; Anderson, R. T.; Nevin, K. P.; Lovley, D. R. *Soil Sed. Contamin.* 2002, *11*, 339-357.

(9) Holmes, D. E.; Finneran, K. T.; O'Neil, R. A.; Lovley, D. R. *Appl. Environ. Microbiol.* 2002, *68*, 2300-2306.

(10) Petrie, L.; North, N. N.; Dollhopf, S. L.; Balkwill, D. L.; Kostka, J. E. *Appl. Environ. Microbiol.* 2003, *69*, 7467-7479.

(11) North, N. N.; Dollhopf, S. L.; Petrie, L.; Istok, J. D.; Balkwill, D. L.; Kostka, J. E. *Appl. Environ. Microbiol.* 2004, *70*, 4911-4920.

(12) Chang, Y. J.; Long, P. E.; Geyer, R.; Peacock, A. D.; Resch, C. T.; Sublette, K.; Pfiffner, S.; Smithgall, A.; Anderson, R. T.; Vrionis, H. A.; Stephen, J. R.; Dayvault, R.; Ortiz-Bernad, I.; Lovley, D. R.; White, D. C. *Environ. Sci. Technol.* 2005, *39*, 9039-9048.

(13) Vrionis, H. A.; Anderson, R. T.; Ortiz-Bernad, I.; O'Neill, K. R.; Resch, C. T.; Peacock, A. D.; Dayvault, R.; White, D. C.; Long, P. E.; Lovley, D. R. *Appl. Environ. Microbiol.* 2005, *71*, 6308-6318.

(14) Peacock, A. D.; Chang, Y. J.; Istok, J. D.; Krumholz, L. R.; Geyer, R.; Kinsall, B.; Watson, D.; Sublette, K. L.; White, D. C. *Microb. Ecol.* 2004, *47*, 284-292.

(15) Gu, B.; Wu, W.-M.; Ginder-Vogel, M. A.; Yan, H.; Fields, M. W.; Zhou, J.; Fendorf, S.; Criddle, C. S.; Jardine, P. M. *Environ. Sci. Technol.* 2005, *39*, 4841-4847.

(16) Wu, W. M.; Gu, B.; Fields, M. W.; Gentile, M.; Ku, Y. K.; Yan, H.; Tiquias, S.; Yan, T.; Nyman, J.; Zhou, J.; Jardine, P. M.; Criddle, C. S. *Bioremediation J.* 2005, *9*, 49-61.

(17) Wan, J.; Tokunaga, T. K.; Brodie, E.; Wang, Z.; Zheng, Z.; Herman, D.; Hazen, T. C.; Firestone, M. K.; Sutton, S. R. *Environ. Sci. Technol.* 2005, *39*, 6162-6169.

(18) Moon, J. W.; Roh, Y.; Phelps, T. J.; Phillips, D. H.; Watson, D. B.; Kim, Y. J.; Brooks., S. C. *J. Environ. Qual* 2006, *35*, 1731-1741.

(19) Parkhurst, D. A.; Appelo, C. A. *Water-Resources Investigation Report 99-4259* 1999.

(20) Guillaumont, R.; Fanghanel, T.; Fugen, J.; Grenthe, I.; Neck, V.; Palmer, D. A.; Rand, M. H. *Update on the Chemical Thermodynamics of Uranium, Neptunium, Plutonium, Americium, and Technicium*; Elsevier Science Publ.: Amsterdam, 2003.

(21) Bernhard, G.; Geipel, G.; Reich, T.; Brendler, V.; Amayri, S.; Nitsche, H. *Radiochimica Acta* 2001, *89*, 511-518.
(22) Phillips, E. J. P.; Landa, E. R.; Lovley, D. R. *J Ind Microbiol* 1995, *14*, 203-207.
(23) Jeon, B. H.; Kelly, S. D.; Kemner, K. M.; Barnett, M. O.; Burgos, W. D.; Dempsey, B. A.; Roden, E. E. *Environ. Sci. Technol.* 2004, *38*, 5649-5655.
(24) Weber, K. A.; Picardal, F. W.; Roden, E. E. *Environ. Sci. Technol.* 2001, *35*, 1644-1650.
(25) Wetzel, R. G.; Likens, G. E. *Limnological analyses*; Springer-Verlag: New York, 1991.
(26) Stumm, W.; Morgan, J. J. *Aquatic Chemistry*; 2nd ed.; John Wiley & Sons, Inc.: New York, 1996.
(27) Kukkadapu, R. K.; Zachara, J. M.; Fredrickson, J. K.; Kennedy, D. W. *Geochim. Cosmochim. Acta* 2004, *68*, 2799-2814.
(28) Rancourt, D. G.; Ping, J. Y. *Nucl. Instrum. Meth. Phy. Rev.* 1991, *58*, 85-97.
(29) Bligh, E. G.; Dyer, W. J. *Can J Biochem Physiol* 1954, *37*, 911-917.
(30) White, D. C.; Stair, J. O.; Ringelberg, D. B. *J Ind Microbiol* 1996, *17*, 185-196.
(31) Guckert, J. B.; Antworth, C. P.; Nichols, P. D.; White, D. C. *FEMS Microbiol. Ecol.* 1985, *31*, 147-158.
(32) Mayberry, W. R.; Lane, J. R. *J Microbiol Methods* 1993, *18*, 21-32.
(33) Lytle, C. A.; Gan, Y. D.; Salone, K.; White, D. C. *Environ Microbiol* 2001, *3*, 265-272.
(34) Lytle, C. A.; J., V. B. G.; White, D. C. *49th American Society for Mass Spectroscopy Meeting Proceedings, Chicago, IL May 27-31, TPC 074.* 2001.
(35) Hurt, R.; Qiu, X.; Wu, L.; Roh, Y.; Palumbo, A. V.; Tiedje, J. M.; Zhou, J. *Appl. Environ. Microbiol* 2001, *67*, 4495-4503.
(36) Altschul, S. F.; Madden, T. L.; Schaffer, A. A.; Zhang, J. H.; Zhang, Z.; Miller, W.; Lipman, D. J. *Nucleic Acids Res.* 1997, *25*, 3389-3402.
(37) Cole, J. R.; Chai, B.; Marsh, T. L.; Farris, R. J.; Wang, Q.; Kulam, S. A.; Chandra, S.; McGarrell, D. M.; Schmidt, T. M.; Garrity, G. M.; Tiedje, J. M. *Nucleic Acids Res.* 2003, *31*, 442-443.
(38) Gillis, M.; Vandamme, P.; DeVos, P.; Swings, J.; Kersters, K. In *Bergey's Manual of Systematic Bacteriology*; Second ed.; Boone, D. R., Castenholz, R. W., Eds.; Springer: New York, 2001; Vol. 1, pp 43-48.
(39) Hedrick, D. B.; White, D. C. *J Microbiol Methods* 1986, *5*, 243-254.
(40) Kukkadapu, R. K.; Zachara, J. M.; Fredrickson, J. K.; Kennedy, D. W.; Smith, S. C.; Dong, H. *Geochim. Cosmochim. Acta* 2006, *70*, 3662-3676.
(41) Stucki, J. W.; Lee, K.; Goodman, B. A.; Kostka, J. E. *Geochim. Cosmochim. Acta* 2007, *71*, 835-843.
(42) Lovley, D. R.; Giovannoni, S. J.; White, D. C.; Champine, J. E.; Phillips, E. J. P.; Gorby, Y. A.; Goodwin, S. *Arch. Microbiol* 1993, *159*, 336-344.
(43) Zhang, C. L. L.; Li, Y. L.; Ye, Q.; Fong, J.; Peacock, A. D.; Blunt, E.; Fang, J. S.; Lovley, D. R.; White, D. C. *Chem. Geol.* 2003, *195*, 17-28.
(44) Wilkinson, S. G. In *Microbial Lipids*; Ratledge, C., Wilkinson, S. G., Eds.; Academic Press: New York, 1988; Vol. 1, pp 299-323.
(45) Coates, J. D.; Michaelidou, U.; Bruce, R. A.; O'Connor, S. M.; Crespi, J. N.; Achenbach, L. A. *Appl. Environ. Microbiol.* 1999, *65*, 5234-5241.
(46) Weber, K. A.; Churchill, P. F.; Urrutia, M. M.; Kukkadapu, R. K.; Roden, E. E. *Environ. Microbiol.* 2006, *8*, 100-113.
(47) Smith, R. L.; Strohmaier, F. E.; Oremland, R. S. *Arch. Microbiol.* 1985, *141*, 8-13.

(48) Smith, R. L.; Oremland, R. S. *Appl. Environ. Microbiol.* 1983, *46*, 106-113.
(49) Reardon, C. L.; Cummings, D. E.; Petzke, L. M.; Kinsall, B. L.; Watson, D. B.; Peyton, B. M.; Geesey, G. G. *Appl. Environ. Microbiol* 2004, *70*, 6037-6046.
(50) Kuhner, C.; Hartman, P.; Allison, M. *Appl. Environ. Microbiol.* 1996, *62*, 2494-2500.
(51) Dawson, K. A.; Allison, M. J.; Hartman, P. A. *Appl. Environ. Microbiol.* 1980, *40*, 833-839.
(52) Taylor, J.; Parkes, R. J. *J. Gen. Microbiol.* 1983, *129*, 3303-3309.
(53) Dowling, N. J. E.; Widdel, F.; White, D. C. *J. Gen. Microbiol.* 1986, *132*, 1815-1825.
(54) Londry, K. L.; Jahnke, L. L.; Marais, D. J. D. *Appl. Environ. Microbiol.* 2004, *70*, 745-751.
(55) Lovley, D. R.; Roden, E. E.; Phillips, E. J. P.; Woodward, J. C. *Mar. Geol.* 1993, *113*, 41-53.
(56) Ponnamperuma, F. N. *Adv. Agron.* 1972, *24*, 29-96.
(57) Zehnder, A. J. B.; Stumm, W. In *Biology of anaerobic microorganisms*; Zehnder, A. J. B., Ed.; John Wiley & Sons: New York, 1988; pp 1-38.
(58) Lovley, D. R.; Chapelle, F. H. In *Mathematical Modeling in Microbial Ecology*; Koch, A. L., Robinson, J. A., Milliken, G. A., Eds.; Cahpman and Hall: New York, 1998; pp 196-209.
(59) Roden, E. E. In *Kinetics of Water-Rock Interactions*; Springer: New York, 2008.
(60) Jakobsen, R.; Albrechtsen, H. J.; Rasmussen, M.; Bay, H.; Bjerg, P.; Christensen, T. H. *Environ. Sci. Technol.* 1998, *32*, 2142-2148.
(61) Jakobsen, R.; Postma, D. *Geochim. Cosmochim. Acta* 1999, *63*, 137-151.
(62) Froelich, P. N.; Klinkhammer, G. P.; Bender, M. L.; Luedtke, N. A.; Heath, G. R.; Cullen, D.; Dauphin, P.; Hammond, D.; Hartman, B.; Maynard, V. *Geochim. Cosmochim. Acta* 1979, *43*, 1075-1090.
(63) Banwart, S. A.; Thornton, S. F. In *Bioremediation: A Critical Review*; Head, I. M., Singleton, I., Milner, Eds.; Horizon Scientific: Wymondham, 2003; pp 93-138.
(64) Scott, M. J.; Morgan, J. J. In *Chemical Modeling of Aqueous Systems II*; Melchoir, D. C., Basset, R. L., Eds.; American Chemical Society: Washington, DC, 1990.
(65) Buffle, J.; Stumm, W. In *Chemical and biological regulation of aquatic systems*; Buffle, J., DeVitre, R. R., Eds.; Lewis: Boca Raton, 1994; pp 1-43.
(66) Thauer, R. K.; Jungermann, K.; Decker, K. *Bacteriol. Rev.* 1977, *41*, 100-180.
(67) Davis, J. A.; Kent, D. B. In *Mineral-water interface geochemistry*; Hochella, M. F., White, A. F., Eds.; Mineralogical Society of America: Washington, DC, 1990; pp 177-260.
(68) Istok, J. D. *Manuscript in prep* 2007.
(69) Ortiz-Bernad, I.; Anderson, R. T.; Vrionis, H. A.; Lovley, D. R. *Appl. Environ. Microbiol.* 2004, *70*, 7558-7560.
(70) Jeon, B. H.; Barnett, M. O.; Burgos, W. D.; Dempsey, B. A.; Roden, E. E. *Environ. Sci. Technol.* 2005, *39*, 5642-5649.
(71) Barnett, M. O.; Jardine, P. M.; Brooks, S. C. *Environ. Sci. Technol.* 2002, *36*, 937-942.
(72) Ginder-Vogel, M.; Criddle, C. S.; Fendorf, S. *Environ. Sci. Technol.* 2006, *40*, 3544-3550.
(73) Lovley, D. R.; Coates, J. D.; Blunt-Harris, E. L.; Phillips, E. J. P.; Woodward, J. C. *Nature* 1996, *382*, 445-448.
(74) Jin, Q.; Zu, C.; Zhen, Z. *Groundwater* 2007, *Submitted for publication*.

(75) Watson, I. A.; Oswald, S. E.; Mayer, R. U.; Wu, Y.; Banwart, S. A. *Environ. Sci. Technol.* 2003, *37*, 3910-3919.
(76) Wirtz, K. A. *FEMS Microbial Ecology* 2003, *46*, 295-306.
(77) Thullner, M.; Van Cappellen, P.; Regnier, P. *Geochim. Cosmochim. Acta* 2005, *69*, 5005-5019.
(78) Jin, Q.; Mohanty, S. R.; Roden, E. E. *Geomicrobiol. J.* 2007, *Submitted for publication*.
(79) Roden, E. E.; Fang, Y.; Scheibe, T. D.; Brooks, S. C. *Available at: http://public.ornl.gov/nabirfrc/frcdoc12.cfm* 2005.
(80) Fang, Y.; Yeh, G. T.; Burgos, W. D. *Wat. Resour. Res.* 2003, *39*, 1083-1108.
(81) Fang, Y.; Yabusaki, S. B.; Yeh, G. T. *Comp. Geosci.* 2006, *32*, 64-72.
(82) Yeh, G. T.; Li, Y.; Jardine, P. M.; Burgos, W. D.; Fang, Y. L.; Li, M. H.; Siegel, M. D. 2004.

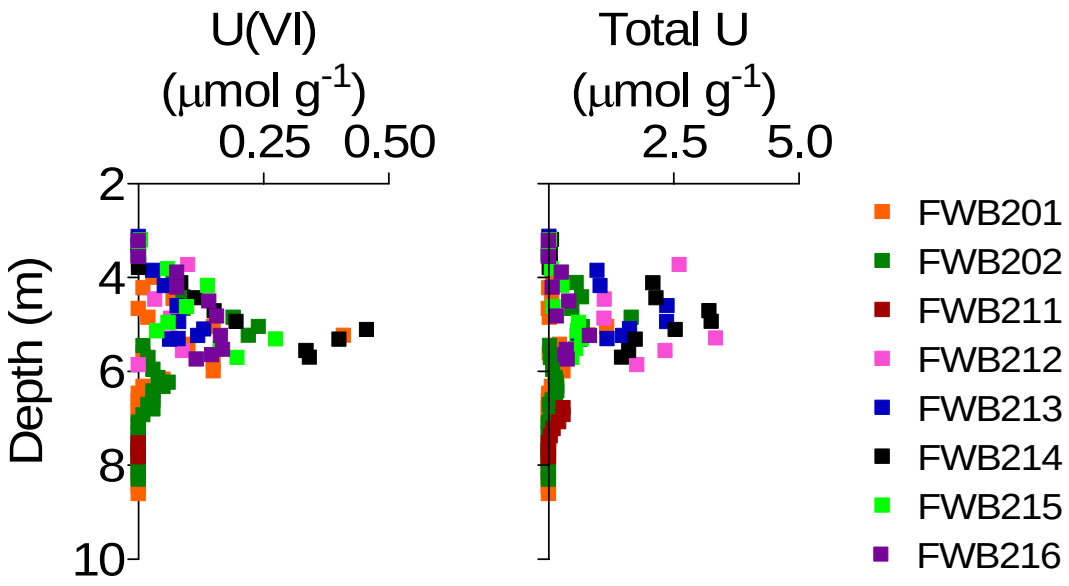

Figure S1. Total, 10% HNO_3-extractable and 100 mM $NaHCO_3$-extractable U(VI) concentrations in Area 2 sediments. Different colored symbols correspond to different cores collected within the same ca. 10 m × 10 m study area. Each symbol represents the average of duplicate or triplicate extraction of ca. 1 g of wet sediment in 10 mL of extractant. Uranium concentrations in the extracts were determined by KPA as described in the text.

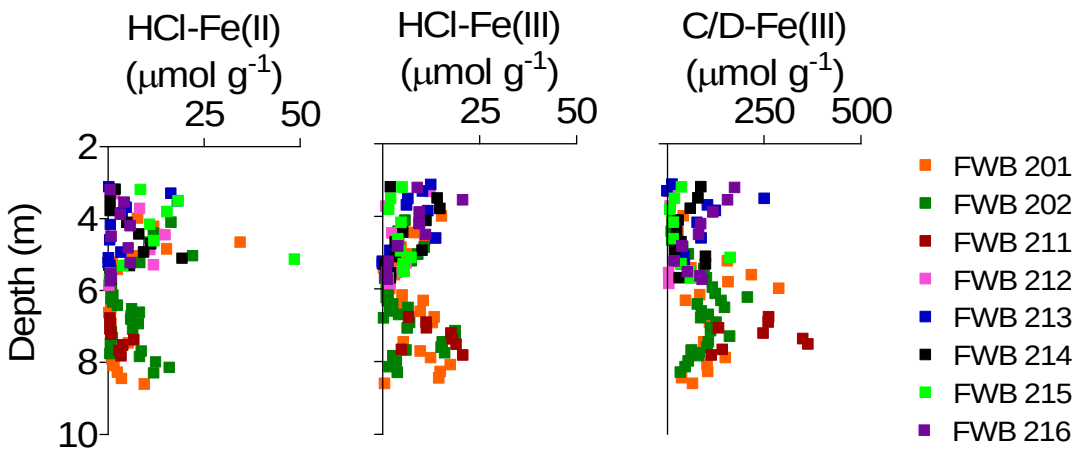

Figure S2. Dilute (0.5M) HCl-extractable Fe(II) and Fe(III), and citrate/dithionite (C/D) Fe(III) concentrations in Area 2 sediments. Different colored symbols correspond to different cores collected within the same ca. 10 m × 10 m study area. Each symbol represents the average of duplicate or triplicate extraction of ca. 1 g of wet sediment in 10 mL of extractant. Fe concentrations in the extracts were determined spectrophotometrically using Ferrozine.

Table S1. Input file for PHREEQC simulation

```
# Define ethanol and uranium as master species in solution
SOLUTION_MASTER_SPECIES
C(-1.5)   CH3CH2OH  0.0     CH3CH2OH   46
U       U+4     0.0     238.0290     238.0290
U(4)    U+4     0.0     238.0290
U(6)    UO2+2   0.0     238.0290

SURFACE_MASTER_SPECIES
# Define goethite surface
Gt      GtOH
# Define an additional generic surface
Surf    SurfOH

# Redefine NO3-/NH4+ log K to inhibit formation of NH4+
SOLUTION_SPECIES
NO3- + 10 H+ + 8 e- = NH4+ + 3 H2O
          log_k     0.0

# Define ethanol redox equilibria
CH3CH2OH = CH3CH2OH
   log_k     0.0
2 CO3-2 + 16 H+ + 12 e-  =  CH3CH2OH + 5H2O
   log_k     54.65

#Define uranium aqueous-phase and redox speciation
U+4 = U+4
          log_k         0.0
U+4 + 4 H2O = U(OH)4 + 4 H+
          log_k         -10.05
U+4 + 4 CO3-2 = U(CO3)4-4
          log_k         35.13
U+4 + 2H2O = UO2+2 + 4H+ + 2e-
          log_k         -9.07
UO2+2 + CO3-2 = UO2CO3
          log_k         9.96
UO2+2 + 2 CO3-2 = UO2(CO3)2-2
          log_k         16.64
UO2+2 + 3 CO3-2 = UO2(CO3)3-4
          log_k         21.86
Ca+2 + UO2+2 + 3CO3-2 = CaUO2(CO3)3-2
          log_k         25.38
2 Ca+2 + UO2+2 + 3CO3-2 = Ca2UO2(CO3)3
          log_k         30.43
```

```
PHASES
# Define solubility of uraninite
Uraninite
        UO2 + 4 H+ = U+4 + 2 H2O
        log_k   1.48

# Define solubility of goethite
Goethite
        FeOOH + 3 H+ = Fe+3 + 2 H2O
        log_k   -1.41

# Define solubility of FeS
FeS(ppt)
        FeS + H+ = Fe+2 + HS-
        log_k   -2.96

# Define mock phase to fix pH
Fix_pH
        H+ = H+
   log_k 0

SURFACE_SPECIES
# Define goethite surface species
GtOH = GtOH
   log_k  0.0

GtOH + Fe+2 = GtOHFe+2
   log_k 3.8

# Define additional generic surface species
SurfOH = SurfOH
   log_k  0.0

SurfOH + Fe+2 = SurfOHFe+2
   log_k  4.8

# Define initial solution composition
SOLUTION  1
      units     mmol/L
      Ca                3.35
      K           0.16
      Mg                1.1
      Na                15.5 charge
      C(4)        0.5
      N(5)      1.16
      S(6)      1.07
```

```
    U(6)        0.09
    Cl      6.06
END

EQUILIBRIUM_PHASES 1
    Goethite    0       0.032
    Uraninite   0       0
    FeS(ppt)    0               0
    Fix_pH      -6.61   HCl 0.1

SURFACE 1
    GtOH    Goethite  equilibrium_phase  0.0410  1.068e4
    SurfOH  0.022           25      227
    -no_edl
END

# Define ethanol oxidation as a series of reaction steps
REACTION 1
    CH3CH2OH    1
    9 mmol in 450 steps #Add 9 mM ethanol in 450 increments
END

# Put reactants together for simulation
INCREMENTAL_REACTIONS TRUE
USE SOLUTION 1
USE EQUILIBRIUM_PHASES 1
USE SURFACE 1
USE REACTION 1
SAVE SOLUTION 1
SAVE EQUILIBRIUM_PHASES 1
SAVE SURFACE 1
```

TEAPREVU: A numerical simulation model of Terminal Electron-Accepting Processes in a Representative Elementary Volume of Uranium-contaminated subsurface sediment

Developed by[1]:

Eric E. Roden[2], The University of Alabama
Yilin Fang and Tim Scheibe, Pacific Northwest National Laboratory
Scott Brooks, Oak Ridge National Laboratory

January 2005

[1] Through support of the U.S. Department of Energy, Office of Biological and Environmental Research, Natural and Accelerated Bioremediation Research Program

[2] Corresponding author; (205) 348-0556; **eroden@bsc.as.ua.edu**

Description of TEAPREVU Model

1. Overview

TEAPREVU is a reaction-based model of Terminal Electron Accepting Processes (TEAP) and other biogeochemical reactions in a hypothetical Representative Elementary Volume (REV) of Uranium-contaminated subsurface sediment. The model (which includes 30 primary dependent variables listed in Table 1), was developed to simulate the results of a batch slurry experiment with FRC Area 2 sediment (Mohanty et al., 2004), with the idea that the developed framework will eventually be incorporated into a field-scale reactive transport simulation of in situ biostimulation at Area 2. The model envisions flow of ethanol-containing fluid through a single reactor cell (the fluid flow rate is set equal to zero to model the batch slurry experiment). The incoming fluid contains soluble electron acceptors (O_2, NO_3^-, U(VI), SO_4^{2-}) whose abundance, together with the abundance of solid-phase electron acceptors (MnO_2, FeOOH, S^0) in the sediment, control the relative rates of various terminal electron accepting processes (TEAP) and other biogeochemical reactions over time in the reactor. The model accounts for complete (to HCO_3^-) or incomplete (to acetate) oxidation of ethanol, as well as oxidation of acetate to HCO_3^- and/or CH_4, via 18 different TEAP pathways (see Fig. 1 and Table 2). Each of the TEAP reactions are dependent on the biomass of one or more distinct microbial populations (8 total; see Table 1) chosen based on current knowledge of the kinds of organisms likely to proliferate in response to biostimulation of subsurface sediments. Growth of these populations is described using the bioenergetics-based approach developed by Rittman and McCarty (2001) for simulation of wastewater (i.e. sewage) treatment, in which the partitioning of organic carbon flow between energy generation and cell biomass production (see Fig. 2) is dependent on the free energy of the corresponding TEAP, which is computed dynamically during the simulation as a function of the abundance (concentration and/or activity) of the reactants and products involved in the process. This approach alleviates the need for making a priori assumptions about the biomass yield for the different physiological functional populations. Kinetic constants for uptake of electron donors, electron acceptors, and inorganic nitrogen compounds, as well for the inhibition of specific RTEAPs (37 total; see Table 3) by the presence of more favorable electron acceptors, were either chosen arbitrarily or constrained by the physiological properties of pure culture representatives and/or by values required to reproduce the results of the batch slurry experiment. Each of the RTEAPs results in production of various inorganic compounds, which either accumulate in solution or undergo reactions (sorption and/or mineral precipitation) with the solid-phase. The model also accounts for a wide variety of secondary redox reactions (sensu Van Cappellen and Wang (1996)) that may potentially occur in sedimentary environments (e.g. oxidation of reduced species such as Mn(II), Fe(II), U(IV), S(-II), S^0, and CH_4 by aqueous or solid-phase electron acceptors such as O_2, NO_3^-, MnO_2, and FeOOH; see Table 4 for a complete list of reactions), as well as for precipitation/dissolution of mineral phases that may be associated with microbial activity in sediments (see Table 5). In this way the model is capable of simulating time-dependent changes in the abundance of various oxidized and reduced species and mineral phases as a function of the input of external electron acceptors/donors and other aqueous species. This capacity is critical for field-scale simulation of biogeochemical processes in subsurface environments (Hunter et al., 1998).

The current version of the model consists of a system of differential (kinetic reactions) and algebraic (equilibrium speciation reactions) equations (summarized in Tables 3-12) that were assembled manually and directly based on our current conception of the reaction network. The differential equations are solved using a fifth-order Runge-Kutta algorithm (Press et al., 1992) as previously described (Roden, 2004), and the equilibrium speciation equations are solved with the MICROQL algorithm (Westall, 1986), which operated within the ODE solver routine. This manual system is being converted to the reaction-based batch biogeochemical simulator BIOGEOCHEM (Fang et al., 2003) en route to inclusion of the developed reaction network in field-scale modeling of subsurface biostimulation at Area 2.

2. Rational for TEAPs and microbial physiological functional groups

As outlined in Table 2, the model includes 18 separate TEAP reactions, each of which is catalyzed by at least one physiological functional group of microorganisms. This approach is analogous to that employed by Lensing et al. (1994) for simulation of TEAPs in leachate-contaminated aquifer sediments in Germany, which itself was based on the pioneering work of F. Molz, M. Celia, and colleagues on modeling of O_2 and NO_3^- respiration in porous media (Molz et al., 1986; Widdowson et al., 1988; Celia et al., 1989; Kindred and Celia, 1989). The TEAPs represent the standard suite of inorganic electron-accepting pathways known to be active in natural systems (Lovley and Chapelle (1995)) coupled to the metabolism of ethanol or acetate. The physiological functional groups were defined based on the known physiology of soil/sediment microorganisms. Strictly aerobic microorganisms (AMs) were assumed to utilize only O_2 as an electron acceptor, whereas denitrifying microorganisms (DMs) were assumed to be able to utilize either O_2 or NO_3^-, in keeping with the almost universal facultative anaerobic physiology of such organisms (Tiedje, 1988). These organisms were assumed to oxidize both ethanol and acetate directly to HCO_3^-. Three different groups of "dissimilatory reducing microorganisms" (DRM1, DRM2, DRM3) were included: the first group was assumed to catalyze only dissimilatory reduction of nitrate to ammonium (DNRA) coupled to partial oxidation of ethanol to acetate, and as such are assumed to represent obligate anaerobes that catalyze DNRA during fermentative rather than oxidative metabolism (Tiedje, 1988). The second group was assumed to catalyze both DNRA and dissimilatory reduction of Mn(IV)/Fe(III) oxides and U(VI) coupled to either partial oxidation of ethanol to acetate or complete oxidation of acetate to HCO_3^-. These organisms are assumed to represent mesophilic dissimilatory metal-reducing microorganisms such as *Geobacter* which are well-known for their ability to oxidize organic carbon compounds with Mn(IV)/Fe(III) or NO_3^- as an electron acceptor (Lovley, 2002). The third group of DRMs was assumed to be able to carry-out SO_4^{2-} and S^0 reduction in addition to NO_3^-, Mn(IV)/Fe(III), and U(VI) reduction. This group is the least well-recognized in terms of pure culture representatives, with *Desulfotomaculum reducens* (Tebo and Obraztsova, 1998) being the only isolate known to date. Although inclusion of this group of organisms was not required to simulate the results of the Area 2 slurry experiment, it was included so as to maximize flexibility in modeling the interplay between Fe(III) and SO_4^{2-} reduction in FRC sediments. The other groups of organisms included in the model are SO_4^{2-} reducing microorganisms proper (SO4RM), S^0 reducing microorganisms (S0RM), and methanogenic microorganisms (MGM), each of which were assumed to either partially oxidize ethanol to acetate, or to oxidize acetate to HCO_3^- (SO4RM and S0RM) or to a mixture of HCO_3^- and CH_4 (MGM). Note that although S^0 is not likely to be abundant in native FRC subsurface sediments (or any other native subsurface sediment), it can be generated during reaction of hydrogen sulfide (HS^-) with Mn(IV) or Fe(III) oxides (e.g. at reaction front where HS^- containing groundwater encounters Mn(IV) and/or Fe(III) oxide-bearing sediment) and subsequently serve as an electron acceptor for organic carbon oxidation. The SO_4^{2-}- and S^0-reducing organisms are assumed by default to be able to reduce U(VI), although this can be turned-off as necessary to consider the potential impact of a switch from Fe(III)-reducing to SO_4^{2-}-reducing conditions on U(VI) reduction.

The different TEAP reactions were subject to inhibition by the presence of higher redox potential electron acceptors according to standard noncompetitive inhibition functions (Rawn, 1983). Such inhibition functions account for either preferential utilization of more energetically favorable electron acceptors (which is generally under linked genetic/physiological control, as in the case of O_2 vs. NO_3^- respiration in denitrifying microorganisms (Tiedje, 1988), or NO_3^- vs. Fe(III) respiration in DRMs; D. Lovley, personal communication), for poisoning (or "short-circuiting") of respiratory electron transfer reactions (as in the case of Fe(III) inhibition of acetoclastic methanogenesis; (Bond and Lovley, 2002)), or for general interference posed by the presence of high redox potential couples. It is important to emphasize the distinction between the use of inhibition functions in this physiologically-based manner as compared to how such functions have been used in previous models of TEAP reactions in soil/sedimentary (VanCappellen and Gaillard, 1996; Hunter et al., 1998) environments. In the latter models, degradation

of organic substrates (natural organics and/or hydrocarbon contaminants) and associated consumption of electron acceptors are depicted strictly as a kinetic function of the abundance of the substrate(s) and the electron acceptor(s), with no consideration of the biomass or physiological properties of the organisms catalyzing the TEAPs. As such, inhibition functions (hyperbolic or otherwise) were used in a general way to depict the negative influence of higher redox potential electron acceptors on biodegradation coupled to utilization of lower redox potential electron acceptors – as opposed to their use here to describe effects on specific TEAPs carried out by specific groups of microorganisms.

The relative rates of different TEAP reactions were also assumed to be influenced by the presence or absence of a given organic electron donor. Specifically, ethanol was assumed to inhibit utilization of acetate according to a standard noncompetitive inhibition function. This assumption was required to reproduce the pattern of acetate accumulation during the early stages of the slurry experiment, and is consistent with the expectation that cells would preferentially utilize an energetically more favorable electron donor such as ethanol over a less energetically favorable donor such as acetate. The algorithm for computing the influence of alternative electron donors on TEAP pathways is completely general and can in principle be expanded to include the effect of the presence of multiple electron donors, e.g. the variety of end-products that might arise from fermentation of individual sugars such as glucose or polymeric mixtures of carbohydrates such as those present in molasses or corn syrup.

3. Modeling microbial biosynthesis and growth yield

The bioenergetics approach for modeling microbial biosynthesis and growth yield with either NH_4^+, NO_3^-, or N_2 as a nitrogen source (Rittmann and McCarty, 2001) was modified slightly for use in the TEAP model. First, the free energy available from each TEAP was computed dynamically during the simulation, and these values (rather than values based on standard state calculations) were used to simulate the cell growth yield, assuming a standard energy transfer efficiency of 0.6 (Rittmann and McCarty, 2001) for all TEAP reactions. Although time-dependent free energy effects were insignificant for highly favorable TEAPs such as O_2 and NO_3^- reduction, changes in the free energy of Fe(III) reduction, SO_4^{2-} reduction, and methanogenesis led to 2-5 fold decreases in the fraction of carbon flow into cell biosynthesis vs. energy generation for the batch slurry simulations. The general strategy of Rittmann and McCarty (2001) for computing the free energy requirements for biosynthesis as a function of the nitrogen source (see Table 6 for a summary of biosynthetic reactions) was retained, but the nitrogen source used for biosynthesis was not assumed to be constant during the simulation. Instead, cells were assumed to take up NH_4^+ preferentially over NO_3^-, and in turn to take up NO_3^- in preference to N_2 (i.e. to N_2 fixation). The amount of these different N sources consumed for biosynthesis of the different microbial populations was computed based on the total fixed N requirement at each time step and hyperbolic kinetic functions which account for preferential uptake the different N sources (see Table 10). A similar approach was used to simulate the influence of the presence of alternative (i.e. relative to the primary organic electron donor involved in a given TEAP) fixed carbon sources on the energetics of cellular carbon biosynthesis (see Table 8). In this case, the sequence (and relative percent) of carbon substrate utilization for biosynthesis was assumed to be identical to the sequence (and relative percent) of primary carbon substrate utilization for a given TEAP process.

4. Uranium speciation and reduction

In its current configuruation, the model includes two basic process which affect aqueous/solid-phase uranium speciation: (1) adsorption of U(VI) to Fe(III) oxide surfaces according to a non-electrostatic version of the two-site Waite et al. (1994) model; and (2) enzymatic reduction of dissolved (but not sorbed) U(VI) to insoluble UO_2(s) (uraninite) according to a standard Monod-style rate expression. Abiotic reduction of U(VI) by Fe(II), a potentially important mechanism for U(VI) reduction in Fe(III)-

reducing systems (Fredrickson et al., 2000), was omitted from the model due to uncertainties in the rate/extent of this process in natural Fe(II)-rich sediments (Jeon et al., 2005).

Stability constants for aqueous U(VI) species were those used by Waite et al. (1994), whereas the stability constants for sorption of U(VI) to oxide surfaces were obtained from fitting of data from a U(VI) sorption isotherm experiment with Oyster, VA sediment (B.H. Jeon and E.E. Roden, unpubl data). Experiments designed to parameterize U(VI) sorption to FRC Area 2 sediments are being conducted through the Scheibe et al. and Burgos et al. NABIR projects, and this information will be incorporated into the model as it becomes available. Kinetic constants for U(VI) bioreduction were constrained by published results for *Shewanella* and *Geobacter* (Truex et al., 1997; Liu et al., 2002; Roden and Scheibe, 2005).

5. Selection of parameter values

The model contains a large number of parameters (summarized in Table 13), not all of which could be independently defined or constrained by existing experimental results or information from the literature. The selection of parameter values was therefore based on a combination of existing information (referred to as "independent" parameter values), values that could constrained from literature or other sources of information (referred to as "constrained" parameter values), values that were assigned arbitrarily based on general knowledge not specific to the particular process under consideration (referred to as "arbitrary" parameter values), and finally values that were determined by trial-and-error in order to reproduce the results of the Area 2 sediment slurry experiment (referred to as "model-derived" parameter values). Although this approach may not be appealing from a rigorous scientific point of view, it is defensible in the case of complex biogeochemical models where the processes involved are more well-understood (relatively) than are the values for parameters involved those processes (VanCappellen and Wang, 1995, 1996).

6. Area 2 slurry incubation experiment simulation results

The central goal in simulating the Area 2 sediment slurry experiment was to reproduce the basic patterns of organic substrate metabolism, consumption of electron acceptors, and accumulation of reduced end-products of anaerobic respiration. In general the optimized model reproduced these patterns rather well (Fig. 3A,B). Although the timing and magnitude of the predicted accumulation of acetate resulting from partial oxidation of ethanol (and the subsequent utilization of acetate) did not exactly match the experiment results (Fig. 3A), the general agreement between the simulation and the data suggests that the developed reaction network provides a reasonable explanation for this pattern of substrate metabolism. The strategy for simulating the interaction between the different TEAPs also seems generally valid, given the close resemblance of the predicted and observed patterns of electron acceptor (NO_3^-, Fe(III), SO_4^{2-}) consumption and reduced end-product accumulation (Fe(II) and CH_4; note that the abundance of reduced sulfur compounds (e.g. HS^-, FeS) was not determined). Together these results suggest that the current version of the model is appropriate for incorporation into exploratory field-scale simulations (i.e. numerical experimentation) of ethanol metabolism and major TEAP reactions at the Area 2 field site. However, the predicted aqueous/solid speciation of uranium did not match the experimental data (Fig. 3C). A significant fraction (ca. 50%) of solid-associated U(VI) failed to desorb during biostimulation and therefore remained unreduced at the end of the incubation, a result consistent with other recent studies of enzymatic reduction of sorbed U(VI) (Jeon et al., 2004; Ortiz-Bernad et al., 2004). Understanding the controls on reduction of solid-associated U(VI) (both biotic and abiotic) and development of strategies for accurately simulating the fate of uranium in biostimulated FRC Area 2 sediments is a key goal the new Burgos et al. NABIR project ("Reaction-Based Reactive Transport Modeling of Iron Reduction and Uranium Immobilization at Area 2 of the NABIR Field Research Center").

6. References

Berg, P., S. Rysgaard, and B. Thamdrup. 2003. Dynamic modeling of early diagenesis and nutrient cycling. A case study in an arctic marine sediment. Am. J. Sci. 303:905-955.
Bond, D. R., and D. R. Lovley. 2002. Reduction of Fe(III) by methanogens in the presence and absence of extracellular quinones. Environ. Microbiol. 4:115-124.
Celia, M. A., J. S. Kindred, and I. Herrera. 1989. Contaminant transport and biodegradation 1. A numerical model for reactive transport in porous media. Wat. Resour. Res. 25:1141-1148.
Davis, J. A., and D. B. Kent. 1990. Surface complexation modeling in aqueous geochemistry. In M. F. Hochella, and A. F. White (eds.). Mineral-water interface geochemistry, pp. 177-260. Mineralogical Society of America, Washington, DC.
Fang, Y., G. T. Yeh, and W. D. Burgos. 2003. A general paradigm to model reaction-based biogeochemical processes in batch systems. Wat. Resour. Res. 39:1083-1108.
Fredrickson, J. K., J. M. Zachara, D. W. Kennedy, M. C. Duff, Y. A. Gorby, S. W. Li, and K. M. Krupka. 2000. Reduction of U(VI) in goethite (α-FeOOH) suspensions by a dissimilatory metal-reducing bacterium. Geochim. Cosmochim. Acta 64:3085-3098.
Grenthe, I., I. Puigdomenech, M. C. A. Sandino, and M. H. Rand. 1995. Appendix D. Chemical Thermodynamics of Uranium. Chemical Thermodynamics of Americium. Elsevier Science Publ., Amsterdam.
Hunter, K. S., Y. Wang, and P. VanCappellen. 1998. Kinetic modeling of microbially-driven redox chemistry of subsurface environments: coupling transport, microbial metabolism and geochemistry. J. Hydrol. 209:53-80.
Jeon, B. H., M. O. Barnett, W. D. Burgos, B. A. Dempsey, and E. E. Roden. 2005. Chemical reduction of U(VI) by Fe(II) at the solid-water interface using synthetic and natural iron(III) oxides. Environ. Sci. Technol. Submitted for publication.
Jeon, B. H., S. D. Kelly, K. M. Kemner, M. O. Barnett, W. D. Burgos, B. A. Dempsey, and E. E. Roden. 2004. Microbial reduction of U(VI) at the solid-water interface. Environ. Sci. Technol. In press.
Kindred, J. S., and M. A. Celia. 1989. Contaminant transport and biodegradation 2. Conceptual model and test simulations. Wat. Resour. Res. 25:1149-1159.
Langmuir, D. 1997. Aqueous Environmental Geochemistry. Prentice Hall, Upper Saddle River, NJ.
Lensing, H. J., M. Vogt, and B. Herrling. 1994. Modeling of biologically mediated redox processes in the subsurface. J Hydrol 159:125-143.
Liu, C., Y. A. Gorby, J. M. Zachara, J. K. Fredrickson, and C. F. Brown. 2002. Reduction kinetics of Fe(III), Co(III), U(VI), Cr(VI), Tc(VII) in cultures of dissimilatory metal reducing bacteria. Biotechnol. Bioengin. 80:637-649.
Lovley, D. R. 2002. Fe(III)- and Mn(IV)-reducing prokaryotes. In S. F. M. Dworkin, E. Rosenberg, K.H Schleifer, E. Stackebrandt (ed.). The Prokaryotes, p. In press. Springer-Verlag, New York.
Lovley, D. R., and F. H. Chapelle. 1995. Deep subsurface microbial processes. Rev. Geophys. 33:365-381.
Mohanty, S., B. Kollah, and E. E. Roden. 2004. Biogeochemical processes and microbial community structure in ethanol-stimulated subsurface sediments. Manuscript in preparation.
Molz, F. J., M. A. Widdowson, and L. D. Benefield. 1986. Simulation of microbial growth dynamics coupled to nutrient and oxygen transport in porous media. Wat. Resour. Res. 22:1207-1216.

Ortiz-Bernad, I., R. T. Anderson, H. A. Vrionis, and D. R. Lovley. 2004. Resistance of solid-phase U(VI) to microbial reduction during in situ bioremediation of uranium-contaminated groundwater. Appl. Environ. Microbiol. 70:7558-7560.
Press, W. H., S. A. Teukolsky, W. T. Vetterling, and B. P. Flannery. 1992. Numerical Recipes in FORTRAN. Cambridge University Press, Port Chester, NY.
Rawn, J. D. 1983. Biochemistry. Harper and Row, New York.
Rittmann, B. E., and P. L. McCarty. 2001. Environmental Biotechnology. McGraw-Hill, Boston.
Roden, E. E. 2004. Analysis of long-term bacterial versus chemical Fe(III) oxide reduction kinetics. GCA 68:3205-3216.
Roden, E. E., and J. H. Tuttle. 1993. Inorganic sulfur turnover in oligohaline estuarine sediments. Biogeochemistry 22:81-105.
Roden, E. E., and E. Sedo. 2003. Framework for numerical simulation of bacterial Fe(III) oxide reduction in circumneutral soil and sedimentary environments. EOS Trans. AGU 84(46), Fall Meet Suppl.:Abstract B32A-0375.
Roden, E. E., and T. D. Scheibe. 2005. Conceptual and numerical model of uranium(VI) reductive immobilization in fractured subsurface sediments. Chemosphere In press.
Stumm, W., and J. J. Morgan. 1996. Aquatic Chemistry. John Wiley & Sons, Inc., New York.
Tebo, B. M., and A. Y. Obraztsova. 1998. Sulfate-reducing bacterium grows with Cr(VI), U(VI), Mn(IV) and Fe(III) as electron acceptors. FEMS Microbiol. Lett. 162:193-198.
Thauer, R. K., K. Jungermann, and K. Decker. 1977. Energy conservation in chemotrophic anaerobic bacteria. Bacteriol. Rev. 41:100-180.
Tiedje, J. M. 1988. Ecology of denitrification and dissimilatory nitrate reduction to ammonium. In A. J. B. Zehnder (ed.). Biology of anaerobic microorganisms. John Wiley & Sons, New York.
Truex, M. J., B. M. Peyton, N. B. Valentine, and Y. A. Gorby. 1997. Kinetics of U(VI) reduction by a dissimilatory Fe(III)-reducing bacterium under non-growth conditions. Biotech. Bioengin. 55:490-496.
VanCappellen, P., and Y. Wang. 1995. Metal cycling in surface sediments: modeling the interplay of transport and reaction. In H. E. Allen (ed.). Metal contaminated aquatic sediments, pp. 21-64. Ann Arbor Press, Chelsea, MI.
VanCappellen, P., and Y. Wang. 1996. Cycling of iron and manganese in surface sediments: a general theory for the coupled transport and reaction of carbon, oxygen, nitrogen, sulfur, iron, and manganese. Am. J. Sci. 296:197-243.
VanCappellen, P., and J. F. Gaillard. 1996. Biogeochemical dynamics in aquatic sediments. In P. C. Lichtner, C. I. Steefel, and E. H. Oelkers (eds.). Reactive transport in porous media, pp. 335-376. The Mineralogical Society of America, Washington, DC.
Waite, T. D., J. A. Davis, T. E. Payne, G. A. Waychunas, and N. Xu. 1994. Uranium(VI) adsorption to ferrihydrite: Application of a surface complexation model. Geochim. Cosmochim. Acta 58:5465-5478.
Weber, K. A., E. E. Roden, and F. W. Picardal. 1998. Microbially-catalyzed nitrate-dependent oxidation of solid-phase Fe(II) compounds. Environ. Sci. Technol. Submitted for publication.
Westall, J. C. 1986. MICROQL I. A chemical equilibrium program in BASIC. Report 86-02, Department of Chemistry, Oregon State University, Corvalis, OR.
Widdowson, M. A., F. J. Molz, and L. D. Benefield. 1988. A numerical transport model of oxygen- and nitrate-based respiration linked to substrate and nutrient availability in porous media. Wat. Resour. Res. 24:1553-1565.

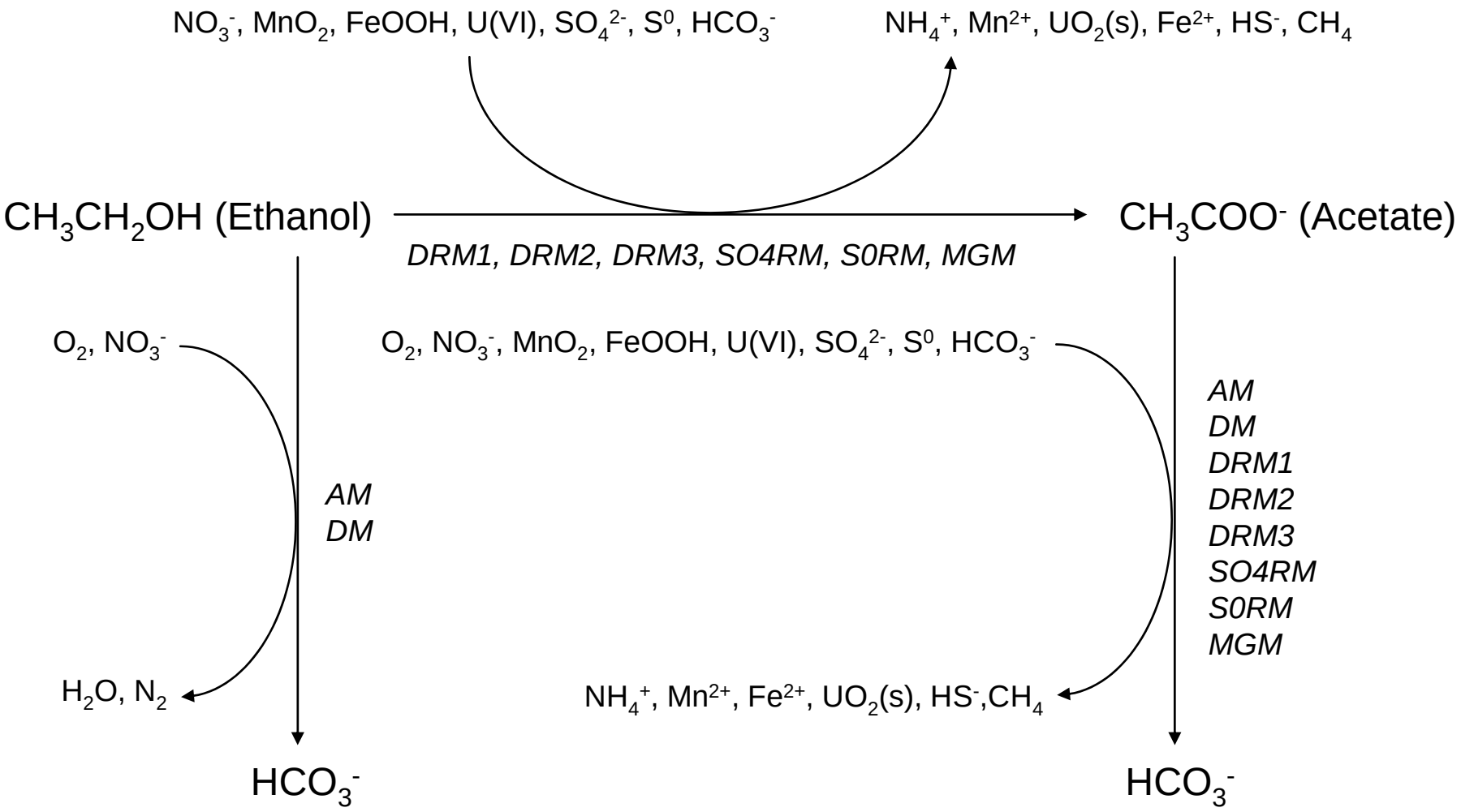

Fig. 1. Diagram of substrate metabolism and electron flow in the TEAPREV simulation model.

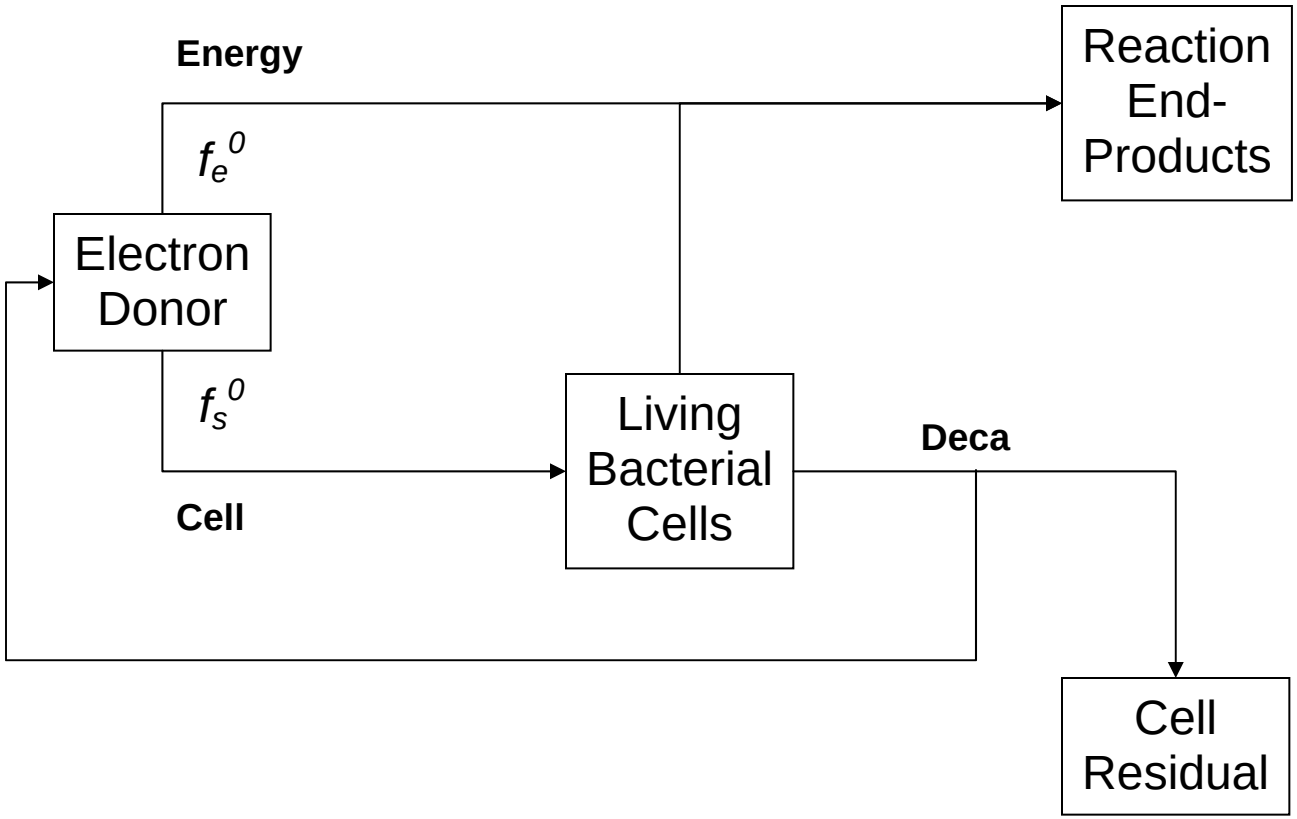

Fig. 2. Diagram of substrate partitioning between energy production and cell biosynthesis during microbial respiration. Modified from Fig. 2.1 in Rittmann and McCarty (2001).

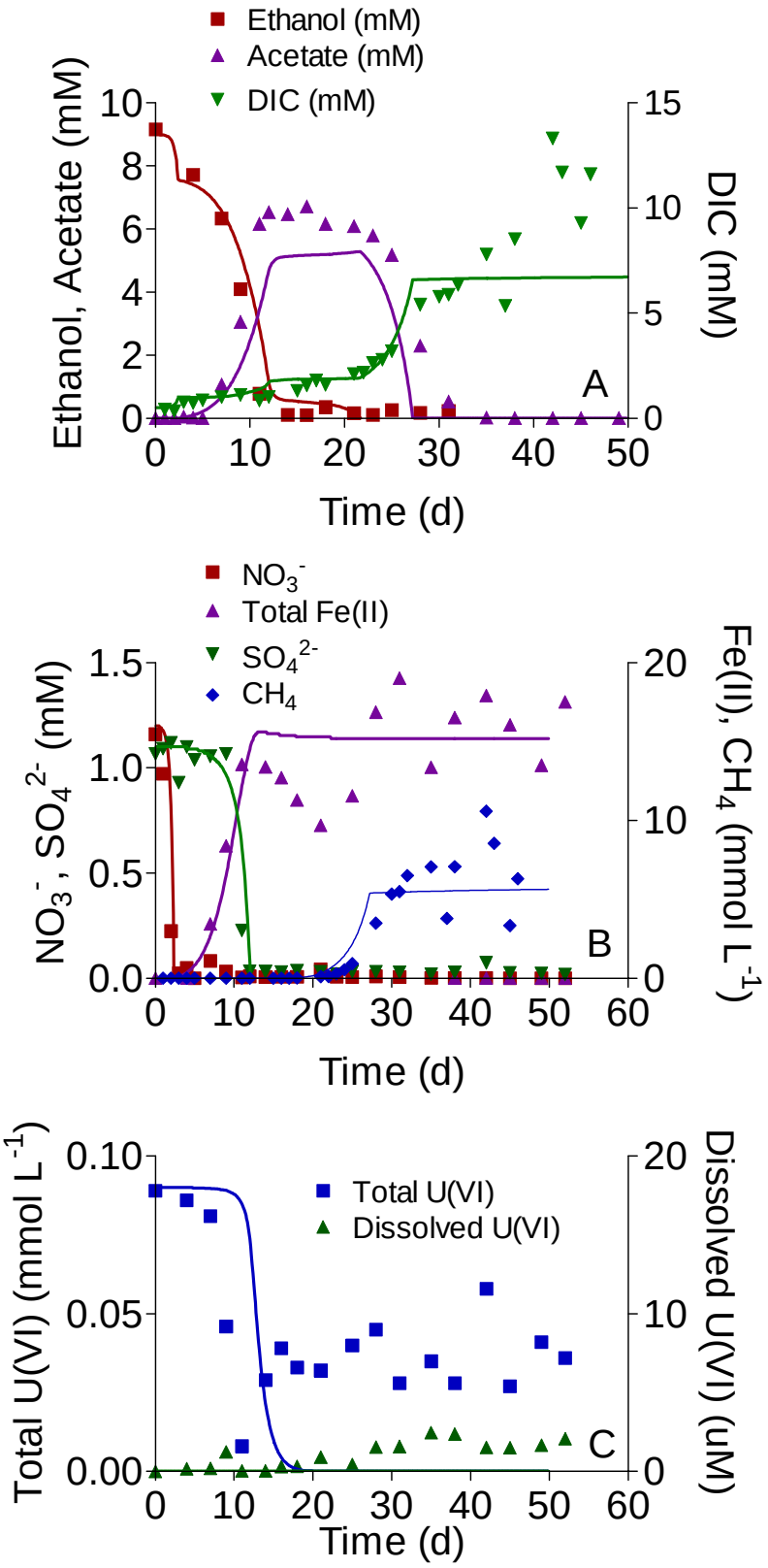

Figure 3. Results of TEAPREVU simulation of the Area 2 sediment slurry experiment. Data points show means of duplicate slurries; solid lines show simulation results.

Table 1. Primary dependent variables

Number	Type	Name	Fortran Name	Initial Value
(1)	Electron Donor	CH_3CH_2OH (Ethanol)	CH3CH2OH	0.009 (mol L^{-1})
(2)	Electron Donor	CH_3COO^- (Acetate)	CH3COO	0.0 (mol L^{-1})
(3)	Electron Acceptor	O_2	O2	0.0 (mol L^{-1})
(4)	Electron Acceptor	NO_3^-	NO3	0.0012 (mol L^{-1})
(5)	Electron Acceptor	NO_2^-	NO2	0.0 (mol L^{-1})
(6)	Electron Acceptor	MnO_2(s)	MnO2	0.0 (mol L^{-1})
(7)	Electron Acceptor	FeOOH(s)	FeOOH	0.3 (mol L^{-1})
(8)	Electron Acceptor	SO_4^{2-}	SO4	0.0011 (mol L^{-1})
(9)	Electron Acceptor	S^0(s)	S0	0.0 (mol L^{-1})
(10)	Electron Acceptor	UVI	UVI	0.00009 (mol L^{-1})
(11)	Respiration End Product	HCO_3^-	HCO3	0.005 (mol L^{-1})
(12)	Respiration End Product	N_2	N2	0.0005 (mol L^{-1})
(13)	Respiration End Product	NH_4^+	NH4	0.0001 (mol L^{-1})
(14)	Respiration End Product	Mn(II)	Mn2	0.0 (mol L^{-1})
(15)	Respiration End Product	Fe(II)	Fe2	0.0 (mol L^{-1})
(16)	Respiration End Product	HS^-	HS	0.0 (mol L^{-1})
(17)	Respiration End Product	CH_4	CH4	0.0 (mol L^{-1})
(18)	Respiration End Product	UO_2(s)	UO2	0.0 (mol L^{-1})
(19)	Reactant/Product	TOTH	TOTH	0.0212 (mol L^{-1})
(20)	Mineral Precipitate	$MnCO_3$(s)	MnCO3	0.0 (mol L^{-1})
(21)	Mineral Precipitate	$FeCO_3$(s)	FeCO3	0.0 (mol L^{-1})
(22)	Mineral Precipitate	FeS(s)	FeS	0.0 (mol L^{-1})
(23)	Microbial Biomass	Aerobic Microorganisms	AM	0.00005 (g L^{-1})
(24)	Microbial Biomass	Denitrifying Microorganisms	DM	0.00005 (g L^{-1})
(25)	Microbial Biomass	Group 1 Dissimilatory-Reducing Microorganisms	DRM1	0.000005 (g L^{-1})
(26)	Microbial Biomass	Group 2 Dissimilatory-Reducing Microorganisms	DRM2	0.0000025 (g L^{-1})
(27)	Microbial Biomass	Group 3 Dissimilatory-Reducing Microorganisms	DRM3	0.0000025 (g L^{-1})
(28)	Microbial Biomass	Sulfate-Reducing Microorganisms	SO4RM	0.000005 (g L^{-1})
(29)	Microbial Biomass	Elemental S-Reducing Microorganisms	S0RM	0.000005 (g L^{-1})
(30)	Microbial Biomass	Methanogenic Microorganisms	MGM	0.000005 (g L^{-1})

Table 2. Metabolic energy-generating terminal electron-accepting processes (TEAPs)

Number	Reaction	Catalyzed By
(1)	$CH_3CH_2OH + 3O_2 \rightarrow 2HCO_3^- + H_2O + 2H^+$	AM, DM
(2)	$CH_3CH_2OH + 2.4NO_3^- + 0.4H^+ \rightarrow 2HCO_3^- + 1.2N_2 + 2.2H_2O$	DM
(3)	$CH_3CH_2OH + 0.5NO_3^- \rightarrow CH_3COO^- + 0.5NH_4^+ + 0.5H_2O$	DRM1, DRM2, DRM3
(4)	$CH_3CH_2OH + 2MnO_2 + 3H^+ \rightarrow CH_3COO^- + 2Mn^{2+} + 3H_2O$	DRM2, DRM3
(5)	$CH_3CH_2OH + 4FeOOH + 7H^+ \rightarrow CH_3COO^- + 4Fe^{2+} + 7H_2O$	DRM2, DRM3
(6)	$CH_3CH_2OH + 0.5SO_4^{2-} \rightarrow CH_3COO^- + 0.5HS^- + 0.5H^+ + H_2O$	DRM3, SO4RM
(7)	$CH_3CH_2OH + 2S^0 + H_2O \rightarrow CH_3COO^- + 2HS^- + 3H^+$	DMR3, S0RM
(8)	$CH_3CH_2OH + 0.5HCO_3^- \rightarrow CH_3COO^- + 0.5CH_4 + 0.5H^+ + 0.5H_2O$	MGM
(9)	$CH_3COO^- + 2O_2 \rightarrow 2HCO_3^- + H^+$	AM, DM
(10)	$CH_3COO^- + 1.6NO_3^- + 0.6H^+ \rightarrow 2HCO_3^- + 0.8N_2 + 0.8H_2O$	DM
(11)	$CH_3COO^- + NO_3^- + H_2O + H^+ \rightarrow 2HCO_3^- + NH_4^+$	DRM2, DRM3
(12)	$CH_3COO^- + 4MnO_2 + 7H^+ \rightarrow 2HCO_3^- + 4Mn^{2+} + 4H_2O$	DRM2, DRM3
(13)	$CH_3COO^- + 8FeOOH + 15H^+ \rightarrow 2HCO_3^- + 8Fe^{2+} + 12H_2O$	DRM2, DRM3
(14)	$CH_3COO^- + SO_4^{2-} \rightarrow 2HCO_3^- + HS^-$	DRM3, SO4RM
(15)	$CH_3COO^- + 4S^0 + 4H_2O \rightarrow 2HCO_3^- + 4HS^- + 5H^+$	DRM3, S0RM
(16)	$CH_3COO^- + H_2O \rightarrow HCO_3^- + CH_4$	MGM
(17)	$CH_3CH_2OH + 2UO_2(CO_3)_2^{2-} + H_2O \rightarrow CH3COO^- + 4HCO_3^- + 2UO_2(s) + H^+$	DRM2, DRM3, [SO4RM, S0RM]*
(18)	$CH_3COO^- + 4UO_2(CO_3)_2^{2-} + 4H_2O \rightarrow 10HCO_3^- + 4UO_2(s) + H^+$	DRM2, DRM3, [SO4RM, S0RM]*

* Reduction of U(VI) by SO4RM and S0RM is optional

Table 3. Terminal electron-accepting process reactions (RTEAPs)

Number	Reaction	Catalyzed By
(1,1)	$CH_3CH_2OH + 3O_2 \rightarrow 2HCO_3^- + H_2O + 2H^+$	AM
(1,2)	$CH_3CH_2OH + 3O_2 \rightarrow 2HCO_3^- + H_2O + 2H^+$	DM
(2,1)	$CH_3CH_2OH + 2.4NO_3^- + 0.4H^+ \rightarrow 2HCO_3^- + 1.2N_2 + 2.2H_2O$	DM
(3,1)	$CH_3CH_2OH + 0.5\ NO_3^- \rightarrow CH_3COO^- + 0.5NH_4^+ + 0.5H_2O$	DRM1
(3,2)	$CH_3CH_2OH + 0.5\ NO_3^- \rightarrow CH_3COO^- + 0.5NH_4^+ + 0.5H_2O$	DRM2
(3,3)	$CH_3CH_2OH + 0.5\ NO_3^- \rightarrow CH_3COO^- + 0.5NH_4^+ + 0.5H_2O$	DRM3
(4,1)	$CH_3CH_2OH + 2MnO_2 + 3H^+ \rightarrow CH_3COO^- + 2Mn^{2+} + 3H_2O$	DRM2
(4,2)	$CH_3CH_2OH + 2MnO_2 + 3H^+ \rightarrow CH_3COO^- + 2Mn^{2+} + 3H_2O$	DRM3
(5,1)	$CH_3CH_2OH + 4FeOOH + 7H^+ \rightarrow CH_3COO^- + 4Fe^{2+} + 7H_2O$	DRM2
(5,2)	$CH_3CH_2OH + 4FeOOH + 7H^+ \rightarrow CH_3COO^- + 4Fe^{2+} + 7H_2O$	DRM3
(6,1)	$CH_3CH_2OH + 0.5SO_4^{2-} \rightarrow CH_3COO^- + 0.5HS^- + 0.5H^+ + H_2O$	DRM3
(6,2)	$CH_3CH_2OH + 0.5SO_4^{2-} \rightarrow CH_3COO^- + 0.5HS^- + 0.5H^+ + H_2O$	SO4RM
(7,1)	$CH_3CH_2OH + 2S^0 + H_2O \rightarrow CH_3COO^- + 2HS^- + 3H^+$	DRM3
(7,2)	$CH_3CH_2OH + 2S^0 + H_2O \rightarrow CH_3COO^- + 2HS^- + 3H^+$	S0RM
(8,1)	$CH_3CH_2OH + 0.5HCO_3^- \rightarrow CH_3COO^- + 0.5CH_4 + 0.5H^+ + 0.5H_2O$	MGM
(9,1)	$CH_3COO^- + 2O_2 \rightarrow 2HCO_3^- + H^+$	AM
(9,2)	$CH_3COO^- + 2O_2 \rightarrow 2HCO_3^- + H^+$	DM
(10,1)	$CH_3COO^- + 1.6NO_3^- + 0.6H^+ \rightarrow 2HCO_3^- + 0.8N_2 + 0.8H_2O$	DM
(11,1)	$CH_3COO^- + NO_3^- + H_2O + H^+ \rightarrow 2HCO_3^- + NH_4^+$	DRM2
(11,2)	$CH_3COO^- + NO_3^- + H_2O + H^+ \rightarrow 2HCO_3^- + NH_4^+$	DRM3
(12,1)	$CH_3COO^- + 4MnO_2 + 7H^+ \rightarrow 2HCO_3^- + 4Mn^{2+} + 4H_2O$	DRM2
(12,2)	$CH_3COO^- + 4MnO_2 + 7H^+ \rightarrow 2HCO_3^- + 4Mn^{2+} + 4H_2O$	DRM3
(13,1)	$CH_3COO^- + 8FeOOH + 15H^+ \rightarrow 2HCO_3^- + 8Fe^{2+} + 8H_2O$	DRM2
(13,2)	$CH_3COO^- + 8FeOOH + 15H^+ \rightarrow 2HCO_3^- + 8Fe^{2+} + 8H_2O$	DRM3
(14,1)	$CH_3COO^- + SO_4^{2-} \rightarrow 2HCO_3^- + HS^-$	DRM3
(14,2)	$CH_3COO^- + SO_4^{2-} \rightarrow 2HCO_3^- + HS^-$	SO4RM
(15,1)	$CH_3COO^- + 4S^0 + 4H_2O \rightarrow 2HCO_3^- + 4HS^- + 5H^+$	DRM3
(15,2)	$CH_3COO^- + 4S^0 + 4H_2O \rightarrow 2HCO_3^- + 4HS^- + 5H^+$	S0RM
(16,1)	$CH_3COO^- + H_2O \rightarrow HCO_3^- + CH_4$	MGM
(17,1)	$CH_3CH_2OH + 2UO_2(CO_3)_2^{2-} + H_2O \rightarrow CH3COO^- + 4HCO_3^- + 2UO_2(s) + H^+$	DRM2
(17,2)	$CH_3CH_2OH + 2UO_2(CO_3)_2^{2-} + H_2O \rightarrow CH3COO^- + 4HCO_3^- + 2UO_2(s) + H^+$	DRM3
(17,3)	$CH_3CH_2OH + 2UO_2(CO_3)_2^{2-} + H_2O \rightarrow CH3COO^- + 4HCO_3^- + 2UO_2(s) + H^+$	SO4RM
(17,4)	$CH_3CH_2OH + 2UO_2(CO_3)_2^{2-} + H_2O \rightarrow CH3COO^- + 4HCO_3^- + 2UO_2(s) + H^+$	S0RM
(18,1)	$CH_3COO^- + 4UO_2(CO_3)_2^{2-} + 4H_2O \rightarrow 10HCO_3^- + 4UO_2(s) + H^+$	DRM2
(18,2)	$CH_3COO^- + 4UO_2(CO_3)_2^{2-} + 4H_2O \rightarrow 10HCO_3^- + 4UO_2(s) + H^+$	DRM3
(18,3)	$CH_3COO^- + 4UO_2(CO_3)_2^{2-} + 4H_2O \rightarrow 10HCO_3^- + 4UO_2(s) + H^+$	SO4RM
(18,4)	$CH_3COO^- + 4UO_2(CO_3)_2^{2-} + 4H_2O \rightarrow 10HCO_3^- + 4UO_2(s) + H^+$	S0RM

Table 4. Secondary redox reactions (SRRs)

Number	Reaction
(1)	$0.5Mn^{2+}(aq) + 0.25O_2 + 0.5H_2O \rightarrow 0.5MnO_2 + H^+$
(2)	$0.5{\equiv}Mn^+ + 0.25O_2 + 0.25H_2O \rightarrow 0.5MnO_2 + 0.5H^+$
(3)	$0.5MnCO_3 + 0.25O_2 + 0.5H_2O \rightarrow 0.5MnO_2 + 0.5HCO_3^- + 0.5H^+$
(4)	$Fe^{2+}(aq) + 0.25O_2 + 1.5H_2O \rightarrow FeOOH + 2H^+$
(5)	${\equiv}Fe^+ + 0.25O_2 + 1.0H_2O \rightarrow FeOOH + H^+$
(6)	$FeCO_3 + 0.25O_2 + 1.5H_2O \rightarrow FeOOH + HCO_3^- + H^+$
(7)	$HS^- + 2O_2 \rightarrow SO_4^{2-} + H^+$
(8)	$S^0 + 1.5O_2 + H_2O \rightarrow SO_4^{2-} + 2H^+$
(9)	$FeS + 2O_2 \rightarrow Fe^{2+} + SO_4^{2-}$
(10)	$CH_4 + 2O_2 \rightarrow HCO_3^- + H^+ + H_2O$
(11)	$Fe^{2+}(aq) + 0.2NO_3^- + 1.4H_2O \rightarrow FeOOH + 0.1N_2 + 1.8H^+$
(12)	${\equiv}Fe^+ + 0.2NO_3^- + 1.4H_2O \rightarrow FeOOH + 0.1N_2 + 0.8H^+$
(13)	$FeCO_3 + 0.2NO_3^- + 1.4H_2O \rightarrow FeOOH + HCO_3^- + 0.1N_2 + 0.8H^+$
(14)	$HS^- + 1.6NO_3^- + 0.6H^+ \rightarrow SO_4^{2-} + 0.8N_2 + 0.8H_2O$
(15)	$S^0 + 1.2NO_3^- + 0.4H_2O \rightarrow SO_4^{2-} + 0.6N_2 + 0.8H^+$
(16)	$FeS + 1.6NO_3^- + 1.6H^+ \rightarrow Fe^{2+} + SO_4^{2-} + 0.8N_2 + 0.8H_2O$
(17)	$Fe^{2+}(aq) + 0.5MnO_2 + H_2O \rightarrow FeOOH + 0.5Mn^{2+} + H^+$
(18)	${\equiv}Fe^+ + 0.5MnO_2 + 0.5H_2O \rightarrow FeOOH + 0.5Mn^{2+} + H^+$
(19)	$FeCO_3 + 0.5MnO_2 + H_2O \rightarrow FeOOH + 0.5Mn^{2+} + HCO_3^-$
(20)	$0.5HS^- + 0.5MnO_2 + 1.5H^+ \rightarrow 0.5S^0 + 0.5Mn^{2+} + H_2O$
(21)	$FeS + 1.5MnO_2 + 3H^+ \rightarrow FeOOH + S^0 + 1.5Mn^{2+} + H_2O$
(22)	$0.5HS^- + FeOOH + 3H^+ \rightarrow 0.5S^0 + Fe^{2+} + 2H_2O$
(23)	$4S^0 + 4H_2O \rightarrow 3HS^- + SO_4^{2-} + 5H^+$
(24)	$0.125NH_4^+ + 0.25O_2 \rightarrow 0.125NO_3^- + 0.125H_2O + 0.25H^+$
(25)	$UO_2(s) + 0.5O_2 + 2HCO_3^- \rightarrow UO_2(CO_3)_2^{2-} + H_2O$
(26)	$UO_2(s) + 0.4NO_3^- + 2HCO_3^- + 0.4H^+ \rightarrow UO_2(CO_3)_2^{2-} + 0.2N_2 + 1.2H_2O$
(27)	$UO_2(s) + MnO_2 + 2HCO_3^- + 2H^+ \rightarrow UO_2(CO_3)_2^{2-} + Mn^{2+} + 2H_2O$

Table 5. Mineral precipitation reactions (MPRs)

Number	Reaction
(1)	$Mn^{2+}(aq) + CO_3^{2-} = MnCO_3$
(2)	$Fe^{2+}(aq) + CO_3^{2-} = FeCO_3$
(3)	$Fe^{2+}(aq) + HS^- = FeS + H^+$
(4)	$Fe^{2+}(ads) + HS^- = FeS$
(5)	$FeCO_3 + HS^- = FeS + HCO_3^-$

Table 6. Biosynthetic reaction pathways

Number	Reaction
(1)	$0.25HCO_3^- + 0.05NH_4^+ + 1.2H^+ + e^- \rightarrow 0.05C_5H_7O_2N + 0.65H_2O$
(2)	$0.179HCO_3^- + 0.0357NO_3^- + 1.214H^+ + e^- \rightarrow 0.0357C_5H_7O_2N + 0.571H_2O$
(3)	$0.217HCO_3^- + 0.0217N_2 + 1.217H^+ + e^- \rightarrow 0.0435C_5H_7O_2N + 0.564H_2O$

Table 7. Key end-products of equilibrium speciation reactions (see Tableau for summary of reactions)

Name	Fortran Name	Description	Role in Simulation
Mn^{2+}(aq)	Mn2aq	Conc of aqueous Mn^{2+}	Participation in SRRs, MPRs
Mn^{2+}(ads)	Mn2ads	Conc of adsorbed Mn^{2+}	Attenuation of MnO_2 reduction; participation in SRRs
Fe^{2+}(aq)	Fe2aq	Conc of aqueous Fe^{2+}	Participation in SRRs, MPRs
Fe^{2+}(ads)	Fe2ads	Conc of adsorbed Fe^{2+}	Attenuation of FeOOH reduction; participation in SRRs, MPRs
{CH_3COO^-}	aCH3COO	Activity of CH_3COO^-	Free energy of TEAPs, SRRs
{NO_3^-}	aNO3	Activity of NO_3^-	Free energy of TEAPs, SRRs
{$UO_2(CO_3)_2^{2-}$}	aUO2CO32	Activity of U(VI)-carbonate	Free energy of TEAPs, SRRs
{SO_4^{2-}}	aSO4	Activity of SO_4^{2-}	Free energy of TEAPs, SRRs
{NH_4^+}	aNH4	Activity of NH_4^+	Free energy of TEAPs, SRRs
{H^+}*	aH	Activity of H^+	Free energy of TEAPs, SRRs
{Mn^{2+}}	aMn2aq	Activity of Mn^{2+}(aq)	Free energy of TEAPs, SRRs, MPRs
{Fe^{2+}}	aFe2aq	Activity of Fe^{2+}(aq)	Free energy of TEAPs, SRRs, MPRs
{HS^-}	aHS	Activity of HS^-	Free energy of TEAPs, SRRs, MPRs
{HCO_3^-}	aHCO3	Activity of HCO_3^-	Free energy of TEAPs, SRRs, MPRs
{CH_4(aq)}	aCH4	Activity of CH_4(aq)	Free energy of TEAPs, SRRs, MPRs

TEAPs = Terminal Electron Accepting Processes
SRRs = Secondary Redox Reactions
MPRs = Mineral Precipitation Reactions

* pH was fixed at 6.9 for the simulation of the Area 2 sediment slurry experiment

Table 8. General TEAP kinetic reaction equations

Soluble electron acceptors

RTEAP(i,j) = Vmax(i,j)*FED(i,j)*FEA(i,j)*FTTEAP(i)*FIED(i,j)*FIEA(i,j)*BM(i) (mol e^- L^{-1} d^{-1})

Vmax(i,j) = μmax(i,j)/YCells(i,j)

μmax = maximum specific growth rate for cells catalyzing RTEAP(i,j) (d^{-1})

YCells(i,j) = Yield coefficient for RTEAP(i,j) (mol cells/electron)

= fs0(i,j)*gmwcells/biomasscoefdenom(i,j))

Solid-phase electron acceptors

RTEAP(i,j) = Vmax(i,j)*FED(i,j)*FEA(i,j)*FTTEAP(i)*FIED(i,j)*FIEA(i,j)*BM(i)´/(KmDRM(i)+BM(i)´)

Vmax(i,j) = VmaxEA(i,j) × EAfss **(solid-phase electron acceptors)**

VmaxEA(i,j) = maximum reduction rate constant at high biomass (mol/mol sites/d)

EAfss = concentration of free surface sites (mol L^{-1})

BM(i)´ = BM(i)/Eafss (g cells/mol free surface sites)

KmDRM(i) = half-saturation constant for the biomass-dependent rate of e^- transfer to free surface sites (g cells/mol free surface sites)

FED(i,j) = ED(i)/(KmED(i,j) + ED(i))

ED(i) = concentration of e^- donor for TEAP(i) (mol L^{-1})

KmED(i,j) = half-saturation constant for uptake of ED(i) via RTEAP(i,j) (mol L^{-1})

FEA(i,j) = EA(i)/(KmED(i,j) + EA(i))

EA(i) = concentration of e^- acceptor TEAP(i) (mol L^{-1})

KmEA(i,j) = half-saturation constant for uptake of EA(i) via RTEAP(i,j) (mol L^{-1})

FTTEAP(i) = max(0, (1-exp(dGrxnTEAP(i) × nelecTEAP(i)-dGmin(i))/0.008314/(273 + Temp))))

dGrxnTEAP(i) = free energy for TEAP(i) (kJ/electron)

nelecTEAP(i) = number of e^- transferred in TEAP(i)

dGmin(i) = minimum free energy for biological energy conservation (-20 kJ/rxn)

Temp = temperature (K)

$$FIED(i,j) = \prod_k KmIED(i,j,k)/(KmIED(i,j,k) + EDI(i,j,k))$$

KmIED(i,j,k) = half-saturation concentration of e^- donor k inhibiting RTEAP(i,j)

EDI(i,j,k) = concentration of e^- donor k inhibiting RTEAP(i,j)

$$FIEA(i,j) = \prod_k KmIEA(i,j,k)/(KmIEA(i,j,k) + EAI(i,j,k))$$

KmIEA(i,j,k) = half-saturation concentration of e^- acceptor k inhibiting RTEAP(i,j)

EAI(i,j,k) = concentration of e^- acceptor k inhibiting RTEAP(i,j)

BM(i) = Biomass of micoorganisms catalyzing TEAP(i) (g cells L^{-1})

Table 9. General TEAP reactant/product flux equations

---

1. Electron Donors

$$RED(i) = \sum_{j} RTEAP(i,j) \times Reaccoef(i,1) \text{ (mol } L^{-1}\ d^{-1})$$

Where:

RED(i) = total rate of e^- donor consumption coupled to TEAP(i) (mol e^- L^{-1} d^{-1})
RTEAP(i,j) = rate of e^- transfer coupled to RTEAP(i,j) (mol e^- L^{-1} d^{-1})
Reaccoef(i,1) = mol e^- donor consumed per e^- in TEAP(i) (mol/mol e^-)

2. Electron Acceptors

$$REA(i) = \sum_{j} fe0(i,j) \times RTEAP(i,j) \times Reaccoef(i,2) \text{ (mol } L^{-1}\ d^{-1})$$

Where:

REA(i) = total rate of e^- acceptor consumption coupled to TEAP(i) (mol e^- L^{-1} d^{-1})
fe0(i,j) = fraction of e^- donor used in RTEAP(i,j) that goes toward energy generation
Reaccoef(i,2) = mol e^- acceptor consumed per e^- transferred in TEAP(i) (mol/mol e^-)
(see below for additional definitions)

3. Other Reactants

$$ROR(i) = \sum_{j} fe0(i,j) \times RTEAP(i,j) \times Reaccoef(i,k) \text{ (mol } L^{-1}\ d^{-1})$$

Where:

ROR(i) = total rate of other reactant consumption coupled to TEAP(i) (mol L^{-1} d^{-1})
Reaccoef(i,k) = mol reactant k consumed per e^- transferred in TEAP(i) (mol/mol e^-)

4. Reaction End Products

$$REP(i) = \sum_{j} fe0(i,j) \times RTEAP(i,j) \times Prodcoef(i,k) \text{ (mol } L^{-1}\ d^{-1})$$

Where:

REP(i) = total rate of end product accumulation coupled to TEAP(i) (mol L^{-1} d^{-1})
Reaccoef(i,k) = mol end product k produced per e^- transferred in TEAP(i) (mol/mol e^-)
fe0(i,j) = 1.0 - fs0(i,j)
fs0(i,j) = 1.0/(1 + A)
A = -(dGp(i,j)/(epsiln(i,j)^ndenom(i)) + dGpC(i,j)/epsiln(i,j))/(dGrxnTEAP(i) × epsiln(i,j))
dGp(i,j) = dGfPyruvate - dGc0(i,j)
dGfPyruvate = ΔG_f of pyruvate (assumed to be the central biosynthetic intermediate in the synthesis of cellular organic carbon)

Table 9. Continued

$$dGc0(i,j) = FEDCS(i,j,k) \times dGc0EDCS(i,j,k) + \left(1 - \sum_{k} FEDCS(i,j,k)\right) \times dGc0HCO3$$

FEDCS(i,j,k)= function depicting kinetic control on utilization of organic e^- donor as a carbon source for production of BM(i) via RTEAP(i,j) *(see yield.f90 for details)*

dGc0ED(i,j,k) = free energy required to synthesize organic e^- donor k from HCO_3^-

dGcHCO3 = free energy required to liberate an electron from H_2O for use in HCO_3^- fixation

epsiln(i,j) = energy transfer efficiency for RTEAP(i,j)

dGpc(i,j) = free energy required to synthesize biomass

= FNNH4(i)*dGpCNH4+FNNO3(i)*dGpCNO3+FNN2(i)*dGpCN2

FNNH4(i) = fraction of cellular nitrogen obtained from NH_4^+

dGpCNH4 = free energy required to synthesize biomass with NH_4^+ as a N source

FNNO3(i) = fraction of cellular nitrogen obtained from NO_3^-

dGpCNO3 = free energy required to synthesize biomass with NO_3^- as a N source

FNN2(i) = fraction of cellular nitrogen obtained from N_2

dGpCN2 = free energy required to synthesize biomass with N_2 as a N source

(see below for additional definitions)

Table 10. Microbial biosynthesis and nitrogen metabolism equations

---

1. Microbial Biosynthesis

$$RBM(i) = \sum_{i^*, j^*} fs0(i, j) \times RTEAP(i^*, j^*) \times Prodcoef BS(i, j,1) \times gmwcells \,(\text{mol } L^{-1}\ d^{-1})$$

Where:

RBM(i) = Total rate of BM(i) biosynthesis (g cells L^{-1} d^{-1})
fs0(i,j) = Fraction of e^- donor used to produce biomass in RTEAP(i*,j*)
RTEAP(i*,j*) = Rate of electron transfer coupled to RTEAP(i*,j*) (mol e^- L^{-1} d^{-1})
i*, j* refer to RTEAPs that involve BM(i)
ProdcoefBS(i,j,1) = mol cells produced per e^- in biosynthesis coupled to RTEAP(i*,j*)
ProdcoefBS(i,j,1)=FNNH4(i,j)*0.05+FNNO3(i,j)*0.0357+FNN2(i,j)*0.0435
biomasscoefdenom(i,j)=FNNH4(i,j)*20.0+FNNO3(i,j)*28.0+FNN2(i,j)*23.0
(see section 2 for further definition of terms)
gmwcells = molecular weight of cell biomass (g/mol)

2. Microbial Nitrogen Metabolism

RNTot(i,j) = Total rate of N uptake for biosynthesis
= fs0(i,j) × RTEAP(i*,j*) × ReaccoefBS(i,j,2) × gmwcells
ReaccoefBS(i,j,1)=FNNH4(i,j)*0.25+FNNO3(i,j)*0.179+FNN2(i,j)*0.217
ReaccoefBS(i,j,2)=FNNH4(i,j)*0.05+FNNO3(i,j)*0.0357+FNN2(i,j)*0.0435
RNNH4(i,j) = Rate of NH_4^+ consumption for biosynthesis coupled to RTEAP(i,j)
= FNNH4(i,j)*RNTot(i,j)
RNNO3(i,j) = Rate of NO_3^- consumption for biosynthesis coupled to RTEAP(i,j)
= FNNO3(i,j)*RNTot(i,j)
RNN2(i,j) = Rate of N_2 consumption for biosynthesis coupled to RTEAP(i,j)
= FNN2(i,j)*RNTot(i,j)
FNNH4(i,j) = NH4/(KmNH4(i,j)+NH4N)
KmNH4 = half saturation constant for uptake of NH_4^+ coupled to RTEAP(i,j)
FNNO3(i,j)=(1-FNNH4(i,j))*(NO3/(KmNO3(i,j)+NO3))
KmNO3 = half saturation constant for uptake of NO_3^- coupled to RTEAP(i,j)
FNN2(i,j)=(1-FNNH4(i,j))*(1-(NO3/(KmNO3(i,j)+NO3)))
KmN2 = half saturation constant for uptake of N_2 coupled to RTEAP(i,j)

Table 11. Secondary redox reaction equations

$RSRR(i) = kRedOxid \times Red \times Oxid \times FTSRR(i,j)$

Where:

kRedOxid = second-order reaction rate coefficient $(mol\ L^{-1})^{-1}d^{-1}$
Red = Concentration of reducing reactant
Oxid = Concentration of oxidizing reactant
FTSRR(i) = max(0, (1-exp(dGrxnSRR(i))/0.008314/(273 + Temp))))
dGrxnSRR(i) = free energy for SRR(i) (kJ/electron)
Temp = temperature (K)

Table 12. Mineral recipitation equations

$RMPR(i) = kprecip(i) \times (OMEGA(i) - 1.0), OMEGA(i) \geq 1$
$RMPR(i) = kdiss(i) \times Min(i) \times (OMEGA(i) - 1.0), OMEGA(i) < 1$

Where:

$kprecip(i)$ = mineral i precipitation rate constant (mol L^{-1} d^{-1})
$kdiss(i)$ = mineral i dissoluation rate constant (d^{-1})
$Min(i)$ = concentration of mineral i (mol L^{-1})
$OMEGA(i) = \exp(-dGrxnMPR(i)/0.008314/(273 + Temp))$
dGrxnMPR(i) = free energy for RMPR(i) (kJ/mol)
Temp = temperature (I)

Table 13. Parameter values used in simulation of the sediment slurry experiment. (I) Independent, (C) Constrained, (A) Arbitrary, and (M) Model-derived parameters. (NA) Not Applicable.

Description	Parameter	Value	Units	Type	Source
Maximum growth rate	umax(1,1)	5.0	d^{-1}	C	(Rittmann and McCarty, 2001)
	umax(1,2)	5.0	d^{-1}	C	(Rittmann and McCarty, 2001)
	umax(2,1)	3.0	d^{-1}	C	(Rittmann and McCarty, 2001)
	umax(3,1)	2.0	d^{-1}	C	(Rittmann and McCarty, 2001)
	umax(3,2)	2.0	d^{-1}	C	(Rittmann and McCarty, 2001)
	umax(3,3)	2.0	d^{-1}	C	(Rittmann and McCarty, 2001)
	umax(6,1)	1.5	d^{-1}	M	
	umax(6,2)	1.5	d^{-1}	M	
	umax(7,1)	1.5	d^{-1}	M	
	umax(7,2)	1.5	d^{-1}	M	
	umax(8,1)	0.5	d^{-1}	M	
	umax(9,1)	5.0	d^{-1}	C	(Rittmann and McCarty, 2001)
	umax(9,2)	5.0	d^{-1}	C	(Rittmann and McCarty, 2001)
	umax(10,1)	3.0	d^{-1}	C	(Rittmann and McCarty, 2001)
	umax(11,1)	2.0	d^{-1}	C	(Rittmann and McCarty, 2001)
	umax(11,2)	2.0	d^{-1}	C	(Rittmann and McCarty, 2001)
	umax(14,1)	2.0	d^{-1}	M	
	umax(14,2)	1.5	d^{-1}	M	
	umax(15,1)	1.5	d^{-1}	M	
	umax(15,2)	1.5	d^{-1}	M	
	umax(16,1)	0.5	d^{-1}	M	
	umax(17,1)	1.5	d^{-1}	M	
	umax(17,2)	1.5	d^{-1}	M	
	umax(17,3)	1.5	d^{-1}	M	
	umax(17,4)	1.5	d^{-1}	M	
	umax(18,1)	1.5	d^{-1}	M	
	umax(18,2)	1.5	d^{-1}	M	
	umax(18,3)	1.5	d^{-1}	M	
	umax(18,4)	1.5	d^{-1}	M	

Description	Parameter	Value	Units	Type	Source
Oxide mineral surface area	SAMnO2	170	$m^2\ g^{-1}$	A	
	SAFeOOH	170	$m^2\ g^{-1}$	C	
Maximum surface area-specific oxide mineral reduction rate	VmaxDMRM(1)	0.75	mol/mol sites/d	C/M	(Roden and Sedo, 2003)
	VmaxDMRM(2)	0.75	mol/mol sites/d	C/M	(Roden and Sedo, 2003)
	VmaxDIRM(1)	0.75	mol/mol sites/d	C/M	(Roden and Sedo, 2003)
	VmaxDIRM(2)	0.75	mol/mol sites/d	C/M	(Roden and Sedo, 2003)
Half-saturating cell density for oxide mineral reduction	KmDMRM(1)	2.25	g/mol sites	C/M	(Roden and Sedo, 2003)
	KmDMRM(2)	2.25	g/mol sites	C/M	(Roden and Sedo, 2003)
	KmDIRM(1)	2.25	g/mol sites	C/M	(Roden and Sedo, 2003)
	KmDIRM(2)	2.25	g/mol sites	C/M	(Roden and Sedo, 2003)
Cell death rate constant	kDeath(1)	0.2	d^{-1}	C	(Rittmann and McCarty, 2001)
	kDeath(2)	0.2	d^{-1}	C	(Rittmann and McCarty, 2001)
	kDeath(3)	0.05	d^{-1}	C	(Rittmann and McCarty, 2001)
	kDeath(4)	0.05	d^{-1}	C	(Rittmann and McCarty, 2001)
	kDeath(5)	0.05	d^{-1}	C	(Rittmann and McCarty, 2001)
	kDeath(6)	0.05	d^{-1}	C	(Rittmann and McCarty, 2001)
	kDeath(7)	0.05	d^{-1}	C	(Rittmann and McCarty, 2001)
	kDeath(8)	0.05	d^{-1}	C	(Rittmann and McCarty, 2001)
Decayable fraction of dead cells	fdecay	0.9		A	
Half-saturation constant for electron donor uptake	KmED(1,1)	0.000001	mol L^{-1}	A	
	·	0.000001	mol L^{-1}	A	
	·	0.000001	mol L^{-1}	A	
	·	0.000001	mol L^{-1}	A	
	KmED(18,2)	0.000001	mol L^{-1}	A	

Description	Parameter	Value	Units	Type	Source
Half-saturation constant for electron acceptor uptake	KmEA(1,1)	0.000001	mol L^{-1}	A	
	·	0.000001	mol L^{-1}	A	
	·	0.000001	mol L^{-1}	A	
	·	0.000001	mol L^{-1}	A	
	KmEA(4,2)	0.000001	mol L^{-1}	A	
	KmEA(5,1)	0.0001	mol L^{-1}	M	
	KmEA(5,2)	0.0001	mol L^{-1}	M	
	KmEA(6,1)	0.0001	mol L^{-1}	C	(Roden and Tuttle, 1993)
	KmEA(6,2)	0.0001	mol L^{-1}	C	(Roden and Tuttle, 1993)
	KmEA(7,1)	0.0001	mol L^{-1}	A	
	KmEA(7,2)	0.0001	mol L^{-1}	A	
	KmEA(8,1)	NA			
	KmEA(9,1)	0.000001	mol L^{-1}	A	
	·	0.000001	mol L^{-1}	A	
	·	0.000001	mol L^{-1}	A	
	·	0.000001	mol L^{-1}	A	
	KmEA(12,2)	0.000001	mol L^{-1}	A	
	KmEA(13,1)	0.0001	mol L^{-1}	M	
	KmEA(13,2)	0.0001	mol L^{-1}	M	
	KmEA(14,1)	0.0001	mol L^{-1}	C	(Roden and Tuttle, 1993)
	KmEA(14,2)	0.0001	mol L^{-1}	C	(Roden and Tuttle, 1993)
	KmEA(15,1)	0.0001	mol L^{-1}	A	
	KmEA(15,2)	0.0001	mol L^{-1}	A	
	KmEA(16,1)	NA			
	KmEA(17,1)	0.000001	mol L^{-1}	C	(Roden and Scheibe, 2005)
	KmEA(17,2)	0.000001	mol L^{-1}	C	(Roden and Scheibe, 2005)
	KmEA(17,3)	0.000001	mol L^{-1}	C	(Roden and Scheibe, 2005)
	KmEA(17,4)	0.000001	mol L^{-1}	C	(Roden and Scheibe, 2005)
	KmEA(18,1)	0.000001	mol L^{-1}	C	(Roden and Scheibe, 2005)
	KmEA(18,2)	0.000001	mol L^{-1}	C	(Roden and Scheibe, 2005)
	KmEA(18,3)	0.000001	mol L^{-1}	C	(Roden and Scheibe, 2005)
	KmEA(18,4)	0.000001	mol L^{-1}	C	(Roden and Scheibe, 2005)

Description	Parameter	Value	Units	Type	Source
Half-saturation constant	KmNH4(1,1)	0.000001	mol L^{-1}	A	
For uptake of NH_4^+	·	0.000001	mol L^{-1}	A	
for biosynthesis	·	0.000001	mol L^{-1}	A	
as a nitrogen source	·	0.000001	mol L^{-1}	A	
	KmNH4(18,4)	0.000001	mol L^{-1}	A	
Half-saturation constant	KmNO3(1,1,1)	0.000001	mol L^{-1}	A	
For uptake of NO_3^-	KmNO3(1,2,1)	0.000001	mol L^{-1}	A	
as a nitrogen source	·	0.000001	mol L^{-1}	A	
for biosynthesis	·	0.000001	mol L^{-1}	A	
	·	0.000001	mol L^{-1}	A	
	KmNO3(16,1,4)	0.000001	mol L^{-1}	A	
Half-saturation constant	KmIED(1,1,1)	0.000001	mol L^{-1}	A	
for inhibition of primary	KmIED(1,2,1)	0.000001	mol L^{-1}	A	
electron donor uptake by	·	0.000001	mol L^{-1}	A	
another electron donor	·	0.000001	mol L^{-1}	A	
	·	0.000001	mol L^{-1}	A	
	KmIED(8,1)	0.000001	mol L^{-1}	A	
	KmIED(9,1,1)	0.000001	mol L^{-1}	A	
	·	NA			
	·	NA			
	·	NA			
	KmIED(16,1)	NA			
	KmIED(17,1,1)	0.000001	mol L^{-1}	A	
	KmIED(17,1,2)	0.000001	mol L^{-1}	A	
	KmIED(17,1,3)	0.000001	mol L^{-1}	A	
	KmIED(17,1,4)	0.000001	mol L^{-1}	A	
	KmIED(18,1,1)	NA			
	KmIED(18,1,2)	NA			
	KmIED(18,1,3)	NA			
	KmIED(18,1,4)	NA			

Description	Parameter	Inhibiting EA	Value	Units	Type	Source
Half-saturation constant for inhibition of primary electron acceptor (EA) uptake another electron acceptor	KmIEA(1,1,1)	NA				
	KmIEA(1,2,1)	NA				
	KmIEA(2,2,1)	O_2	0.000001	mol L^{-1}	A	
	KmIEA(3,1,1)	O_2	0.000001	mol L^{-1}	A	
	KmIEA(3,2,1)	O_2	0.000001	mol L^{-1}	A	
	KmIEA(3,2,1)	O_2	0.000001	mol L^{-1}	A	
	KmIEA(4,1,1)	O_2	0.000001	mol L^{-1}	A	
	KmIEA(4,2,1)	NO_3^-	0.000001	mol L^{-1}	A	
	KmIEA(4,2,1)	O_2	0.000001	mol L^{-1}	A	
	KmIEA(4,2,2)	NO_3^-	0.000001	mol L^{-1}	A	
	KmIEA(5,1,1)	O_2	0.000001	mol L^{-1}	A	
	KmIEA(5,2,1)	NO_3^-	0.000001	mol L^{-1}	A	
	KmIEA(5,2,1)	O_2	0.000001	mol L^{-1}	A	
	KmIEA(5,2,2)	NO_3^-	0.000001	mol L^{-1}	A	
	KmIEA(6,1,1)	O_2	0.000001	mol L^{-1}	A	
	KmIEA(6,1,2)	NO_3^-	0.000001	mol L^{-1}	A	
	KmIEA(6,1,3)	MnO_2	0.001	mol L^{-1}	M	
	KmIEA(6,1,4)	FeOOH	0.001	mol L^{-1}	M	
	KmIEA(6,2,1)	O_2	0.000001	mol L^{-1}	A	
	KmIEA(6,2,2)	NO_3^-	0.000001	mol L^{-1}	A	
	KmIEA(6,2,3)	MnO_2	0.001	mol L^{-1}	M	
	KmIEA(6,2,4)	FeOOH	0.001	mol L^{-1}	M	
	KmIEA(7,1,1)	O_2	0.000001	mol L^{-1}	A	
	KmIEA(7,1,2)	NO_3^-	0.000001	mol L^{-1}	A	
	KmIEA(7,1,3)	MnO_2	0.001	mol L^{-1}	M	
	KmIEA(7,1,4)	FeOOH	0.001	mol L^{-1}	M	
	KmIEA(7,2,1)	O_2	0.000001	mol L^{-1}	A	
	KmIEA(7,2,2)	NO_3^-	0.000001	mol L^{-1}	A	
	KmIEA(8,1,1)	O_2	0.000001	mol L^{-1}	A	
	KmIEA(8,1,2)	NO_3^-	0.000001	mol L^{-1}	A	
	KmIEA(8,1,3)	MnO_2	0.005	mol L^{-1}	M	
	KmIEA(8,1,4)	FeOOH	0.005	mol L^{-1}	M	

Description	Parameter	Inhibiting EA	Value	Units	Type	Source
	KmIEA(91,1,1)	NA				
	KmIEA(9,2,1)	NA				
	KmIEA(10,2,1)	O_2	0.000001	mol L^{-1}	A	
	KmIEA(11,1,1)	O_2	0.000001	mol L^{-1}	A	
	KmIEA(11,2,1)	O_2	0.000001	mol L^{-1}	A	
	KmIEA(11,2,1)	O_2	0.000001	mol L^{-1}	A	
	KmIEA(12,1,1)	O_2	0.000001	mol L^{-1}	A	
	KmIEA(12,2,1)	NO_3^-	0.000001	mol L^{-1}	A	
	KmIEA(12,2,1)	O_2	0.000001	mol L^{-1}	A	
	KmIEA(12,2,2)	NO_3^-	0.000001	mol L^{-1}	A	
	KmIEA(13,1,1)	O_2	0.000001	mol L^{-1}	A	
	KmIEA(13,2,1)	NO_3^-	0.000001	mol L^{-1}	A	
	KmIEA(13,2,1)	O_2	0.000001	mol L^{-1}	A	
	KmIEA(13,2,2)	NO_3^-	0.000001	mol L^{-1}	A	
	KmIEA(14,1)	O_2	0.000001	mol L^{-1}	A	
	KmIEA(14,2)	NO_3^-	0.000001	mol L^{-1}	A	
	KmIEA(14,3)	MnO_2	0.001	mol L^{-1}	M	
	KmIEA(14,4)	FeOOH	0.001	mol L^{-1}	M	
	KmIEA(14,1)	O_2	0.000001	mol L^{-1}	A	
	KmIEA(14,2)	NO_3^-	0.000001	mol L^{-1}	A	
	KmIEA(14,2,3)	MnO_2	0.001	mol L^{-1}	M	
	KmIEA(14,2,4)	FeOOH	0.001	mol L^{-1}	M	
	KmIEA(15,1,1)	O_2	0.000001	mol L^{-1}	A	
	KmIEA(15,1,2)	NO_3^-	0.000001	mol L^{-1}	A	
	KmIEA(15,1,3)	MnO_2	0.001	mol L^{-1}	M	
	KmIEA(15,1,4)	FeOOH	0.001	mol L^{-1}	M	
	KmIEA(15,2,1)	O_2	0.000001	mol L^{-1}	A	
	KmIEA(15,2,2)	NO_3^-	0.000001	mol L^{-1}	A	
	KmIEA(16,1,1)	O_2	0.000001	mol L^{-1}	A	
	KmIEA(16,1,2)	NO_3^-	0.000001	mol L^{-1}	A	
	KmIEA(16,1,3)	MnO_2	0.005	mol L^{-1}	M	
	KmIEA(16,1,4)	FeOOH	0.005	mol L^{-1}	M	
	KmIEA(17,1,1)	O_2	0.000001	mol L^{-1}	A	

	KmIEA(17,1,2)	NO_3^-	0.000001	mol L^{-1}	A
	KmIEA(17,2,1)	O_2	0.000001	mol L^{-1}	A
	KmIEA(17,2,2)	NO_3^-	0.000001	mol L^{-1}	A
	KmIEA(17,3,1)	O_2	0.000001	mol L^{-1}	A
	KmIEA(17,3,2)	NO_3^-	0.000001	mol L^{-1}	A
	KmIEA(17,4,1)	O_2	0.000001	mol L^{-1}	A
	KmIEA(17,4,2)	NO_3^-	0.000001	mol L^{-1}	A
	KmIEA(18,1,2)	NO_3^-	0.000001	mol L^{-1}	A
	KmIEA(18,2,1)	O_2	0.000001	mol L^{-1}	A
	KmIEA(18,2,2)	NO_3^-	0.000001	mol L^{-1}	A
	KmIEA(18,3,1)	O_2	0.000001	mol L^{-1}	A
	KmIEA(18,3,2)	NO_3^-	0.000001	mol L^{-1}	A
	KmIEA(18,4,1)	O_2	0.000001	mol L^{-1}	A
	KmIEA(18,4,2)	NO_3^-	0.000001	mol L^{-1}	A

Description	Parameter	Value	Units	Type	Source
Energy transfer efficiency	epsiln(1,1)	0.6		C	(Rittmann and McCarty, 2001)
	epsiln(1,2)	0.6		C	(Rittmann and McCarty, 2001)
	.	0.6		C	(Rittmann and McCarty, 2001)
	.	0.6		C	(Rittmann and McCarty, 2001)
	.	0.6		C	(Rittmann and McCarty, 2001)
	epsiln(16,1)	0.6		C	(Rittmann and McCarty, 2001)
Rate constant for secondary redox reaction	kMn2aqO2	1.0D7	$(mol\ L^{-1})^{-1}\ yr^{-1}$	C	(Hunter et al., 1998)
	kMn2adsO2	5.0D6	$(mol\ L^{-1})^{-1}\ yr^{-1}$	C	(VanCappellen and Wang, 1996)
	kMnCO3O2	1.0D7	$(mol\ L^{-1})^{-1}\ yr^{-1}$	A	
	kFe2aqO2	1.0D7	$(mol\ L^{-1})^{-1}\ yr^{-1}$	C	(Hunter et al., 1998)
	kFe2adsO2	5.0D7	$(mol\ L^{-1})^{-1}\ yr^{-1}$	C	(VanCappellen and Wang, 1996)]
	kFeCO3O2	1.0D7	$(mol\ L^{-1})^{-1}\ yr^{-1}$	A	
	kHSO2	1.6D5	$(mol\ L^{-1})^{-1}\ yr^{-1}$	C	(Hunter et al., 1998)
	kS0O2	6.0D4	$(mol\ L^{-1})^{-1}\ yr^{-1}$	A	
	kFeSO2	6.0D4	$(mol\ L^{-1})^{-1}\ yr^{-1}$	C	(Hunter et al., 1998)

Description	Parameter	Value	Units	Type	Source
	kCH4O2	1.0D7	(mol L^{-1})$^{-1}$ yr^{-1}	C	(Hunter et al., 1998)
	kUO2O2	6.0D4	(mol L^{-1})$^{-1}$ yr^{-1}	A	
	kFe2aqNO3	2.0D5	(mol L^{-1})$^{-1}$ yr^{-1}	I	(Weber et al., 1998)
	kFe2adsNO3	2.0D5	(mol L^{-1})$^{-1}$ yr^{-1}	I	(Weber et al., 1998)
	kFeCO3NO3	2.0D5	(mol L^{-1})$^{-1}$ yr^{-1}	I	(Weber et al., 1998)
	kUO2NO3	6.0D4	(mol L^{-1})$^{-1}$ yr^{-1}	A	
	kHSNO3	1.6D5	(mol L^{-1})$^{-1}$ yr^{-1}	A	
	kS0NO3	6.0D4	(mol L^{-1})$^{-1}$ yr^{-1}	A	
	kFeSNO3	6.0D4	(mol L^{-1})$^{-1}$ yr^{-1}	A	
	kFe2aqMnO2	2.0D5	(mol L^{-1})$^{-1}$ yr^{-1}	C	(Hunter et al., 1998)
	kFe2adsMnO2	2.0D5	(mol L^{-1})$^{-1}$ yr^{-1}	C	(Hunter et al., 1998)
	kFeCO3MnO2	2.0D5	(mol L^{-1})$^{-1}$ yr^{-1}	A	
	kHSMnO2	2.0D4	(mol L^{-1})$^{-1}$ yr^{-1}	C	(Hunter et al., 1998)
	kFeSMnO2	2.0D4	(mol L^{-1})$^{-1}$ yr^{-1}	A	
	kUO2MnO2	2.0D4	(mol L^{-1})$^{-1}$ yr^{-1}	A	
	kHSFeOOH	8.0D3	(mol L^{-1})$^{-1}$ yr^{-1}	C	(Hunter et al., 1998)
	kS0disp	1.0D2	yr^{-1}	C	(Berg et al., 2003)
	kNH4O2	5.0D6	(mol L^{-1})$^{-1}$ yr^{-1}	C	(Hunter et al., 1998)
Rate constant for mineral precipitation or dissolution	kprecipMnCO3	1.0D-4	mol L^{-1} yr^{-1}	C	(Hunter et al., 1998)
	kdissMnCO3	1.0D-4	mol L^{-1} yr^{-1}	C	(Hunter et al., 1998)
	kprecipFeCO3	0.0	mol L^{-1} yr^{-1}	M	
	kdissFeCO3	0.0	mol L^{-1} yr^{-1}	M	
	kprecipFeS	6.0D-5	mol L^{-1} yr^{-1}	C	(Hunter et al., 1998)
	kdissFeS	1.0D-4	mol L^{-1} yr^{-1}	C	(Hunter et al., 1998)
	kHSFe2ads	1.0D4	(mol L^{-1})$^{-1}$ yr^{-1}	A	
	kHSFeCO3	1.0D4	(mol L^{-1})$^{-1}$ yr^{-1}	A	
Molecular weight	MWMnO2	86.9	g mol^{-1}	I	
	MWFeOOH	89.0	g mol^{-1}	I	

Description	Parameter	Value	Units	Type	Source
Mineral surface site density	SSD	3.84D-6	sites m^{-2}	C	(Davis and Kent, 1990)
Free energy of formation (non-living materials)	dGfCH3CH2OH	-181.75	kJ mol^{-1}	I	(Thauer et al., 1977)
	dGfCH3COO	-369.41	kJ mol^{-1}	I	(Thauer et al., 1977)
	dGfPyruvate	34.2	kJ mol^{-1}	I	(Thauer et al., 1977)
	dGfO2	16.32	kJ mol^{-1}	I	(Stumm and Morgan, 1996)
	dGfNO3	-111.3	kJ mol^{-1}	I	(Stumm and Morgan, 1996)
	dGfMnO2	-460.0	kJ mol^{-1}	I	(Stumm and Morgan, 1996)
	dGfFeOOH	-487.0	kJ mol^{-1}	M	
	dGfUO2CO32	-2105.4	kJ mol^{-1}	I	(Grenthe et al., 1995)
	dGfSO4	-744.6	kJ mol^{-1}	I	(Stumm and Morgan, 1996)
	dGfS0	0.0	kJ mol^{-1}	I	(Stumm and Morgan, 1996)
	dGfHCO3	-586.8	kJ mol^{-1}	I	(Stumm and Morgan, 1996)
	dGfCO3	-527.9	kJ mol^{-1}	I	(Stumm and Morgan, 1996)
	dGfN2	-18.26	kJ mol^{-1}	I	(Stumm and Morgan, 1996)
	dGfNH4	79.37	kJ mol^{-1}	I	(Stumm and Morgan, 1996)
	dGfMn2	-228.0	kJ mol^{-1}	I	(Stumm and Morgan, 1996)
	dGfFe2	-78.87	kJ mol^{-1}	I	(Stumm and Morgan, 1996)
	dGfUO2	-979.7	kJ mol^{-1}	I	(Grenthe et al., 1995)
	dGfHS	12.05	kJ mol^{-1}	I	(Stumm and Morgan, 1996)
	dGfCH4	-34.39	kJ mol^{-1}	I	(Stumm and Morgan, 1996)
	dGfH	0.0	kJ mol^{-1}	I	(Stumm and Morgan, 1996)
	dGfH2O	-237.2	kJ mol^{-1}	I	(Stumm and Morgan, 1996)
	dGfMnCO3	-816.0	kJ mol^{-1}	I	(Stumm and Morgan, 1996)
	dGfFeCO3	-666.7	kJ mol^{-1}	I	(Stumm and Morgan, 1996)
	dGfFeS	-83.71	kJ mol^{-1}	I	(Langmuir, 1997)
Free energy of formation (other; see above)	dGc0CH3CH2OH	30.4	kJ mol^{-1}	I	
	dGc0CH3COO	26.9	kJ mol^{-1}	I	
	Gc0HCO3	-82.7	kJ mol^{-1}	I	

Description	Parameter	Value	Units	Type	Source
	dGpcNH4	18.8	kJ mol^{-1}	C	(Rittmann and McCarty, 2001)
	dGpcNO3	13.5	kJ mol^{-1}	C	(Rittmann and McCarty, 2001)
	dGpcN2	16.4	kJ mol^{-1}	C	(Rittmann and McCarty, 2001)
Molecular weight of cell biomass	gmwcells	113.0	g mol^{-1}	C	(Rittmann and McCarty, 2001)